CHARACTERIZATION AND USE OF POLLEN AS A BIORENEWABLE FILLER FOR POLYMER COMPOSITES

A Thesis
Presented to
The Academic Faculty

by

Oluwatimilehin Fadiran

In Partial Fulfillment
Of the Requirements for the Degree
Doctor of Philosophy in the
School of Chemical and Biomolecular Engineering

Georgia Institute of Technology
May 2015

COPYRIGHT 2015 OLUWATIMILEHIN FADIRAN

CHARACTERIZATION AND USE OF POLLEN AS A BIORENEWABLE FILLER FOR POLYMER COMPOSITES

Approved by:

Dr. J. Carson Meredith, Advisor
School of Chemical and
Biomolecular Engineering
Georgia Institute of Technology

Dr. Yulin Deng
School of Chemical and
Biomolecular Engineering
Georgia Institute of Technology

Dr. Meisha Shofner
School of Materials Science &
Engineering
Georgia Institute of Technology

Dr. William Koros
School of Chemical and
Biomolecular Engineering
Georgia Institute of Technology

Dr. Peter Ludovice
School of Chemical and
Biomolecular Engineering
Georgia Institute of Technology

Date Approved: March 2015

This work is dedicated to my family.

ACKNOWLEDGEMENTS

I would like to thank my family for their love and support all my life. To my parents, Emmanuel and Omotunde Fadiran, thank you for you love and support, your friendship, teaching me the importance of hard work, and always leading me by example. I would not be where I am today without you. To my siblings, Tope and Toyin, thank you for being my best friends and always lending a listening ear in my times of need. To my family in Atlanta, the Afons, the Dele-Tunjis, and the Abodurins, thank you for your support throughout my time here in Atlanta.

To my advisor, Dr. Carson Meredith, thank you for your leadership and mentorship during my studies. I truly appreciate the opportunity you gave me to do unique research that challenged me throughout my studies. You allowed me to develop and think independently, but were also consistently available whenever I needed assistance. I especially appreciate the times you listened to me and gave me valuable career advice as I was considering different options. I would like to thank my committee members, Dr. Yulin Deng, Dr. Meisha Shofner, Dr. William Koros, and Dr. Peter Ludovice for providing me with valuable feedback, support throughout my PhD process, opportunities for collaboration, and access to valuable instrumentation. Additionally, I would like to acknowledge the organizations that provided funding for my PhD programs and for my research: the U.S. Air Force Office for Scientific Research, Georgia Tech's RBI PSE fellowship, and Georgia Tech's FACES fellowship.

There is a host of individuals and organizations that have influenced my life and the course of my education. I would like to thank my middle school teachers Mr. Reddington and Mrs. Engelman for being great teachers that I will never forget. In high school the STARs program, Dr. Hirsch, Mr. Pratt, and Mr. Bascom, were extremely influential in developing my interest in STEM fields. I am very grateful to my basketball coaches Kirk Lawder, Tim Holton,

and Thomas Lang for being very influential in my life as well. I was blessed to be a part of the Meyerhoff scholarship program at UMBC, which prepared me pursue an advanced degree. I am so grateful to all the Meyerhoff staff and my Meyerhoff colleagues for getting me to where I am today. I am thankful to Dr. Timmie Topoleski for being a great professor and advisor that pushed me to use my imagination to solve engineering problems. I would like to thank Dr. Edwin Fuller, Dr. Ryan Kershner, and Dr. Matthew Lang for outstanding summer research experiences during my undergraduate career. I would like to thank Georgia Tech's BGSA for being a great community for support throughout my PhD process as well. I am also very thankful to Dr. Sue Ann Bidstrup-Allen and Dr. Martha Grover for giving me the opportunity to become a mentor and leader through the ExxonMobil Success Program. This experience has given me a unique opportunity to grow as a person and become a role-model for other students.

I thank the current and some past members of the Meredith research group, Dr. Ismael Gomez, Dr. Jie Wu, Dr. Sangil Han, Dr. Shanhong Xu, Dr. Haisheng Lin, Dr. Zifu Li, Natalie Girouard, Yi Zhang, Donglee Shin, Zihao Qu, and Songcheng Wang, for sharing your knowledge and friendships with me. I appreciate all the discussions, collaborations, and laughs we've shared throughout my time in the group.

Lastly, I'd like to thank my friends, who have contributed to my quality of life during my time at Georgia Tech. First, I would like to thank my classmates Lindsay Arnold, Brennen Mueller, Abiola Shitta, Maria Elena Casas, Andrew Peters, and Matthew Mistillis for not only being great colleagues that were vital to my success in our first few semesters, but also for being great friends. I would also like to thank Vyran George for his friendship and mentorship over he years. Finally, I'd like to give special thanks to Patricia Andre for sharing many adventures with me and supporting me throughout my PhD education.

Table of Contents

LIST OF TABLES

LIST OF FIGURES

LIST OF APPENDIX FIGURES

SUMMARY

The incorporation of filler particles into polymer matrices is a common industrial practice for the production of many commercial polymer products. Fillers are often thought of as a means to reduce cost. However, fillers can also be exploited in order to synergistically improve mechanical, thermal and transport properties. High filler-matrix compatibility is often important to achieve such improvements. Many studies have illustrated the successful use of non-biological materials ranging from inorganic particles to carbon nanotubes as reinforcing fillers in fabricating composite materials. With the increase in concerns over environmental issues and the desire to create more versatile polymer-based materials, interest in polymers filled with natural organic fillers continues to grow. This work explores the hypothesis that pollen, a natural particle, has the potential to be an effective biorenewable reinforcing filler due to its unique surface architectures, high strength, chemical stability, and low density. These properties may enhance stress transfer between polymer and pollen filler, increase the energy absorption of pollen filler while under stress, enhance chemical resistance, and effectively maintain or lower material density. Pollens from sources such as ragweed plants are ubiquitous natural materials that are based on sustainable, non-food resources. Pollen is a remarkable example of evolutionary-optimized microscale particle with structures and/or chemistries tailored for effective adhesion to a variety of surfaces and protection of genetic material under different dynamic and environmental conditions. The pollen shell is perhaps the most chemically resistant naturally occurring material. As many pollens achieve pollination simply by being carried by wind, they are very light-weight. These properties make pollen an attractive option as a natural filler for polymers.

This research aims to characterize pollen interfacial properties and utilize pollen as an effective reinforcing filler in polymer materials. In this work, interfacial properties are characterized using Fourier transform infrared spectroscopy (FTIR), the BET method, and inverse liquid chromatography (ILC). These techniques were useful in determining the effect of surface treatments and further chemical modifications on pollen interfacial properties. Characterizing these properties allowed for improved understanding and utilization of pollen as a filler by revealing the enhanced surface interactions and surface properties of acid-base treated pollens when compared to as received untreated pollens. Epoxy and polyvinyl acetate (PVAc) matrices were used to demonstrate the effectiveness of pollen as a filler, as a function of pollen loading and surface treatments/chemical modifications. Scanning electron microscopy (SEM) was used to determine interfacial morphology, a high throughput mechanical characterization device (HTMECH) was used to determine mechanical properties, and differential scanning calorimetry (DSC) was used to determine glass transition behavior. In epoxy, pollen was an effective load bearing filler only after modifying its surface with acid-base hydrolysis. In PVAc, pollen was an effective load bearing filler only after an additional functionalization with a silane coupling agent. Finally, the species of pollen incorporated in PVAc matrices was varied in order determine the effect of the size of surface nano- and micro- structures on wetting, adhesion, and composite properties. Composites containing pollen displayed enhanced wetting and interfacial adhesion when compared to composites with smooth silica particles. Additionally, it was observed that pollen with smaller surface structures were wetted more effectively by the polymer matrix than pollen with larger structures. However, mechanical properties did not suggest significant changes in interfacial adherence with varied pollen microstructure size. The results of

this work highlight the feasibility and potential of utilizing pollen as a natural filler for creating high strength, light-weight polymer composites with sustainable filler.

CHAPTER 1

INTRODUCTION

1.1 Fillers and Polymer Composites

The use of fillers in various materials has a long history, likely arising from the desire to lower costs of materials. Fillers continue to play a very important role today, and their use has expanded much further than simply cost reduction. In 2006 nearly 52 million tons of fillers were consumed worldwide and it is estimated that in 2016, 74 million tons will be consumed at a value of nearly 60 billion US dollars [1]. Fillers can be defined as "solid material capable of changing the physical and chemical properties of a material by surface interaction or its lack thereof and by its own physical properties" [2]. Fillers are able to alter mechanical, optical, thermal, and transport properties, to name a few. Some of the most widely filled polymers include polyvinyl chloride, polypropylene, polyamides, and polyesters [2]. Widely used fillers today include carbon black, calcium carbonate ($CaCO_3$), talc, and kaolin clay amongst many others. The applications for fillers are vast including plastics, construction, paper, etc. These facts distinguish a field where research advances can have high impact. Current interests in the field include nanofillers, filler mixtures, filler surface modification, and low cost reinforcing fillers, to name a few [2, 3].

Although cost reduction is often mentioned as the motivation for using fillers, it can be challenging to achieve for two reasons. First, there are additional costs for compounding the filler into the polymer. Secondly, fillers are often sold by weight, but the quantities required in practice are determined by their volume, since they replace a portion of the polymer volume. Inorganic fillers typically have densities 2-3 times that of polymers, diminishing cost savings.

Thus, the focus and motivation for using fillers usually includes additional goals of achieving improvements in composite functional properties, such as mechanical, thermal, and optical properties to name a few [4-6].

For the most part, fillers are inorganic substances. Synthetic fillers require additional chemical precursors to produce and synthesis can be quite expensive (carbon nanotubes). Some of the widely used fillers mentioned above are non-renewable minerals that are consumed at a faster rate than they are replaced by natural processes. Mineral fillers are generally formed by geological processes over millions of years. For example, some chalk formations with calcium carbonate were deposited between 70 and 130 million years ago [7]. Additionally, widely-used mineral fillers require various forms of mining and further processing such as crushing, grinding and milling. Even with further processing, most filler particles (natural as well as synthetic) are irregular in shape and particle size distributions. Figure 1.1 shows common filler geometries. This has not limited their use, but makes it challenging to describe particle shape in predictive models for composite properties based on uniform model shapes. Additionally, distinguishing between primary particles, agglomerates, aggregates, and even fragments is difficult. In applications that call for uniform stress distribution, monodisperse uniformly shaped particles are ideal [8].

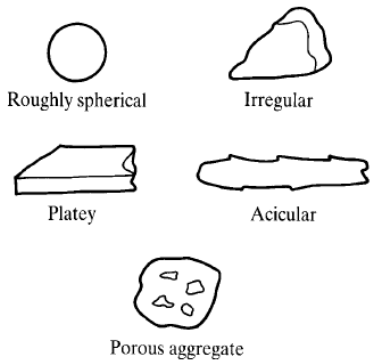

Figure 1.1: Typical filler geometries [9].

Many filler attributes affect the final properties of composites. These attributes must be well understood in order to make effective particulate composites. Some attributes include cost, particle size and shape, filler-polymer interactions, and surface chemistry. For example, in order to improve mechanical properties of a polymer, surface chemistry and filler-polymer interactions, are particularly important because they affect interfacial adhesion [10]. In order to provide improve tensile strength, adhesion between the phases is critical for effective stress transfer. Stiffness(e.g., Young's modulus) is readily improved with filler addition because fillers are typically stiffer than polymer matrices and modulus is a property of low deformations [11]. On the other hand, softer elastomers decrease the stiffness of the final material, but usually increase strain at break and toughness [12-15]. Hard particles typically increase strength more effectively than soft particles, when there is sufficient adhesion. Adhesion is achieved by intimate contact, wetting of polymer with the filler surface, and engineering compatible surface energy. The effects of interfacial interactions can be understood by considering the work of adhesion, the theoretical work required to separate two different surfaces, and the work of cohesion, the theoretical work required to separate identical surfaces (Figure 1.2). The work of adhesion and cohesion are given by Equations 1.1 and 1.2 respectively.

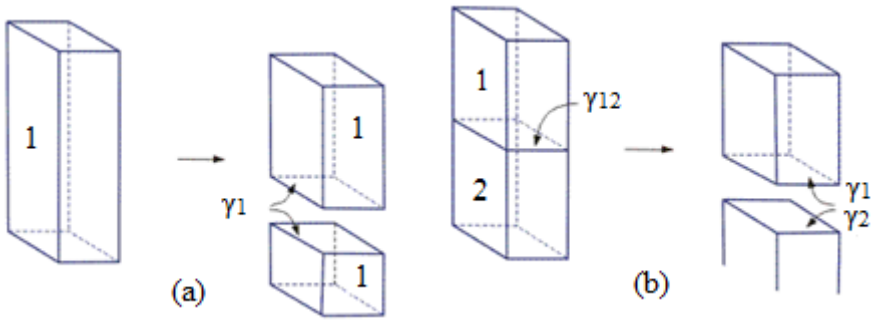

Figure 1.2: Schematic of theoretical reversible works of cohesion (a) and adhesion (b) [16].

$$W_A = W_{12} = \gamma_1 + \gamma_2 - \gamma_{12} \quad (1.1)$$

$$W_C = W_{11} = 2\gamma_1 \quad (1.2)$$

In a composite, subscripts 1 and 2 would correspond with the polymer and the filler, respectively. Equation 1.1 suggests that it is important to maximize the surface free energies ($\gamma_1 and\ \gamma_2$) and minimize the interfacial energy (γ_{12}) for optimal adhesion. Complicating this optimization is the fact that changes in chemistry that would alter γ_1 and γ_2, will invariably alter γ_{12}. Previous experimental work has shown that equalizing the two neat surface free energies corresponds to minimizing the interfacial energy [17-19]. In addition to optimizing adhesion energy per unit area between the polymer and filler in the finished composite, the wetting of polymer solution or melt on the filler during processing is also critical to producing high interfacial area. The spreading coefficient (the negative of free energy of wetting) can also be considered (Equation 13).

$$S = -\Delta G_{wet} = \gamma_2 - \gamma_1 - \gamma_{12} = W_{12} - W_{11} \quad (1.3)$$

Equation 1.3 suggests that it is important to maximize the surface free energy of the solid while minimizing the surface free energy of the liquid and the interfacial free energy. Taking Equations 1.2 and 1.3 together, one can conclude that increasing only the solid component surface energy decreases liquid contact angles allowing for more intimate wetting, while maximizing both liquid and solid component energies allows for enhanced adhesion. Thus there is a competition between maximum adhesion and maximum spreading. If the surface chemistry and energy of filler and polymer are understood, then the thermodynamic criteria above can be used as a guideline to optimize filler performance through selection and modification of polymer and filler.

Works of adhesion and spreading are attributable to intermolecular and intramolecular forces. Van der waals forces are present in any system. Hydrogen bonding is possible in some

systems and covalent bonding can even be achieved by utilizing surface modifiers that crosslink filler into the polymer matrix. This leads to another aspect of adhesion, chemical structure of filler and polymer. The functional moieties on both components determine the possible interactions and the strength of interactions. For example, if one component has hydrogen bond donor moieties and the other component has hydrogen bond acceptor moieties, then hydrogen bonding will be possible in this system, affecting adhesion. Increasing strength of attractive interactions between matrix and filler results in enhanced adhesion and wetting through minimization of γ_{12}.

The degree of adhesion and affects the ability of a filler to enhance mechanical and thermal properties of polymers. Adhesion strength at the polymer-filler interface determines load transfer between the phases, affecting both composite tensile strength (maximum stress before necking) and toughness (ability to absorb energy and plastically deform without fracture). In the case of poor adhesion, stress transfer at the interface is ineffective. Thus the filler cannot carry any load and discontinuities cause strength decreases. High adhesion leads to effective stress transfer at the interface and thus material reinforcement. Improvements in toughness have been attributed to increased crack growth resistance before material deformation and stress redistribution [3]. With poor adhesion crack pinning is ineffective and the load bearing area of the material is reduced. This decreases the energy required to fracture. Particle size and particle loading are also important variables when considering such mechanical properties. Smaller particles have increased surface area, interacting with a greater volume of polymer matrix and thus increasing reinforcement [3, 20, 21]. Depending on the filler-polymer system, there exists a critical filler loading at which any gained improvements begin to degrade due to increased stress concentration attributed to agglomerates formed by filler at higher loading.

Often the surfaces of fillers are modified to enhance filler-polymer interactions [22-25]. Surface modifications are most frequently used to improve reinforcement and interface adhesion. However, they also can improve filler processing, melt viscosities, filler dispersion, allow for higher filler loadings, and improve composite properties. Surface reactive chemicals can have single functionality or dual functionality. Single functionality reagents react only with the filler surface and improve dispersion and wetting by the polymer matrix. For example, stearic acid is an example of such a reagent in which the acid groups can react with surface groups like carbonates on $CaCO_3$ resulting in an outer surface of hydrocarbons. Dual functionality reagents are able to interact with the filler surface as well as crosslink with the polymer matrix creating a continuous chemical bond. Organosilanes have dual functionality and are the most popular materials for filler modification. Silane compounds improve composite mechanical properties through strong chemical bonds with the filler and the matrix. These compounds have the formula R_nSiX_{4-n} where R is the group for polymer binding (i.e. methacrylate group), X is a group that combines with the filler (i.e. methoxy groups), and Si is the silicon atom. The X group combines with the filler surface through hydrolysis or a condensation reaction while the R group reacts into the matrix during free radical polymerization [10]. The specific filler surface chemistry determines the appropriate surface modification. Figure 1.3 shows the simplified mechanism for silane coupling.

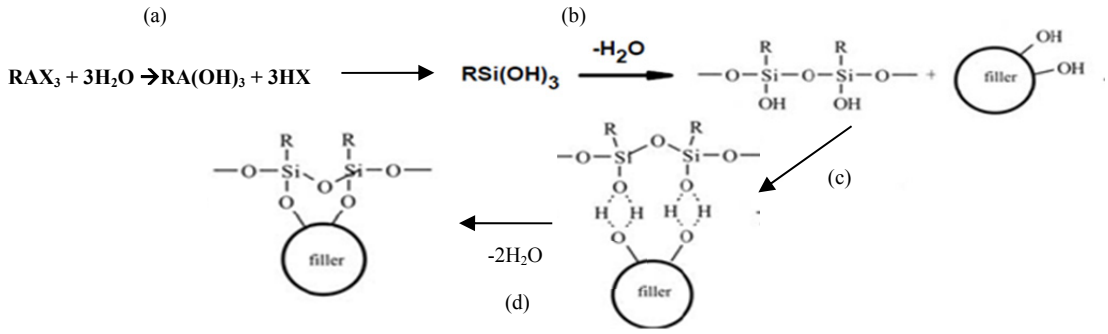

Figure 1.3: (a) Organosilane is hydrolyzed. (b) Hydrolyzedsilane undergoes condensation reaction. (c) Hydrogen bonding occurs. (d) Chemical bonds are formed and water is released [26].

1.2 Organic Fillers

Many studies have illustrated the successful use of non-biological materials ranging from inorganic particles to carbon nanotubes as reinforcing fillers in fabricating composite materials. Pairing non-biodegradable oil-based polymers with these non-renewable resources often makes reuse and recycling quite difficult. With the increase in concerns over environmental issues and the desire to create more versatile polymer-based materials, there is increasing interest in polymers filled with natural organic fillers. These new alternatives, or "green composites", are able to replace traditional polymer composites and lower environmental impact. The first attempts in this area involved incorporation of natural-organic fillers in recyclable polymers, such as polyolefins, reducing the use of non-biodegradable polymer and non-renewable mineral resources. Additionally, these natural fillers are derived from relatively abundant plant sources, making them cheap. They are also less abrasive to processing machinery than mineral resources, less dangerous to production employees via inhalation, are easily incinerated, often lead to composites with low specific weight versus mineral fillers, and allow for unique material properties.

Wood flour and fiber are some of the most widely used natural organic-fillers. Other examples include cellulose, cotton, flax, kenaf, and starch to name a few. Polymers often used to

form green composites include polyethylene, polypropylene, and polystyrene to name a few. Materials filled with natural fillers often suffer from poor adhesion between the fillers (hydrophilic) and the polymer matrix (generally hydrophobic), low impact strength, and low thermal decomposition over 200 °C. Thus, research is often focused on utilizing chemical modifications and adhesion promoters to improve the interfacial adhesion and dispersion of natural organic fillers in polymer matrices. Further, processing of green composites (extrusion, injection molding, compression molding, etc.) is challenging due to the hydrophilic and often hygroscopic nature of natural fillers, as well as their poor thermal resistance, resulting in processing temperatures that are kept below approximately 200 °C. The hydrophilic and hygroscopic characteristics of natural fillers influence both filler dispersion and interfacial adhesion. The presence of humidity can lead to the formation of water vapor during processing, which in turn can cause void formation and poor mechanical properties.

Finally, entirely "green composites" can be fabricated by incorporating natural fillers with biodegradable polymer matrices such as polyesters, polysaccharides, natural rubbers, and some polyamides, to name a few. Fully biodegradable composites have a few limitations as well. First, biodegradable polymers are more expensive than their traditional counterparts. Biodegradable polymers have recently become less expensive, however, their use most increase much more in order to drive their cost down further. Next, as previously mentioned, filler dispersion and interfacial adhesion still present a challenge in many cases. Depending on the biodegradable polymer, dispersion and adhesion may be more satisfactory because of the presence of polar groups in the polymer backbone. However, it is still sometimes necessary to improve adhesion with chemical treatments, which is neither convenient nor cheap from an industrial perspective.

1.3 Pollen as a Filler

Pollen is a natural particle which has the potential to be an effective biorenewable reinforcing filler due to its unique surface architectures, high strength, chemical stability, and low density. These properties may enhance stress transfer between polymer and pollen filler, increase the energy absorption of pollen filler while under stress, enhance chemical resistance, and effectively maintain or lower material density. Pollens from sources such as ragweed plants are ubiquitous natural materials that are based on sustainable, non-food resources. Pollen is a remarkable example of evolutionary-optimized microscale particle with structures and/or chemistries tailored for effective adhesion to a variety of surfaces and protection of genetic material under different dynamic and environmental conditions. The pollen shell is perhaps the most chemically resistant naturally occurring material. Some pollens are anemophilus, or dispersed by wind, and thus are very light-weight.

Pollen's chemical inertness, mechanical strength, thermal resistance, and unique architectures has led to a growing interest in pollens practical use and as a model particle. Some unique studies have explored pollen microcapsules for drug delivery [27, 28]. Food supplements and drugs can be loaded into empty pollen shells, through a variety of means, for targeted delivery. Pollen shells have also been explored as micro-reactors for in situ preparation of nanoparticles [29]. Much work has been done using pollen as a biotemplate for fabrication of microparticles and as a carrier particle of nanoparticles [30-33]. Pollen can be coated with various substances such as silicon dioxide and iron oxides, through methods such as sol-gel processes, and then subsequently burned off leaving behind hollow microparticles with well controlled surface structures. Finally, the Meredith group had been the leader in researching pollen as a model particle for understanding and mimicking biostructural based adhesion [34-

36]. This is primarily achieved with colloidal probe atomic force microscopy, in which pollen grains are attached to tipless cantilevers and contacted to different surfaces in order to measure adhesion forces.

1.3.1 Pollen Chemistry

Pollen grains are the carrier of the male gametes for plant reproduction. The pollen wall has three main domains: the exine, intine, and pollen coat [37, 38]. The outermost shell, known as the exine, is composed of sporopollenin, a highly crosslinked biopolymer network. Sporopollenin is insoluble to most solvents and extremely resistant to non-oxidative physical, biological, and chemical degradation. The outer shell is also very mechanically tough [39]. Chemical analysis of sporopollenin is limited due to its insolubility in commons acids and solvents, making its exact chemical composition difficult elucidate [40]. However, nonoxidative, extraction-hydrolysis methods have been used to isolate pollen exines of different plant classes for analysis with solid state techniques. ^{13}C NMR spectra obtained from exines indicated that sporopollenin from different pollen species are distinct substances [41]. Sporopollenin can therefore be categorized as a class of biopolymers rather than a single, homogeneous macromolecule. FTIR spectra of acetolyzed sporopollenin of *Magnolia grandiflora* Linn. and *Hibiscus syracus* Linn. suggest that the main structure of sporopollenin is a simple aliphatic polymer with aromatic and conjugated groups in the side chains [42]. ^{1}H-^{1}H-COSY NMR spectra of silyl and acetyl derivatives of *Typhaangustifolia* L. have revealed that phenols are integral compounds of the sporopollenin skeleton through the identification of 4-hydroxy-cinnamic acid from [43-45]. Exposing sporopollenin from *Typhaangustifolia* L. to a series of 36 subsequent acidic methanolysis procedures indicated that the sporopollenin possesses alkyl chains containing at least ten CH_2 groups and the polymers are linked by ether bridges [46].

Pyrolysis GC-MS revealed that p-coumaric acid and ferulic acid were both present in sporopollenin of *Betulapendula* and *Pinussylvestris* [47]. Solid state ^{13}C NMR and RuO_4 chemical degradation, combined with pyrolysis results, have led to a tentative structure for sporopollenin, shown in Figure 1.4, in which long-chain (C_{24}-C_{28}) highly aliphatic units form the backbone of sporopollenin with cinnamic acids as cross-linking units, ether cross-linkers, and ester functions [48].

Further structural elucidation has been achieved through derivatisations of sporopollenin in order to identify functional groups. Bromination of sporopollenin highlighted the high degree of carbon-carbon double bond unsaturation in its structure [49, 50]. Gravimetric results were used to estimate the loading of unsaturations as 2.5 mmol/g [51, 52]. Hydroxyl groups have been substituted with chlorine using chemicals such as phosphorus pentachloride and 9-fluorenylmethyl carbamate (Fmoc) [51, 52]. The amount of hydroxyl groups has also been quantified in various studies to be between 1.15 to 9.8 mmol/g with techniques such as radiochemical analysis to determine the release of acetyl attachments following acetylation of sporopollenin and UV analysis of released Fmoc-piperidine [50, 51, 53, 54]. Carbonyls on sporopollenin were reacted with 2,4-dinitrophenylhydrazine forming corresponding hydrazones which were easily detectable by IR due to the introduction of nitrogen and the number of carbonyl sites were estimated to be .6 mmol/g with elemental combustion [51, 52]. Finally, the amount of acidic functions (i.e. carboxyls, lactones, phenols) was estimated to be 1.3 mmol/g with back titrations against dilute sodium hydroxide [51].

Beneath the exine layer is the intine, which is rich in cellulose and hemicelluloses, similar to the primary walls of common plant cells [55]. While the intine and exine are solids, some species of pollen have liquid lipoidal surface substances, called the pollen coat or pollenkitt.

Pollenkitt is a viscous adhesive material that is primarily located in the cavities of the exine as well as the surface of the exine. Amongst its functions, pollenkitt has adhesive properties facilitating pollen transmission with insects and other animals and offers protection against water loss, fungi or bacteria, and UV radiation. Despite its importance for pollen dispersal and subsequent germination, relatively little is known about the chemical composition of the pollenkitt [38]. Analysis of the volatiles from the pollenkitt of *Rosa rugosa* revealed that the coating extract comprised half of the volatiles found in pollen (aromatics, C_{11}-C_{16}aliphatics, and terpenoids) and proportionately more C_{16} acetate [56]. Pollenkitt volatiles of different species of pollen have also been found to be distinct [56]. Other components found in pollenkitt include non-glyceride neutral lipids (hydrocarbons, fatty acid methyl esters, sterol esters, aldehydes, and ketones), very few polar lipids, and pigments (yellow carotenoids and flavenoids) [57]. Pollenkitt is present in pollens of the entomophilus taxa (dispersed by adherence to insects), secondary anemophilous members which belong to entomophilus families, and variably in zoophilus (dispersed by adhering to vertebrates) plants [58, 59]. Finally, within the interior of the pollen grain is a large vegetative cell consisting of a nucleus that lies within the cytoplasm which is densely packed with storage oil bodies, endoplasmic reticulum, vesicles around the periphery cytoplasm, and two sperm cells [38, 60]. These intracellular pollen lipids and membranes are composed of triacylglycerols and membrane-associated phospholipids [38].

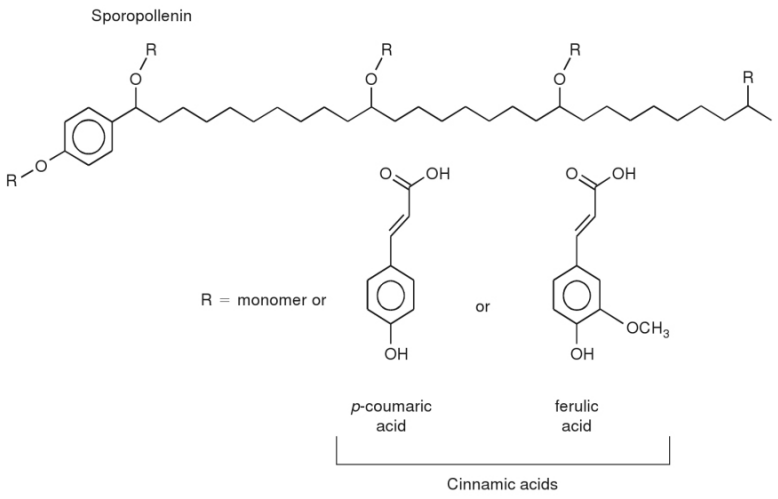

Figure 1.4: Monomer and macromer precursors of sporopollenin [61].

1.3.2 Pollen Shape

Pollen is a micrsoscale particle that can range from 5-200 μm, depending on the plant species. Additionally, different species display unique micro and nano scaled surface structures such as spines, grooves, pores, etc, as shown in Figure 1.5. In nature, pollen structure plays a vital role to its successful dispersal and transport. The exine wall in anemophilous pollen species is often modified to enhance buoyancy. The exine wall in entomophilous and zoophilous pollen species often displays surface rods, spines, and other features to enhance interactions between animal and insect vectors [60, 62, 63]. As a result, the structure and sculpture of the exine is what gives pollen its distinct microscopic and submicroscopic morphology [62]. Figure 1.7 displays the known basic architectures of the outer sculptured layer of the exine and sexine, which are defined by size, shape, and arrangement further explained in Table 1.1 [64].

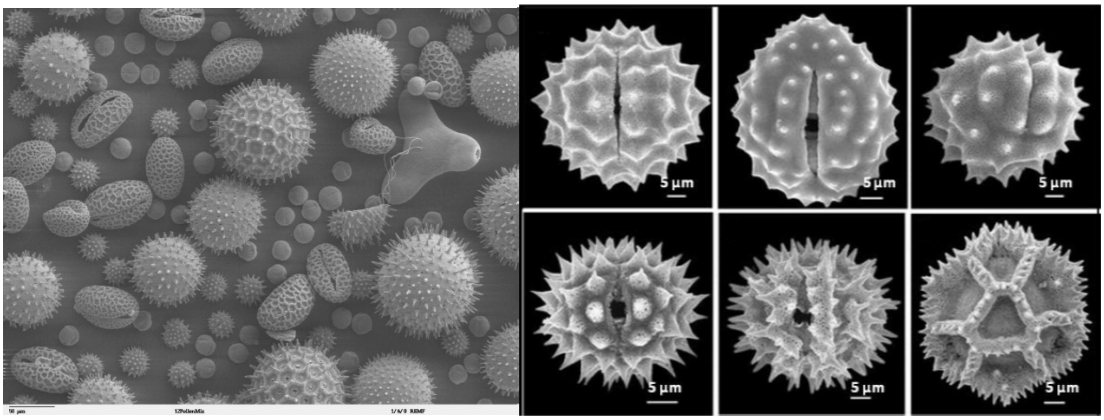

Figure 1.5: Representative scanning electron micrographs of the structural diversity of (a) diatom, (b) spore, and (c) pollen microparticles. Images were taken from references. Pollen from a variety of common plants (left, 50 µm scale bar) [65, 66].

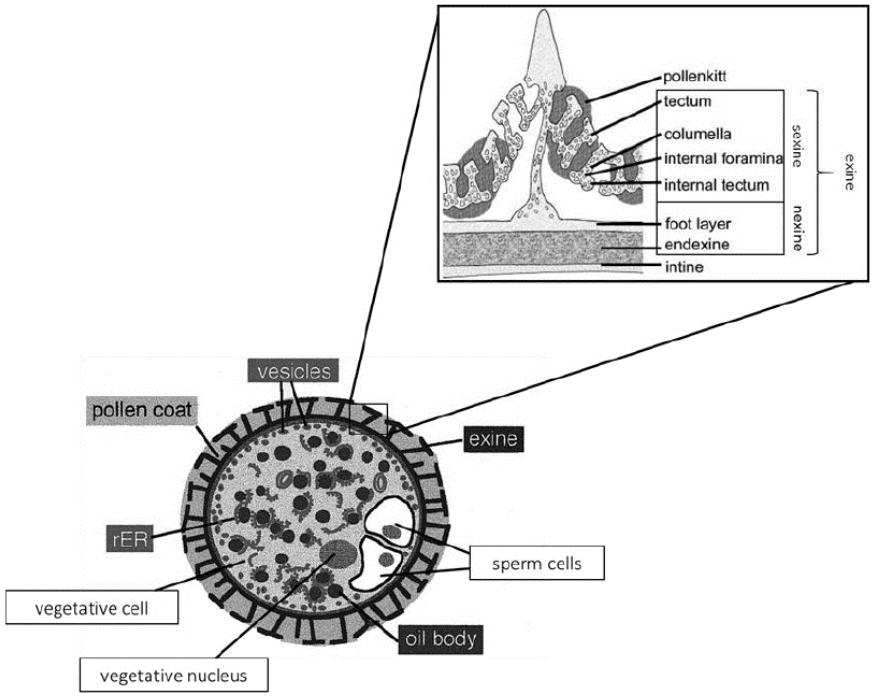

Figure 1.6: Ultrastructure of a typical mature pollen grain. Extracellular features include the inner intine, outer exine, and pollen coat (pollenkitt) filling the cavities of the exine sculpture. The exine is further divided into the sexine (tectum, columella, formina) and nexine (foot layer and endexine). Intracellular features include oil bodies, rough endoplasmic reticulum (rER), numerous vesicles, a vegetative nucleus, a vegetative cell, and sperm cells. Representations were taken from references [38, 67].

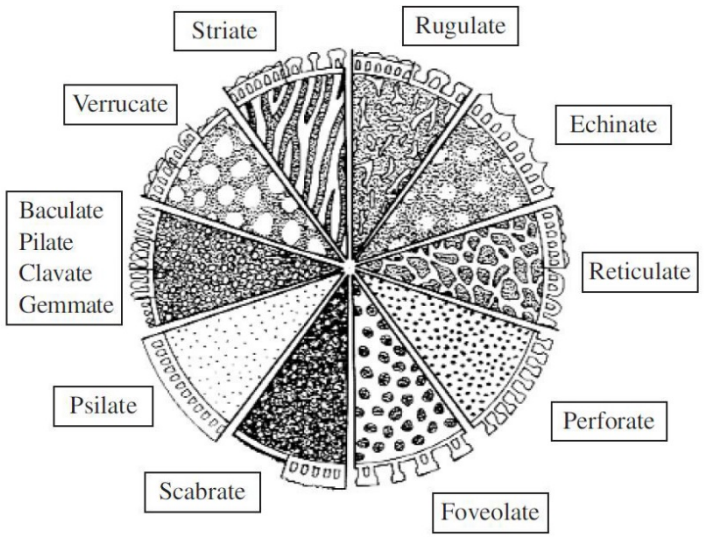

Figure 1.7: Surface sculpturing elements of pollen taken from reference [64]. Raised areas are shown light and lower areas are shown dark. Cross-sections of the exine are located around the perimeter.

Table 1.1: Characteristic surface structures of pollen grains [62].

Architecture	**Characteristic**
Psilate	Smooth surface
Foveolate	Pitted surface
Fossulate	Grooved surface
Perforate	Numerous openings in the tectum
Scabrate	Sculptured elements < 1 μm in any dimension
Verrucate	Sculptured elements > 1 μm with near equal height and width
Gemmate	Sculptured elements with diameters equal to, or greater than, the height with a constricted base of > 1 μm
Baculate	Rod-like elements > 1 μm of greater height than width
Clavate	Elements > 1 μm long of greater height than width with a constricted base or club-shaped tip
Echinate	Pointed spines 1-3 μm long
Rugulate	Horizontally elongated elements in an irregular pattern
Striate	Horizontally elongated elements in an irregular pattern
Reticulate	Horizontally elongated elements forming a net-like pattern

Pollens, with their wide variety of architectures, offer unique shapes relative to other fillers available which are typically confined to simple geometries. Additionally, pollens display well defined shapes that are more uniform in shape and size than conventional fillers. Its uniformity eliminates the need for processing such as crushing, grinding and milling and makes it interesting as a model particle for investigating particle shape effects in predictive models for composite properties. Additionally, distinguishing between primary particles, agglomerates, aggregates, and even fragments is simple with pollen. In applications that call for uniform stress distribution, monodisperse uniformly shaped particles are ideal, making pollen an interesting candidate.

The shapes and sizes of pollen grains may impact its performance as a filler. The unique shape of pollen raises many questions when considering it as a filler, such as how might surface features of some pollen affect wetting and adhesion of the polymer matrix on the pollen surface? Since there are few examples of inorganic or conventional filler particulates with these types of structures, these questions remain relatively unexplored in composite science. Thus, investigating pollen as a filler may shed light upon how fillers with well defined, complex architectures affect composite properties. Pollen surface structures increase overall interfacial area and are likely to have an affect on the structure of the interphase of the polymer matrix surrounding the filler particles [19, 20, 68]. The interphase consists of polymer adsorbed to filler and has been shown to have an important affect on composite properties, including relaxation behavior, glass transition temperature, and fracture behavior (brittle or ductile). Properties of the interphase differ from bulk properties of the matrix and its thickness is affected by the degree of interaction between phases. Pollen surface structures may enhance stress transfer between the pollen and polymer by increasing interactions with surrounding polymer chains, due to increase

interfacial surface area. This may subsequently increase the energy absorption of pollen filler while the material is under stress (i.e. toughening). Additionally, surface features, such as spines, may act as stress concentrators in the polymer matrix. This stress concentration may serve as initiation points for crazing upon deformation which would toughen the material.

Pollen surface structures are likely to have an effect on the wetting and spreading of the polymer matrix around pollen. It has been observed that microscopically rough or spiked surface can dramatically worsen or improve wettability [69]. Wetting regimes on rough surfaces have been separated into three states: the Cassie state, the Wenzel state, and an intermediate state [70]. The Cassie state is heterogeneous wetting where a droplet does not make full contact with the entire surface and the Wenzel state is homogeneous wetting where the liquid fills the grooves of the surface. The transition between these two states is affected by interactions between fluid and substrate, aspect ratio of structures creating roughness, and spacing to diameter ratio of structures. Thus, wetting of polymer surrounding pollen grains is likely to be affected pollen surface roughness and surface features such as spines. Figure 1.8 shows the two extremes of Cassie and Wenzel states and how they may apply to pollen grains incorporated in a polymer. The exceptional adhesion of the gecko footpad with high aspect ratio structures and superhydrophobicity of the lotus leaf with low aspect ratio structures, have inspired many studies on the tuning of wetting and adhesion [71, 72]. Such studies have shown that patterned surfaces with higher space to diameter ratios and lower aspect ratios are more likely to exist in the Wenzel state. Considering only the geometry of short ragweed pollen, low aspect ratio (spike height/spike base diameter ≅ .73) and low space to diameter ratio (~.51), one might expect it to fall in the Cassie state due to its low space to diameter ratio. This may decrease wetting, however its low aspect ratio as well as other factors may enhance filling of inter-spine spaces. Perhaps,

pollen species with high spike density may display decreased wetting due to a decreased space to diameter ratio. Interestingly, due to inspirations from nature such as the gecko, researchers have aimed to tune adhesion with high aspect ratio patterning [73-75], highlighting the synergistic effects between enhanced adhesion and intimate wetting.

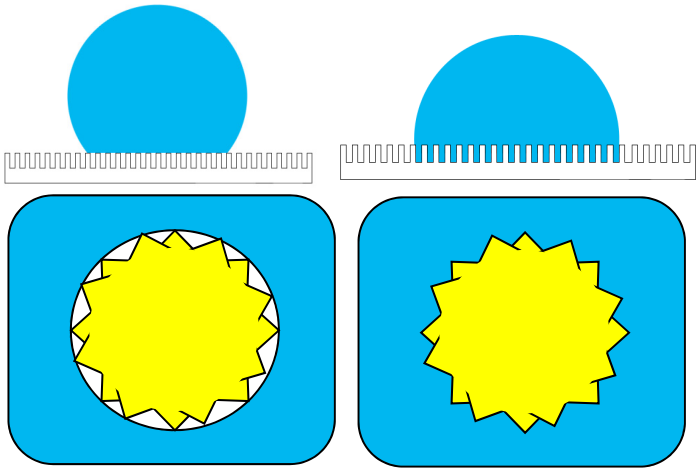

Figure 1.8: Cassie state (left column) and Wenzel state (right column) (top row from [76]).

Polymer chains may also be able to diffuse or flow into the pores of the pollen exine, increasing mechanical stress transfer between polymer and filler. For example, short ragweed pollens display pores between 30 to 100 nm in diameter and many pollens possess large openings, or apertures. Polymer may also become entrapped in pollen grains, possibly leading to a phenomenon known as "occluded polymer", which is widely observed with carbon blacks [77, 78]. This becomes more likely and significant in cleaned pollen with intracellular materials removed. Finally, pollen is very lightweight relative to most fillers, with a density less than or comparable to the density of many polymers. The fact that pollen can be made hollow through relatively simple cleaning steps (acid and base treatments) would render them even lighter and less dense. Sporopollenin has a density slightly larger than 1 g/cm^3. If the surface of hollow pollen grains were coated with some substance in order to entrap air within the pollen grain, even

further weight reduction would be achievable. Thus, potential cost savings with pollen filler may be very feasible. There is tremendous interest in lighter weight composite materials, particularly in transportation applications.

1.3.3 Pollen Sustainability

Pollen is a natural particle produced by plants in large numbers. Pollens from sources such as ragweed plants are ubiquitous natural materials that are based on sustainable, non-food resources. A single ragweed (*Ambrosia artemisiifolia*) plant can produce 8 billion ragweed pollen grains in 5 h [79]. It has been conservatively estimated that 1 million tons ragweed pollen alone are produced annually in the United States [80]. Considering the estimated 352,000 species of flowering, pollen bearing plants, the total yearly production of pollen worldwide may be several orders of magnitude greater. Additionally, pollen production is expected to significantly increase based on predicted future climate conditions. Five CO_2 emission scenarios for the period 1850-2100 project a minimum atmospheric CO_2 level of ~440 ppm, with less conservative estimates approaching ~600 ppm, to be achieved by the year 2100 [81]. Subjecting plants to future CO_2 conditions, a 62% increase in CO_2 levels from the year 2000 to future CO_2 levels results in a 90% increase in pollen production [82]. The pollen shell is perhaps the most chemically resistant naturally occurring material. Intact pollen shells have even been in in fossils that are 500 million years old [83, 84].Pollen exists as individual grains, eliminating the need for mechanical processing such as grinding and milling. The chemicals required to clean and isolate the pollen shell are used in the filler industry as well as other industries and organosilane functionalization is widely practiced in the filler industry as well.

Despite this abundant and potentially sustainable source, there is no current infrastructure for mass pollen collection. Currently a number of companies (e.g. Greer Laboratories, Inc.,

Polysciences, Inc., etc.) offer a wide range of pollen species in lab-scale quantities. Commercial harvesting on this scale is supplied by certified pollen farmers in the U.S. and Europe [85]. One such 400-acre farm collects roughly 30 species of pollen. During ragweed season, which runs from mid-August to October, this farm harvests an average of more than four pounds of ragweed pollen per day, or about 300 pounds total on 10 acres of land [86]. Greer Laboratories, an allergen manufacturer, has demonstrated collection and processing of pollen source materials, such as short ragweed pollen, on the magnitude of tons. Collected pollen is sold to companies at an average cost of 50 cents per gram of pollen and as low as five cents per gram for common pollen such as ragweed (~$23/lb ragweed). Pollen collection and price present the two of the greater challenges to implementing pollen as a filler. In order to replace 10% of the annual silica market, ~11000 tonnes of pollen would be required. However, due to its low density, this is nearly half the weight of the same amount of silica on a volume basis. Based on the 300 pound collection of ragweed on 10 acres, this would require ~776,466 acres of land. Silica is a mass produced filler that ranges from $.90 – 2.50/lb. Although it is unclear how pollen collection on a larger scale may impact the environment, the fact that these pollen farms currently exist demonstrate the potential to sustainably harvest pollen to meet consumer demands. Therefore, opportunities for scaling up and decreasing material cost may be investigated if a sufficient technological motivation were demonstrated. Thus, despite the lack of current infrastructure, the substantial amount of available material and the fact that collection is currently achieved on a smaller scale make such an infrastructure a possibility.

1.3.4 Pollen-Polymer Composites

The Meredith group was the first to demonstrate the incorporation of pollen in polymer matrices [87]. In this study, short ragweed pollen (*Ambrosia artemisiifolia*) is dispersed in polymer solution and then solvent cast to form composite films. The polymers used were poly (ε-caprolactone) (PCL) and polystyrene (PS). Scanning electron microscope (SEM) images revealed better wetting of pollen in PS matrices than in PCL. Sporopollenin contains ester groups and aromatic moieties [40, 88, 89], so the enhanced interaction with PS (aromatic) relative to PCL (esters) was unanticipated. The authors suggested that amorphous nature of PS may facilitate polymer chain interactions with spiny pollen grains, while the ordered crystalline regions in PCL may have hindered interactions. In agreement with interfacial observations, the mechanical properties of PCL degraded with pollen loading, while there was a synergistic effect in elongation in the PS composites. This effect was attributed to a trade off between addition of tough filler at low loadings and inefficient stress transfer at higher loadings. This was also in agreement with a slight glass transition temperature increase indicative of a weak but favorable interaction. This study further shows that pollen-polymer composites are attractive because they could form the basis for a new class of light-weight, high-strength materials with a sustainable plant-based source, displacing petroleum derived materials. However, many filler related properties of pollen must be characterized in order to form a more complete understanding, predict what polymers pollen will be compatible with, and enhance the effectiveness of pollen as a filler. A clearer understanding of these properties will also be useful in choosing proper surface modifications for pollen to further improve pollen-polymer interactions.

These properties make pollen an attractive option as a natural filler for polymers.

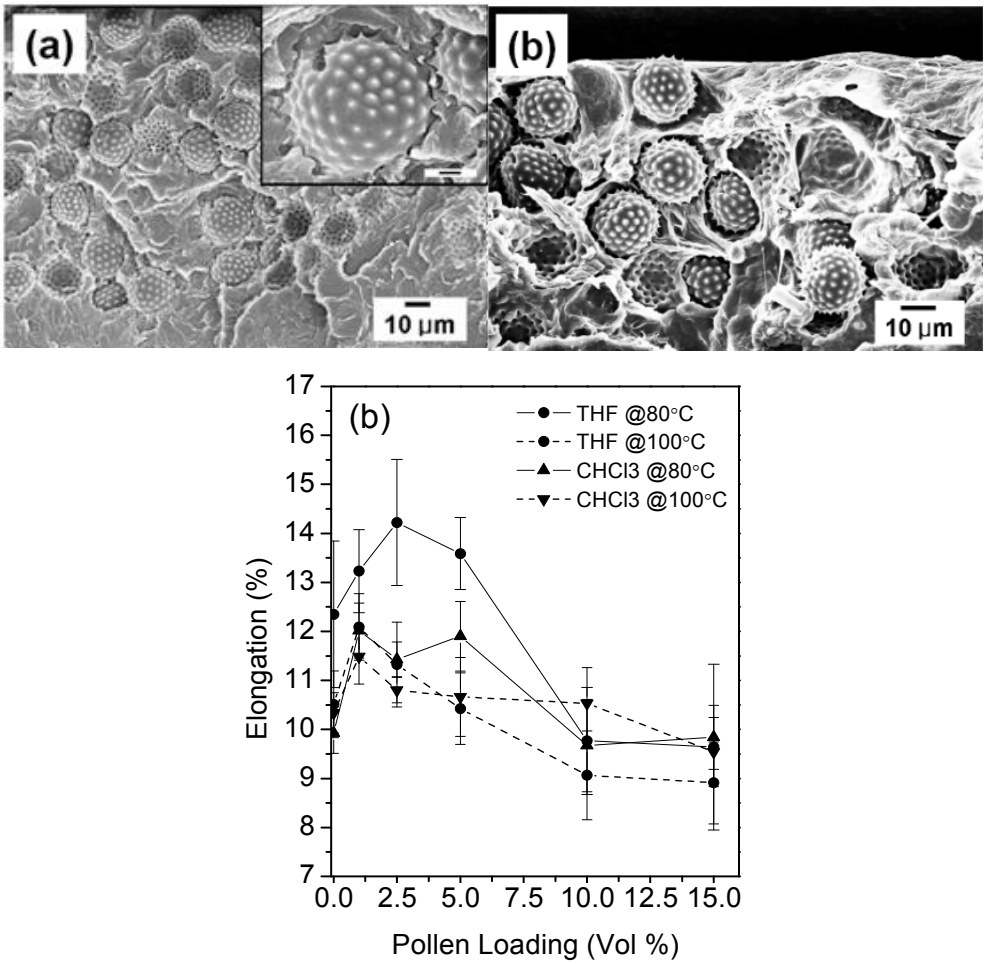

Figure 1.9: Films of ragweed pollen in (a) polycaprolactone, (b) polystyrene, and (c) representative elongation at break curves for the solution cast samples [90].

1.4 Thesis Overview

This research aims to characterize pollen interfacial properties and utilize pollen as an effective reinforcing filler in polymer materials. These particles will allow us to create high strength, light-weight polymer composites with sustainable filler. The main objectives are as follows:

I. Characterize important interfacial properties of pollen.

   a) Optimize an acid-base hydrolysis treatment of as received, defatted pollen.

   b) Investigate the effects of the acid-base hydrolysis treatment on pollen interfacial properties.

c) Develop and use inverse liquid chromatography (ILC) to characterize pollen chemical and physical interactions of pollen with potential matrix chemistries.

II. Engineer a more effective pollen-polymer composite.

a) Explore the effects of the acid-base hydrolysis treatment and organosilane functionalization of pollen in polyvinyl acetate (PVAc) matrices.

b) Explore the effects of the acid-base hydrolysis treatment of pollen in waterborne epoxy matrices.

c) Determine the effects of size of pollen microstructures on wetting, adhesion, and composite properties.

Chapter 2 focuses on understanding pollen interfacial properties of pollen particles using Fourier transform infrared spectroscopy (FTIR), the BET method, and inverse liquid chromatography (ILC). Chapter 3 describes the use of ragweed pollen in PVAc matrices. The effectiveness of pollen as a reinforcing filler is determined as a function of pollen loading and surface treatments/chemical modifications. Scanning electron microscopy (SEM) was used to determine interfacial morphology, a high throughput mechanical characterization device (HTMECH) was used to determine mechanical properties, and differential scanning calorimetry (DSC) was used to determine glass transition behavior. Chapter 4 details the use of ragweed pollen in waterborne epoxy matrices. The effectiveness of pollen as a reinforcing filler is determined as a function of pollen loading and surface treatment and the same techniques utilized in Chapter 2 are used again. Chapter 5 focuses on investigating the effect of surface structure size on wetting, adhesion and composite properties. This was achieved by using three pollen species (Ragweed, Kentucky Blue June, and Dog Fennel) and utilizing the same characterization techniques used in Chapters 3 and 4. Chapter 6 concludes with a summary of the important findings and provides future recommendations based on this work.

1.5 References

1. Eyerer, P. and V. Gettwert, *Properties of Plastics in Structural Components*, in *Polymers - Opportunities and Risks I*, P. Eyerer, Editor. 2010, Springer Berlin Heidelberg. p. 47-165.
2. Wypych, G., *Handbook of Fillers (3rd Edition)*. ChemTec Publishing. p. 1-12.
3. Fu, S.-Y., et al., *Effects of particle size, particle/matrix interface adhesion and particle loading on mechanical properties of particulate–polymer composites.* Composites Part B: Engineering, 2008. **39**(6): p. 933-961.
4. Mitsuishi, K., S. Kodama, and H. Kawasaki, *MECHANICAL-PROPERTIES OF POLYETHYLENE ETHYLENE VINYL-ACETATE FILLED WITH CALCIUM-CARBONATE.* Polymer Composites, 1988. **9**(2): p. 112-118.
5. Bigg, D.M., *MECHANICAL-PROPERTIES OF PARTICULATE FILLED POLYMERS.* Polymer Composites, 1987. **8**(2): p. 115-122.
6. Maiti, S.N. and B.H. Lopez, *TENSILE PROPERTIES OF POLYPROPYLENE KAOLIN COMPOSITES.* Journal of Applied Polymer Science, 1992. **44**(2): p. 353-360.
7. Rothon, R.N., *Particulate-Filled Polymer Composites (2nd Edition)*. Smithers Rapra Technology. p. 53-100.
8. He, J., et al., *Preparation and characterization of monodisperse porous silica microspheres with controllable morphology and structure.* Journal of Polymer Science Part A: Polymer Chemistry, 2012: p. n/a-n/a.
9. Rothon, R.N., *Particulate-Filled Polymer Composites (2nd Edition)*. Smithers Rapra Technology. p. 5-51.
10. Metın, D., et al., *The effect of interfacial interactions on the mechanical properties of polypropylene/natural zeolite composites.* Composites Part A: Applied Science and Manufacturing, 2004. **35**(1): p. 23-32.
11. Zihlif, A.M., et al., *Tensile properties and fracture behaviour of polycarbonate/PAN-based carbon fiber composite.* International Journal of Polymeric Materials, 1995. **29**(3-4): p. 211-220.
12. Pukanszky, B., F.H.J. Maurer, and J.W. Boode, *Impact testing of polypropylene blends and composites.* Polymer Engineering and Science, 1995. **35**(24): p. 1962-1971.
13. Sombatsompop, N. and G.L.A. Sims, *Further studies on the use of pulverised flexible polyurethane foam particles as fillers in natural rubber compounds.* Cellular Polymers, 1996. **15**(5): p. 317-334.
14. Sims, G.L.A. and N. Sombatsompop, *Pulverised flexible polyurethane foam particles as a filler in natural rubber vulcanisates.* Cellular Polymers, 1996. **15**(2): p. 90-104.
15. Bhattacharya, S.K., A.K. Bhowmick, and R.K. Singh, *CRACK-GROWTH RESISTANCE OF FLUOROELASTOMER VULCANIZATES FILLED WITH PARTICULATE AND FIBER FILLER.* Journal of Materials Science, 1995. **30**(1): p. 243-247.
16. Bailey, A.I. *Interfaces*. [Online] 2010 5/1/2012; 7 September 2010:[Available from: http://www.thermopedia.com/content/27/?tid=104&sn=1309.
17. Mittal, K.L. and A.C. Society, *Surface chemical criteria for maximum adhesion and their verification against the experimentally measured adhesive strength values*. Adhesion Science and Technology, ed. L.-H. Lee. 1975: Plenum Press.
18. Kovacevic, V., et al., *Tensile properties of calcium carbonate-reinforced poly(vinyl acetate).* Journal of Adhesion Science and Technology, 1996. **10**(12): p. 1273-1285.

19. Lučić, S., V. Kovačević, and D. Hace, *Mechanical properties of adhesive thin films.* International Journal of Adhesion and Adhesives, 1998. **18**(2): p. 115-123.
20. Kovaevi, V., S. Lui, and M. Leskovac, *Morphology and failure in nanocomposites. Part I: Structural and mechanical properties.* Journal of Adhesion Science and Technology, 2002. **16**(10): p. 1343-1365.
21. Ash, B.J., et al., *Mechanical properties of Al2O3/polymethylmethacrylate nanocomposites.* Polymer Composites, 2002. **23**(6): p. 1014-1025.
22. Jang, J., J. Bae, and D. Kang, *Role of silane coupling agents for performance improvement of poly(vinyl acetate)/tetraethyl orthosilicate hybrid composites prepared by a sol-gel process.* Polymer International, 2001. **50**(11): p. 1247-1251.
23. Suzuki, N. and H. Ishida, *A review on the structure and characterization techniques of silane/matrix interphases.* Macromolecular Symposia, 1996. **108**: p. 19-53.
24. Liauw, C.M., et al., *Filler surface treatments for particulate mineral/thermoplastic composites.* Progress in rubber and plastics technology, 1995. **11**(2): p. 137-153.
25. Domka, L., *MODIFICATION ESTIMATE OF KAOLIN, CHALK, AND PRECIPITATED CALCIUM-CARBONATE AS PLASTOMER AND ELASTOMER FILLERS.* Colloid and Polymer Science, 1994. **272**(10): p. 1190-1202.
26. Wypych, G., *Handbook of Fillers (3rd Edition)*. ChemTec Publishing. p. 285-323.
27. Diego-Taboada, A., et al., *Protein free microcapsules obtained from plant spores as a model for drug delivery: ibuprofen encapsulation, release and taste masking.* Journal of Materials Chemistry B, 2013. **1**(5): p. 707-713.
28. Barrier, S., *Physical and chemical properties of sporopollenin exine particles*, in *Chemistry*. 2008, The University of Hull.
29. Paunov, V.N., G. Mackenzie, and S.D. Stoyanov, *Sporopollenin micro-reactors for in-situ preparation, encapsulation and targeted delivery of active components.* Journal of Materials Chemistry, 2007. **17**(7): p. 609-612.
30. Feng, C. and L. Dong-Xu, *Morphology-controlled synthesis of SiO 2 hollow microspheres using pollen grain as a biotemplate.* Biomedical Materials, 2009. **4**(2): p. 025009.
31. Hall, S.R., H. Bolger, and S. Mann, *Morphosynthesis of complex inorganic forms using pollen grain templates.* Chemical Communications, 2003(22): p. 2784-2785.
32. Wang, Y., et al., *Replication of biological organizations through a supercritical fluid route.* Chemical Communications, 2005(23): p. 2948-2950.
33. Hall, S.R., et al., *Fabrication of Porous Titania (Brookite) Microparticles with Complex Morphology by Sol−Gel Replication of Pollen Grains.* Chemistry of Materials, 2006. **18**(3): p. 598-600.
34. Thio, B.J.R., J.H. Lee, and J.C. Meredith, *Characterization of Ragweed Pollen Adhesion to Polyamides and Polystyrene Using Atomic Force Microscopy.* Environmental Science & Technology, 2009. **43**(12): p. 4308-4313.
35. Goodwin, W.B., et al., *Conversion of Pollen Particles into Three-Dimensional Ceramic Replicas Tailored for Multimodal Adhesion.* Chemistry of Materials, 2013. **25**(22): p. 4529-4536.
36. Lin, H., I. Gomez, and J.C. Meredith, *Pollenkitt Wetting Mechanism Enables Species-Specific Tunable Pollen Adhesion.* Langmuir, 2013. **29**(9): p. 3012-3023.
37. Wiermann, R. and S. Gubatz, *POLLEN WALL AND SPOROPOLLENIN.* International Review of Cytology-a Survey of Cell Biology, 1992. **140**: p. 35-72.

38. Piffanelli, P., J.H.E. Ross, and D.J. Murphy, *Biogenesis and function of the lipidic structures of pollen grains.* Sexual Plant Reproduction, 1998. **11**(2): p. 65-80.
39. Liu, T. and Z. Zhang, *Mechanical properties of desiccated ragweed pollen grains determined by micromanipulation and theoretical modelling.* Biotechnology and Bioengineering, 2004. **85**(7): p. 770-775.
40. Dominguez, E., et al., *Pollen sporopollenin: degradation and structural elucidation.* Sexual Plant Reproduction, 1999. **12**(3): p. 171-178.
41. Guilford, W.J., et al., *High Resolution Solid State 13C NMR Spectroscopy of Sporopollenins from Different Plant Taxa.* Plant Physiology, 1988. **86**(1): p. 134-136.
42. Kawase, M. and M. Takahashi, *Chemical composition of sporopollenin in Magnolia grandiflora (Magnoliaceae) and Hibiscus syriacus (Malvaceae).* Grana, 1995. **34**(4): p. 242-245.
43. Ahlers, F., J. Lambert, and R. Wiermann, *Acetylation and silylation of piperidine solubilized sporopollenin from pollen of Typha angustifolia L.* ZEITSCHRIFT FUR NATURFORSCHUNG C, 2003. **58**(11/12): p. 807-811.
44. Ahlers, F., et al., *1H NMR analysis of sporopollenin from Typha Angustifolia.* Phytochemistry, 1999. **50**(6): p. 1095-1098.
45. Niester-Nyveld, C., et al., *Immunocytochemical localization of phenolic compounds in pollen walls using antibodies againstp-coumaric acid coupled to bovine serum albumin.* Protoplasma, 1997. **197**(3-4): p. 148-159.
46. Bubert, H., et al., *Continuous decomposition of sporopollenin from pollen of Typha angustifolia L. by acidic methanolysis.* Zeitschrift fur Naturforschung C-Journal of Biosciences, 2002. **57**(11-12): p. 1035-1041.
47. Rozema, J., et al., *UV-B absorbance and UV-B absorbing compounds (para-coumaric acid) in pollen and sporopollenin: the perspective to track historic UV-B levels.* Journal of Photochemistry and Photobiology B: Biology, 2001. **62**(1–2): p. 108-117.
48. van Bergen, P.F., et al., 2004: p. Structural biomacromoleules in plants: what can be learnt from the fossil record?. In: Hemsley, A.R. and Poole I. (eds.), Linnean Society Symposium Series, 21, Evolution of Plant Physiology, Elsevier, Amsterdam, p. 134-154.
49. Shaw, G., *THE CHEMISTRY OF SPOROPOLLENIN*, in *Sporopollenin*, J. Brooks, et al., Editors. 1971, Academic Press. p. 305-350.
50. Zetzsche, F. and K. Huggler, *Untersuchungen über die Membran der Sporen und Pollen. I. 1. Lycopodium clavatum L.* Justus Liebigs Annalen der Chemie, 1928. **461**(1): p. 89-109.
51. Kettley, S.J. and H. University of, *Novel derivatives of sporopollenin for potential applications in solid phase organic synthesis and drug delivery*. 2001, Hull: University of Hull.
52. Boasman, A.J., *Ph.D. Thesis*. 2003, Univeristy of Hull: UK.
53. Zetzsche, F. and H. Vicari, *Untersuchungen über die Membran der Sporen und Pollen III. 2. Picea orientalis, Pinus silvestris L., Corylus Avellana L.* Helvetica Chimica Acta, 1931. **14**(1): p. 62-67.
54. Fawcett, P., et al., *Application of Radiochemical Techniques to the Determination of the Hydroxyl Content of Some Sporopollenins.* Grana, 1970. **10**(3): p. 246-247.
55. Schulte, F., et al., *Chemical Characterization and Classification of Pollen.* Analytical Chemistry, 2008. **80**(24): p. 9551-9556.

56. EM Dobson, H., et al., *Pollen and flower volatiles in two< i> Rosa species</i>.* Phytochemistry, 1987. **26**(12): p. 3171-3173.
57. Dobson, H.E.M., *Survey of Pollen and Pollenkitt Lipids -- Chemical Cues to Flower Visitors?* American Journal of Botany, 1988. **75**(2): p. 170-182.
58. Hemsley, A. and I. Ferguson, *Pollen morphology of the genus Erythrina (Leguminosae: Papilionoideae) in relation to floral structure and pollinators.* Annals of the Missouri Botanical Garden, 1985: p. 570-590.
59. Pacini, E. and M. Hesse, *Pollenkitt – its composition, forms and functions.* Flora - Morphology, Distribution, Functional Ecology of Plants, 2005. **200**(5): p. 399-415.
60. Knox, R.B., *Pollen and allergy*. The Institute of Biology's studies in biology. 1979, Baltimore: University Park Press. 59 p.
61. Hemsley, A.R. and I. Poole, *The Evolution of Plant Physiology*. 2004: Elsevier Science.
62. Kapp, R.O., *How to know pollen and spores*. Pictured-key nature series. 1969, Dubuque, Iowa,: W. C. Brown Co. ix, 249 p.
63. Stanley, R.G. and H.F. Linskens, *Pollen: biology, biochemistry, management*. 1974, Berlin, New York,: Springer-Verlag. ix, 307 p.
64. Frenguelli, G., et al., *Pollini allergenici: morfologia e aspetti microscopici.* Giorn It Allergol Immunol Clin, 1991. **1**: p. 389-401.
65. Louisa Howard, C.D. *Pollen Mix*. 2000; Available from: http://remf.dartmouth.edu/images/botanicalPollenSEM/source/12.html.
66. Blackmore, S., et al., *Developmental origins of structural diversity in pollen walls of Compositae.* Plant Systematics and Evolution, 2010. **284**(1-2): p. 17-32.
67. Blackmore, S., et al., *Pollen wall development in flowering plants.* New Phytologist, 2007. **174**(3): p. 483-498.
68. Yue, C.Y. and W.L. Cheung, *THE MORPHOLOGY, CHARACTER AND STRENGTH OF THE INTERFACE IN GLASS-FIBER POLYPROPYLENE COMPOSITES.* Journal of Materials Science, 1991. **26**(4): p. 870-880.
69. Geoghegan, M. and G. Krausch, *Wetting at polymer surfaces and interfaces.* Progress in Polymer Science, 2003. **28**(2): p. 261-302.
70. Lee, J.B., et al., *Wetting Transition Characteristics on Microstructured Hydrophobic Surfaces.* Materials Transactions, 2010. **51**(9): p. 1709-1711.
71. Kulkami, S.A., S.B. Ogale, and K.P. Vijayamohanan, *Tuning the hydrophobic properties of silica particles by surface silanization using mixed self-assembled monolayers.* Journal of Colloid and Interface Science, 2008. **318**(2): p. 372-379.
72. Shah, G.J., M. Sitti, and Ieee, *Modeling and design of biomimetic adhesives inspired by gecko foot-hairs*. IEEE ROBIO 2004: Proceedings of the IEEE International Conference on Robotics and Biomimetics. 2004. 873-878.
73. Zhang, Y., et al., *Replica molding of high-aspect-ratio polymeric nanopillar arrays with high fidelity.* Langmuir, 2006. **22**(20): p. 8595-8601.
74. Lamblet, M., et al., *Adhesion enhancement through micropatterning at polydimethylsiloxane-acrylic adhesive interfaces.* Langmuir, 2007. **23**(13): p. 6966-6974.
75. Greiner, C., A. del Campo, and E. Arzt, *Adhesion of bioinspired micropatterned surfaces: Effects of pillar radius, aspect ratio, and preload.* Langmuir, 2007. **23**(7): p. 3495-3502.
76. *Wetting*. 2012 May 10, 2012 5/1/2012]; Available from: http://en.wikipedia.org/wiki/Wetting.

77. Heinrich, G. and T.A. Vilgis, *Contribution of entanglements to the mechanical properties of carbon black-filled polymer networks.* Macromolecules, 1993. **26**(5): p. 1109-1119.
78. Praveen, S., et al., *Synergistic effect of carbon black and nanoclay fillers in styrene butadiene rubber matrix: Development of dual structure.* Composites Part A: Applied Science and Manufacturing, 2009. **40**(3): p. 309-316.
79. Grater, W.C. and T.R. Stemen, *The plant, the pollen and the patient.* Review of Palaeobotany and Palynology, 1967. **4**(1): p. 187-192.
80. Lewis, A.J., *RAGWEED CONTROL TECHNIQUES - EFFECT ON OLD-FIELD PLANT POPULATIONS.* Bulletin of the Torrey Botanical Club, 1973. **100**(6): p. 333-338.
81. Kharecha, P.A. and J.E. Hansen, *Implications of "peak oil" for atmospheric CO2 and climate.* Global Biogeochemical Cycles, 2008. **22**(3).
82. Ziska, L.H. and F.A. Caulfield, *Rising CO2 and pollen production of common ragweed (Ambrosia artemisiifolia L.), a known allergy-inducing species: implications for public health.* Functional Plant Biology, 2000. **27**(10): p. 893-898.
83. Brooks, J. and G. Shaw, *Chemical structure of the exine of pollen walls and a new function for carotenoids in nature.* 1968.
84. Brooks, J. and G. Shaw, *Geochemistry of sporopollenin.* Chemical Geology, 1972. **10**(1): p. 69-87.
85. Codina, R., R.E. Esch, and W.G. Mahoney. *Testing of Raw Materials Used for the Production of Allergenic Extracts*. 2011 [Cited September 5, 2013]; Available from: http://www.greerlabs.com/files/Library/Manufacturing-and-Testing/Testing_Raw_Materials_EAACI_Meeting_2010_Final_Approved_11_2011.pdf.
86. Bavley, A. *Farmers Cultivate Allergy Sufferers' Worst Nightmare*. 2004 [Cited September 5, 2013]; Available from: http://billingsgazette.com/business/farmers-cultivate-allergy-sufferers-worst-nightmare/article_bbc8de4a-67ea-52ef-82e9-f2aaa06b6f5e.html.
87. Lee, J.-H., et al., *Pollen: A Novel, Biorenewable Filler for Polymer Composites.* Macromolecular Materials and Engineering, 2011: p. n/a-n/a.
88. Jenik, M., et al., *Pollen-imprinted polyurethanes for QCM allergen sensors.* Analytical and Bioanalytical Chemistry, 2009. **394**(2): p. 523-528.
89. Thio, B.J.R., J.-H. Lee, and J.C. Meredith, *Characterization of Ragweed Pollen Adhesion to Polyamides and Polystyrene Using Atomic Force Microscopy.* Environmental Science & Technology, 2009. **43**(12): p. 4308-4313.
90. Lee, J.H., et al., *Pollen: A Novel, Biorenewable Filler for Polymer Composites.* Macromolecular Materials and Engineering, 2011. **296**(11): p. 1055-1062.

CHAPTER 2

CHARACTERIZATING INTERFACIAL PROPERTIES OF POLLEN

This chapter is in preparation for publication.

2.1 Overview

Pollen grains are microscopic particles whose exine exhibits unique surface chemistries tuned by evolution to protect delicate genetic material. However, there are limited quantitative studies on the effect of pollen surface chemistry on surface interactions of pollen grains. The main focus of this work is the measurement of solid-liquid interactions of short ragweed pollen and chemical probes via inverse liquid chromatography (ILC). By measuring retention of probes at various temperatures, heats of interaction are calculated. Native (D) pollen displayed very low variations in retention of probes with varying functionalities likely governed by size exclusion mechanisms. Acid-base treated (AB) pollen displayed increasing retention with increasing probe polarity due to specific interactions. Chemical probes with alcohol and amide groups were most highly retained on acid-base treated pollen. The calculated heats of interaction of chemical probes range from approximately -8 kJ/mole to -30 kJ/mole, with the more highly retained polar probes portraying the largest magnitudes. Additionally, increased asymmetry factors of up to 4 indicate specific interactions of polar probes with surface hydroxyls present on acid-base treated pollen. This information is useful in understanding how chemistry affects dynamic aspects of pollen surface interactions and improves the understanding of pollen physicochemical properties. In addition, it will be helpful in designing composites utilizing pollen as a sustainably-sourced filler. Finally, surface properties of pollen were also investigated with the BET method and DSC/TGA measurements.

2.2 Introduction

Particle adhesion displayed in natural phenomena such as pollination and bacterial, viral, or fungal growth, have been of great scientific interest. Such interest stems from the relevance of particle−surface adhesion in important engineering applications including composites, paints and pigments, and drug delivery [1-6]. Understanding the fundamental mechanisms of these natural phenomena may improve our ability to tune particle adhesion in these various applications.

Pollen grains are microscopic particles exhibiting complex surface chemistries and solid surface features, optimized by evolution for the protection of delicate genetic material for plant reproduction and to facilitate adhesion of pollen to insect and plant surfaces under different dynamic and environmental conditions [7]. The pollen wall has three main domains: the exine, intine, and pollen coat [8, 9]. The outermost shell, known as the exine, is composed of sporopollenin, a highly crosslinked organic substance consisting of fatty acids, phenylpropanoids, and phenolics. It has high chemical stability and is mechanically very tough [10, 11]. Under the exine layer is the intine, which is rich in cellulose and hemicelluloses. While the intine and exine are solids, some species of pollen have liquid lipoidal surface substances, called the pollen coat, in and/or on the exine features. Amongst its functions, the pollen coat has adhesive properties facilitating pollen transmission with insects and other animals [12-14]. Despite pollen's unique surface chemistries, there are only limited quantitative studies on the role of pollen surface chemistry in surface interactions of pollen grains. A quantitative description of the effect of pollen chemistry on surface interactions may be useful for further understanding of pollen adhesion in the natural environment. More specifically, understanding solid-liquid interactions of the pollen surface may be useful in predicting the compatibility of pollen with different polymers, related to previous work on pollen-polymer composites [15].

Inverse liquid chromatography (ILC) is a relatively new technique that can be used to study solid-liquid interactions. It is sensitive to small differences in adsorption properties through measurement of retention times of different chemical probes. ILC has been used to determine the physicochemical characteristics of materials such as silica, coal, xerogels, and zirconia, to name a few [16-18]. ILC is similar to inverse gas chromatography (IGC), a technique that has been used over the past 50 years [19-22]. One advantage of ILC versus IGC is the potential to probe interactions of large molecules, such as oligomers or even polymers. Also, ILC allows the study of solid-liquid interactions relevant to industrial processes under significant conditions such as pH and temperature. One complication with ILC is that the use of a liquid components results in competition between mobile phase and probe molecules for adsorption on the solid phase. This is unlike IGC, where the gaseous mobile phase can be assumed to have negligible in adsorption processes.

ILC retention may be due to multiple mechanisms such as Vander Waals interactions, polar interactions, hydrogen bonding, or size exclusion. Solid-liquid interactions may be influenced by several factors, such as the functional groups in the chemical probes, functional groups on the solid surface and their distributions, and surface area of the solid surface. One ILC approach is based on the determination of the capacity factors of probes, from their net retention times, in the linear domain of the adsorption isotherm (infinite dilution) [23-26]. Column efficiency in ILC could be expected to be less significant than in analytical liquid chromatography. However, peak resolution is not a specific requirement.

Another approach is the determination of adsorption and desorption isotherms with probes at finite concentrations [21, 27-29]. In the present study, the ILC capacity factors of organic compounds in columns packed with pollen grains were observed as a direct measurement of

pollen-liquid interactions. To our knowledge, this is the first use of ILC in characterizing biological particles. Surface properties are also probed with the BET method and DSC/TGA measurements.

2.3 Experimental

2.3.1 Pollen Samples

Short ragweed (A. artemisiifolia, Greer Laboratories) non defatted (N) and defatted (D) pollen grains were obtained from and stored at 4 °C prior to use. D pollen grains were tested as received and also after treatment with an acid base hydrolysis (AB) procedure in order dissolve intracellular material and isolate the exine shell [9, 30]. Briefly, D pollen was stirred in potassium hydroxide (EMD Millipore) at room temperature for 24 hours. This pollen was washed with hot water and hot ethanol and dried in a convection oven. The dried base treated pollen was then stirred in phosphoric acid (BDH chemicals) for 7 days at 50 °C. This acid treated pollen was washed in the same manner as the base step and then dried in a convection oven at 60 °C. This process caused the pollen grains too lose ~80% of their original weight. Treated pollen is referred to as AB pollen. FT-IR spectra were obtained on a Bruker Vertex 80V FT-IR spectrometer equipped with a MIR beamsplitter from 4000 cm^{-1} to 400 cm^{-1}. D and AB pollen were mixed with KBr powders and pressed in pellets for measurement.

2.3.2 Characterization and ILC

A QuadraSorb SI instrument based on adsorption of nitrogen gas by the BET method was used to determine the surface areas of N, D, and AB pollen. In order to obtain suitable measurements, large bulb cells were utilized in order to allow for a large amount of material to be used (> than 1 gram), due to the low surface area of pollens. Pollen was activated overnight in a vaccum oven at 100 °C and again dried on a high vacuum line in the BET bulb cells prior to

testing. A Netzsch STA409PG was used for simultaneous thermogravimetric analysis (TGA) and differential scanning calorimetry (DSC). Approximately 8 mg of pollen (D or AB) were used for each experiment. A heating rate of 10 K/min was used up to 900 °C under a mixed gas stream of nitrogen and air.

For ILC experiments, pollen samples were heated in a vacuum oven at 100 °C before column packing to remove physisorbed water. Pollen was then wet packed with cyclohexane in empty stainless steel columns (i.d. of 4.6 mm, 5 cm long, and with 2 μm frits) with the aid of mechanical vibration and a vacuum pump. HPLC grade cyclohexane (Alfa Aesar) was used as a mobile phase. The HPLC grade organic compounds tested are listed in Table 2.2. ILC experiments were conducted with a Dionex Ultimate 3000 UHPLC instrument equipped with a UV detector with a flow rate of 0.5 mL/min and at various temperatures (30, 40, and 50 °C). The UV detector was operated at a wavelength of 200 nm. 1 to 10 μL injections were made from 0.1 or 1 vol% solutions (depending on strength of UV detection). The dead volume was determined by performing injections with cylcohexane on a smaller column (2.1 mm i.d.) in order to overload the column. This produced double peaks where the second peak is cyclohexane that is adsorbed to the surface, while the first peak is cyclohexane carried by the mobile phase and eluted before the second retained peak because of the low surface area available in the column. The first peak was used to estimate the void time of an unretained probe.

Probe retention is described by the capacity factor, k, as shown in Equation 2.1

$$k=\frac{t_R-t_0}{t_0} \tag{2.1}$$

where t_R is the retention time of an adsorbing probe and t_0 is the void time of a non-adsorbing probe. Asymmetry factors, A_S, are determined with the Chromeleon chromatography data system, as shown in Figure 2.1.

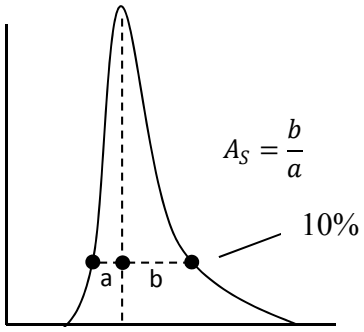

Figure 2.1: Schematic for A_s calculation.

2.4 Results and Discussion

2.4.1 Surface Characterization

The specific surface areas of non-defatted, defatted, and treated pollen shown in Table 2.1 were determined on a QuadraSorb SI instrument based on adsorption of nitrogen gas by the BET method. There was a significant increase in surface area in the order non-defatted < defatted < treated. This is expected as defatting removes soluble surface organics and acid-base hydrolysis removes hydrolysable organics, leaving only the exine shell intact, freeing up surface sites for adsorption. Adsorption isotherms are Type II with limited hysteresis. An SEM image of the exine shell of short ragweed pollen (Figure 2.2) shows a perforated surface with pores ranging from about 30 to 100 nm. Both of these observations suggest the surface of short ragweed pollen is macroporous.

Table 2.1: Specific surface areas of pollen with different treatments.

Pollen Type	Non-Defatted	Defatted	Treated
S_{BET} (m^2/g)	.477	1.953	5.804

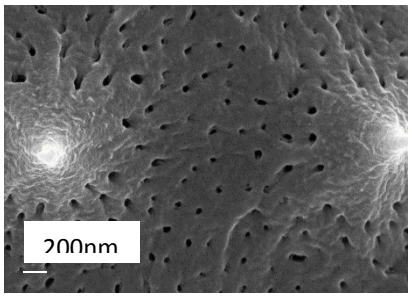

Figure 2.2: Perforated exine surface of ragweed pollen.

Figure 2.3 shows both the percent weight loss and heat flow of both D and AB pollen. Weight loss occurred up to ~500 °C for D pollen and ~560 °C for AB pollen. It has been suggested that the two weight loss event correspond with first the burning off of components with low molecular weight and low boiling point (200 – 400 ˚C) and the second weight loss event corresponds with the decomposition of higher molecular weight components (hemicellulose, cellulose, and sporopollenin, 400 – 550 ˚C) [31]. However, the first event is still clearly present with AB pollen, so it is likely that the burning of hemicelluloses and celluloses occurs in the first event. This would correspond with previously observed weight loss temperature ranges of cellulose as well [32-34]. However, the heat flow plot reveals that the temperature of the first event shifts from 333 ˚C to 344 ˚C for D and AB pollen respectively. Thus, cellulose and hemicelluloses burn off in the first event with other pollen internal materials. Also, AB pollen likely displays a higher temperature of the first event due because more thermally resistant crystalline cellulose is burned off as opposed to amorphous cellulose (dissolved in acid-base treatment). The second event corresponds with the degradation of the high molecular weight, highly crosslinked sporpollenin shell. The heat flow plot also reveals that the temperature of the second event shifts from 483 ˚C to 503 ˚C for D and AB pollen respectively. The weight loss behavior shows that weight loss is continuous and somewhat overlapping. Therefore, with less components present in AB pollen, sporopollenin may

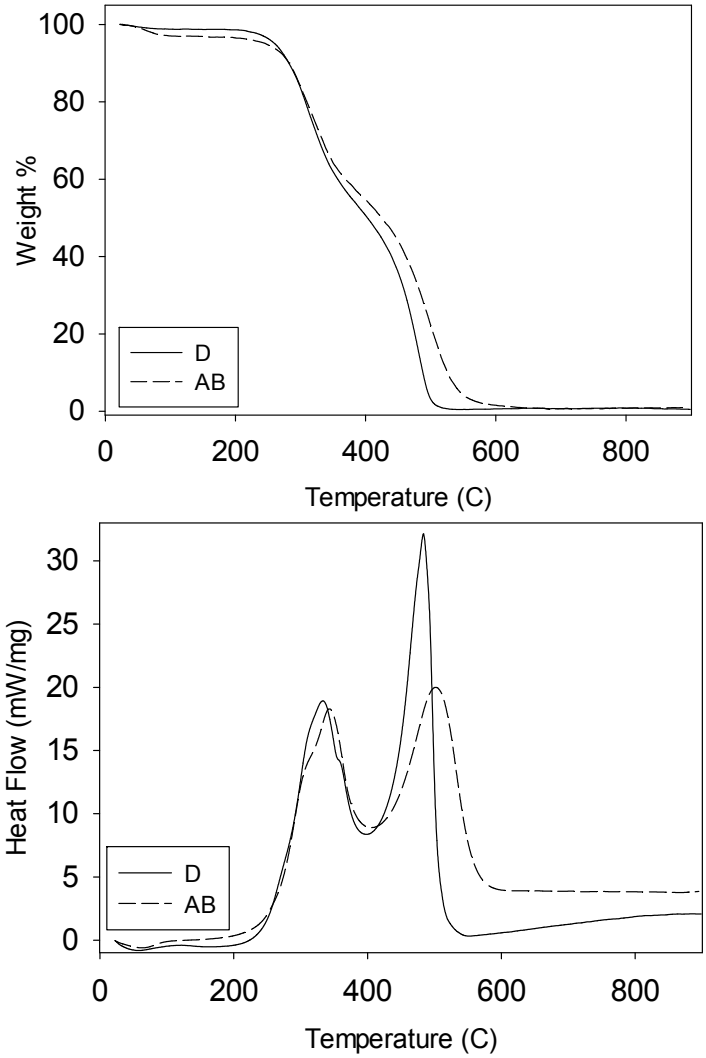

Figure 2.3: Percent weight loss and heat flow for both D and AB pollen.

decompose at a higher temperatures. It is also possible that internal materials react or interact with sporpollenin in such a way that cause it to be less thermally stable and thus the sporopollenin degrades at higher temperatures when these components are absent. This idea may be further supported by the heat flow plot, which reveals that the second decomposition peak of D pollen has a significantly higher magnitude of heat flow than the AB pollen. This means that the decomposition of sporopollenin is more endothermic in D pollen than AB pollen which may be a result of the reaction of intracellular and internal materials with sporopollenin. Finally, the residual masses are .48% and .94% D and AB respectively.

2.4.2 ILC

Retention was first measured on D pollen with the probes listed in Table 2.2. Figure 2.4 shows a few examples of characteristic chromatograms that were obtained for the probes at 30 ˚C. It is observed that for most of probes, retention remains relatively unchanged despite the various probe functionalities. Pyridine, the most polar probe, eluted at 1.439 minutes, barely larger than the void time of 1.36 minutes at 30 ˚C. The exception was ethanol, which eluted at 4.26 minutes at 30 ˚C. Table 2.2 also shows the A_S values for the probes at three different temperatures. Many of the probes, including the solvent peak, have similar A_S values, slightly greater than 1. Some probes of increasing polarity have increased A_S, but a clear trend in A_S values with changing polarity is not clear. Additionally, increased A_S values may be partially due to convoluted peaks due to D pollen's very low selectivity for different probes.

Table 2.2: Peak asymmetry of probes on D pollen.

Probe	A_S 30C	A_S 40C	A_S 50C
Cyclohexane (solvent peak)	1.68	1.72	1.67
Benzene[a]	1.79	1.82	1.84
Ethyl Acetate[b] (EA)	1.79	1.81	1.8
Tetrahydrofuran[c] (THF)	1.67	1.68	1.71
Acetone[d]	2	2.52	3.43
Ethanol[e]	2.61	1.86	2
Propanol[f]	2.15	2.28	2.68
Pyridine[g]	2.63	3.21	4.04

a-e, g-j Sigma-Adlrich, f Alfa Aesar

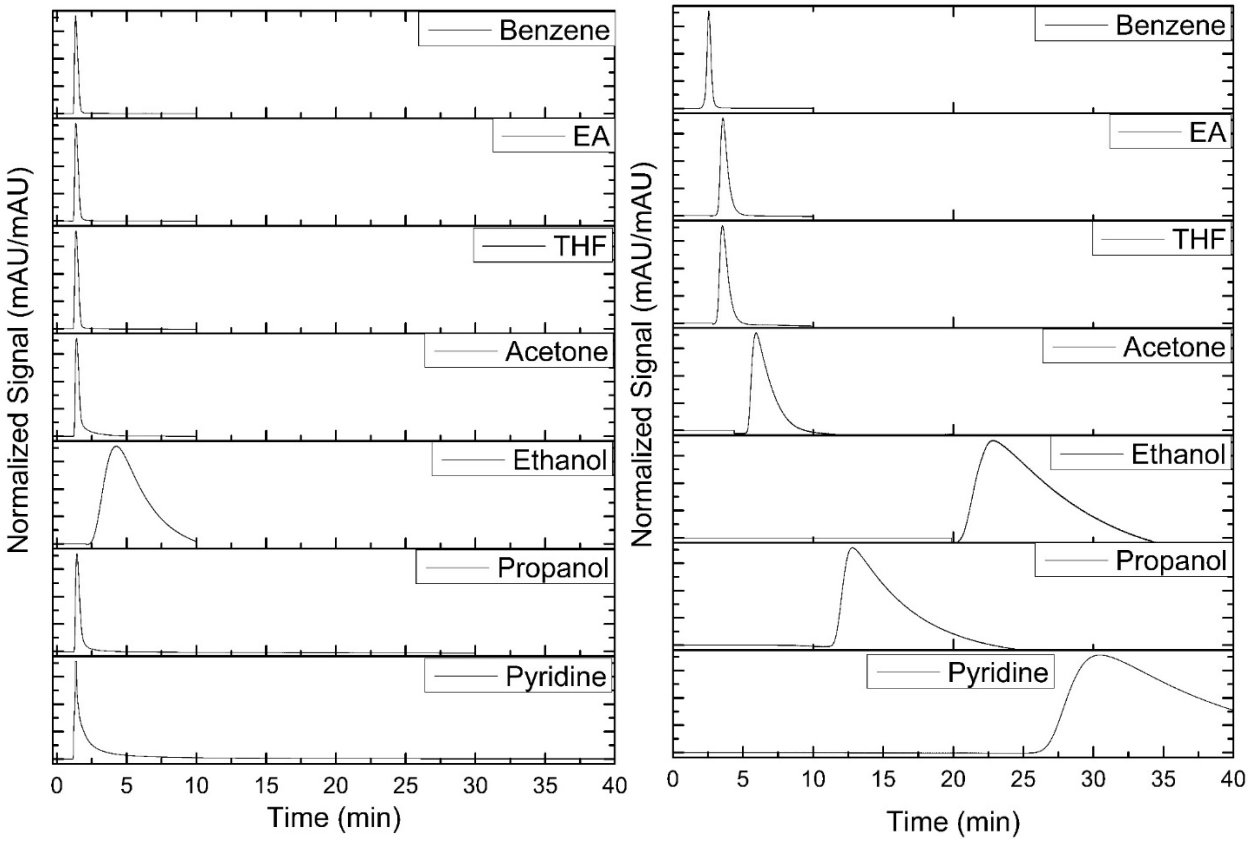

Figure 2.4: Characteristic chromatograms for retention on D pollen at 30 ˚C (left) and AB pollen at 50 ˚C (right).

Considering a tentative and simplified structure of sporopollenin [35] (Figure 1.4) and the unchanging retention time of probes on D pollen, this may suggest that surface interactions are dominated by the intracellular material and/or the aliphatic backbone of sporopollenin, confining interactions to predominantly van der Waals interactions. Figure 2.5 shows the presence of intracellular material in D pollen. This material, which includes storage oil bodies, membrane phospholipids, and pollen cytoplasm, [8] comprises the majority of pollens weight. Therefore, the intracellular material likely dominates interactions since it comprises the majority of D pollen. In the presence of nonpolar cyclohexane mobile phase these components may align in micellar formations with the long nonpolar alkane chains exposed and polar hydroxyl and carboxyl groups inaccessible for surface interactions. Such micelles may also render polar hydroxyl groups in the intine layer inaccessible for adsorption. Ethanol is the smallest molecule

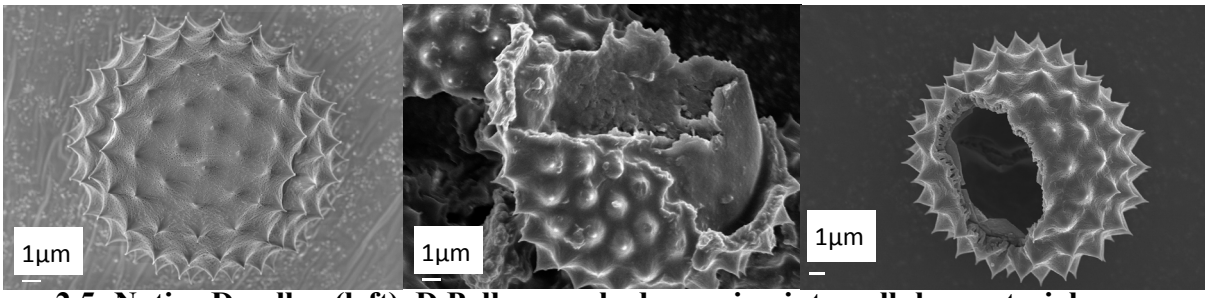

Figure 2.5: Native D pollen (left), D Pollen crushed exposing intracellular material (middle), and hollow AB pollen (right).

Table 2.3: Molecular Diameters of chemical probes.

Probe	Molecular Diam. (Angstroms)
Cyclohexane	6.1
Benzene	6.7
EA	--
THF [36]	6.3
Acetone [37]	6.16
Ethanol	4.4
Propanol [38]	4.8
Pyridine [39]	4.92-5.12

measured (Table 2.3), so its increased retention may indicate that due to weak van der Waals interactions, size exclusion retention mechanisms are significant.

Figure 2.6 shows the FTIR spectra for both D and AB pollen. The spectra of the different pollens are similar, with key differences. The cellulose fingerprint appears in the 1100 to 900 cm^{-1} region on D pollen, due to the presence of polysaccharide material in the pollen [11, 40]. The spectrum for AB pollen shows an important lack of peaks associated with polysaccharides in this range, indicating the full or partial dissolution of pollens cellulosic intine [7, 41]. Additionally, D pollen displays a very broad band at 3375 cm^{-1} due to the O-H stretch of –OH groups that shows a stronger intensity than the –CH stretches of $–CH_2$ groups at 2910 and 2840 cm^{-1}. In contrast,

AB pollen displays a more narrow –OH band with a smaller intensity than the $–CH_2$ peaks. AB pollen's OH band is also shifted to higher wavenumbers around 3450 cm^{-1}, indicating increased stretching of free hydroxyls. The C=O stretch of carboxyl groups also shifts from 1672 cm^{-1} to 1707 cm^{-1} on D and AB pollen, respectively. Therefore, the acid-base hydrolysis decreases the ratio of hydroxyl to methylene groups due to the full or partial dissolution of the intine and makes hydroxyl and carboxyl groups more accessible for surface interactions.

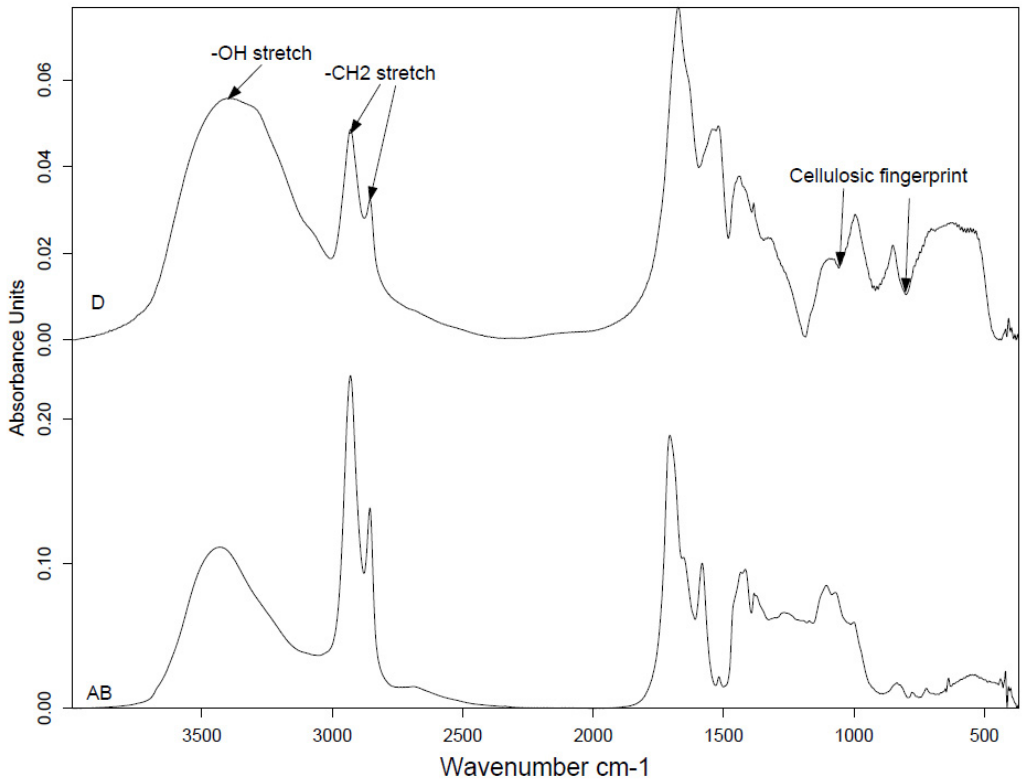

Figure 2.6: FTIR spectra of D pollen (top) and AB pollen (bottom).

Figure 2.4 also shows the characteristic retention chromatograms for AB pollen at 50 ˚C and Table 2.4 shows the capacity factors for probes at three different temperatures. AB pollen displays a significantly different retention behavior than D pollen. The elimination of intracellular material makes hydroxyl and carboxyl groups on the sporopollenin accessible for adsorption, which are capable of polar interactions (e.g. acid-base, hydrogen bonding) [42-44].

As probe polarity is increased, retention increases. Benzene, which has π-electrons that interact with acidic hydrogen sites on the pollen surface [17, 18, 44], displays the lowest capacity factor of 1.07 at 30 ˚C eluting in 2.8 minutes. Oxygen bases are more highly retained, as oxygen may act as electron donors [42-44]. EA and THF show similar retention times. EA eluted in 4.8 minutes at 30 ˚C with a capacity factor of 2.58. Acetone is more highly retained due to its higher electron density. Alcohols show increased interactions due to O-H··O hydrogen bonds alcohol hydrogen or pollen surface hydrogen [44, 45]. For example, propanol, a more polar probe, eluted at 24 minutes at 30 ˚C with a capacity factor of 17. The most polar probe, pyridine, eluted at 70 minutes at 30 ˚C with a capacity factor of 50.31. The lone pair on the nitrogen of pyridine is able interact with an electron accepting hydrogen on polar groups of pollen surface [44]. Additionally, pyridine has negligible self association, unlike the alcohols probed, possibly increasing interactions with the pollen surface [42]. This retention behavior arises from interactions of acidic hydroxyl and carboxyl groups that are accessible after pollen treatment can strongly interact with basic probes. Also, as expected, capacity factors decrease with increased temperature.

Table 2.4: Capacity factors of probes on AB pollen from 30 – 50 ˚C.

Probe	***k* (30C)**	***k* (40C)**	***k* (50C)**
Benzene	1.08	1.022	0.89
EA	2.58	2.02	1.62
THF	2.46	1.97	1.60
Acetone	5.86	4.35	3.34
Ethanol	32.57	24.10	15.75
Propanol	16.79	13.05	8.41
Pyridine	50.31	31.95	21.40

Figure 2.7 shows van't Hoff plots that were used to determine heats of interaction (ΔH) for transfer of probes from the mobile phase to the AB pollen surface according to the following equation:

$$ln(k) = \frac{-\Delta H}{RT} + \frac{\Delta S}{R} + ln\left(\frac{V_s}{V_0}\right) \quad (2.2)$$

Here, ΔS is the entropy for the transfer of the probes from the mobile phase to the stationary phase, R is the gas constant, T is the absolute temperature V_s is the volume of the stationary phase, and V_0 is the void volume. The plot shows that in the temperature range examined, the data is essentially linear. The lowest r^2 value was 0.922. Heat of interaction values ranged from -7.9 to -34.8 kJ/mol (Table 2.5), with the most highly retained probes displaying the largest heats of interaction.

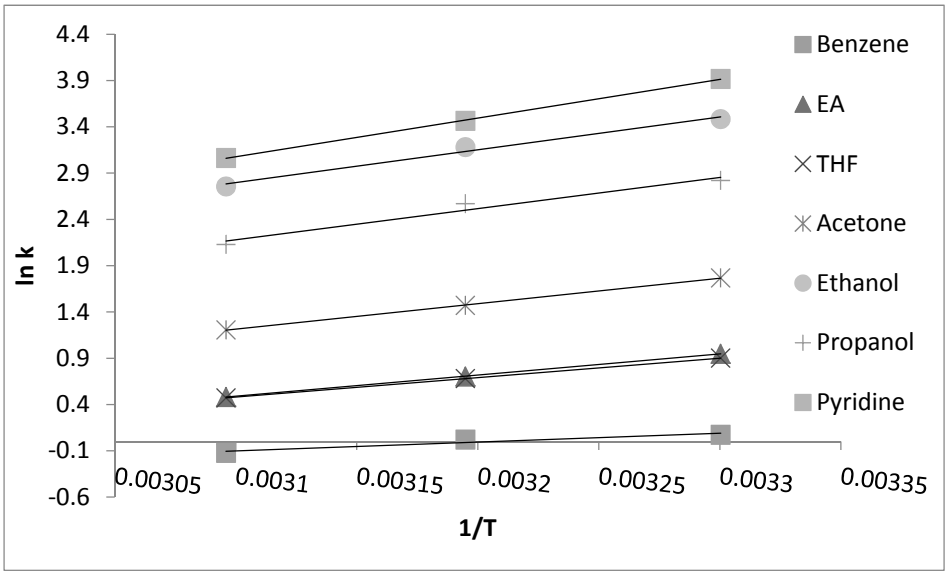

Figure 2.7: Van't Hoff plots probes on AB pollen. The slope of each line gives the heat of interaction.

Table 2.5: Calculated heats of interaction for probes on AB pollen.

Probe	$-\Delta H$ (kJ/mol)
Benzene	7.91
EA	19.02
THF	17.5
Acetone	22.87
Ethanol	29.48
Propanol	28.03
Pyridine	34.79

Table 2.6 shows the A_S values of the probes at three different temperatures. Coupled with increased retention with AB pollen is a significant increase in A_S values with increasing polarity. The least polar probe, benzene, displays A_S factors of 1.06 - 1.15. Propanol displays values of 2.56 - 4.52. Pyridine, the most polar probe, ranges from 3.27 - 4.52. In analytical liquid chromatography, such A_s values would be unacceptable. However, in physicochemical liquid chromatography, ideal peak asymmetry is not a specific requirement, but can be used as indication of additional retention mechanisms such as polar interactions [46].

A_S values for the solvent peak on AB pollen are ideal at 1.02 and .99 indicating effective column packing. The solvent peak for D pollen had A_S values of 1.67 - 1.72. The packing procedures were identical, so the less ideal A_S values for DRW likely arise from different chemistries present in D pollen. This irregular solvent peak is likely due to small differences adsorption properties of the exine (sporopollenin), intine (cellulose), and intracellular material (oil bodies). With the last two components eliminated with acid-base hydrolysis, only a single chemistry is probed during ILC experiments, resulting in a symmetrical solvent peak on AB pollen.

Table 2.6: Peak asymmetry of probes on AB pollen.

Probe	A_s 30C	A_s 40C	A_s 50C
Cyclohexane	1.02	.99	.99
Benzene	1.15	1.1	1.06
Ethyl Acetate	2.34	1.9	1.88
THF	2.13	1.88	1.84
Acetone	3.04	2.94	3.31
Ethanol	-	3.2	3.59
Propanol	2.56	3.08	4.52
Pyridine	3.27	4.51	4.42

As mentioned earlier, these solid-liquid interactions may be useful in predicting the compatibility of pollen with different polymers for composites. Further, it may be useful even for understanding how polymerization reaction components interact with one another. The data may suggest that polymers with alcohol groups or amide groups may have strong surface interactions with AB pollen. In our previous work, untreated pollen was incorporated in both polystyrene (PS) and polycaprolactone (PCL) to create pollen-polymer composites [15]. SEM micrographs revealed large voids and the pollen-polymer interfaces indicating weak surface interactions and poor adhesion. First, the D pollen data shows low surface interactions of untreated pollen with all probes and thus untreated pollen may be unable to interact with the aromatic and ester groups of PS and PCL respectively. However, AB pollen may be a better choice for these polymers considering its retention behavior to improve surface interactions and interfacial adhesion. Paired with a polymer with more polar functional groups, such as polyvinyl alcohol (hydroxyls) or polyvinylpyrrolidone (amides), surface interactions and interfacial adhesion with pollen may be increased further. ILC also allows for the probing of high molecular weight analytes, such as

oligomers and polymers [47]. This would be another route of predicting polymer interactions and may also reveal if size exclusion mechanisms are significant.

2.5 Conclusions

Solid-liquid interactions of short ragweed pollen and chemical probes with varying functionalities were measured with ILC in order to further understand pollen chemistry and physicochemical properties. Retention of probes was measured on as received (D) pollen and acid-base hydrolyzed (AB) pollen over a range of temperatures, allowing the heats of interaction to be calculated. D pollen displayed unchanging retention, while retention increased on AB pollen as probes became increasingly polar, due to interactions with hydroxyl groups on AB pollen. Calculated heats of interaction and peak asymmetry increased with increasing probe polarity on AB pollen. This data suggests that surface interactions are limited to weak van der Waals forces for D pollen, while AB pollen is capable of stronger polar interactions. Considering pollen as a filler for polymer composites, this indicates that AB pollen may be a more useful filler than D pollen. ILC may be used further to probe the retention of high molecular weight probes as well as obtaining solid-liquid adsorption isotherms on pollen surfaces.

2.6 References

1. Rimai, D.S., L.H. Sharpe, and A.S. Meeting, *Advances in Particle Adhesion*. 1996: Gordon and Breach.
2. Binnig, G., C.F. Quate, and C. Gerber, *ATOMIC FORCE MICROSCOPE.* Physical Review Letters, 1986. **56**(9): p. 930-933.
3. Bowen, W.R., et al., *Direct measurement of the force of adhesion of a single biological cell using an atomic force microscope.* Colloids and Surfaces a-Physicochemical and Engineering Aspects, 1998. **136**(1-2): p. 231-234.
4. Dufrene, Y.F., *Recent progress in the application of atomic force microscopy imaging and force spectroscopy to microbiology.* Current Opinion in Microbiology, 2003. **6**(3): p. 317-323.
5. Thio, B.J.R., J.H. Lee, and J.C. Meredith, *Characterization of Ragweed Pollen Adhesion to Polyamides and Polystyrene Using Atomic Force Microscopy.* Environmental Science & Technology, 2009. **43**(12): p. 4308-4313.

6. Thio, B.J.R. and J.C. Meredith, *Quantification of E-coli adhesion to polyamides and polystyrene with atomic force microscopy.* Colloids and Surfaces B-Biointerfaces, 2008. **65**(2): p. 308-312.
7. Barrier, S., *Physical and chemical properties of sporopollenin exine particles*, in *Chemistry*. 2008, The University of Hull.
8. Piffanelli, P., J.H.E. Ross, and D.J. Murphy, *Biogenesis and function of the lipidic structures of pollen grains.* Sexual Plant Reproduction, 1998. **11**(2): p. 65-80.
9. Wiermann, R. and S. Gubatz, *POLLEN WALL AND SPOROPOLLENIN.* International Review of Cytology-a Survey of Cell Biology, 1992. **140**: p. 35-72.
10. Blackmore, S., et al., *Pollen wall development in flowering plants.* New Phytologist, 2007. **174**(3): p. 483-498.
11. Dominguez, E., et al., *Pollen sporopollenin: degradation and structural elucidation.* Sexual Plant Reproduction, 1999. **12**(3): p. 171-178.
12. Lin, H., I. Gomez, and J.C. Meredith, *Pollenkitt Wetting Mechanism Enables Species-Specific Tunable Pollen Adhesion.* Langmuir, 2013. **29**(9): p. 3012-3023.
13. Pacini, E. and M. Hesse, *Pollenkitt – its composition, forms and functions.* Flora - Morphology, Distribution, Functional Ecology of Plants, 2005. **200**(5): p. 399-415.
14. Hesse, M., *The fine structure of the exine in relation to the stickiness of angiosperm pollen.* Review of Palaeobotany and Palynology, 1981. **35**(1): p. 81-92.
15. Lee, J.H., et al., *Pollen: A Novel, Biorenewable Filler for Polymer Composites.* Macromolecular Materials and Engineering, 2011. **296**(11): p. 1055-1062.
16. Donnet, J.B., et al., *Surface energy of silica xerogels and fumed silica by inverse gas chromatography and inverse liquid chromatography.* Rubber Chemistry and Technology, 2002. **75**(5): p. 811-824.
17. Paproski, R.E., C. Liang, and C.A. Lucy, *High temperature normal phase liquid chromatography of aromatic hydrocarbons on bare zirconia.* Journal of Chromatography A, 2011. **1218**(44): p. 7948-7955.
18. Takanohashi, T., et al., *An inverse liquid chromatography study of the interaction of organic compounds with argonne premium coals.* Energy & Fuels, 2000. **14**(3): p. 720-726.
19. Voelkel, A., et al., *Inverse gas chromatography as a source of physiochemical data.* Journal of Chromatography A, 2009. **1216**(10): p. 1551-1566.
20. Rothon, R., *Particulate-filled Polymer Composites*. 2003: Rapra Technology.
21. Yla-Maihaniemi, P.P. and D.R. Williams, *A comparison of frontal and nonfrontal methods for determining solid-liquid adsorption isotherms using inverse liquid chromatography.* Langmuir, 2007. **23**(7): p. 4095-4101.
22. Lloyd, D.R., et al., *Inverse Gas Chromatography: Characterization of Polymers and Other Materials*. 1989: American Chemical Society.
23. Kiso, Y., T. Kitao, and K. Nishimura, *Adsorption properties of cyclic compounds on cellulose acetate.* Journal of Applied Polymer Science, 1999. **71**(10): p. 1657-1663.
24. Kleeman, W.P. and L.C. Bailey, *THERMODYNAMIC EVALUATION OF ACTIVATED-CHARCOAL AS A POISON ANTIDOTE BY HIGH-PERFORMANCE LIQUID-CHROMATOGRAPHY .1. DERIVATION AND VALIDATION OF AN EQUATION FOR GIBBS FREE-ENERGY OF LIQUID SOLID ADSORPTION.* Journal of Pharmaceutical Sciences, 1988. **77**(6): p. 500-505.

25. Huang, H., *Characterization of Leather Powder Using Inverse High Performance Liquid Chromatography*. 2001: Texas Tech University.
26. Kiso, Y., T. Kitao, and K. Nishimura, *Adsorption properties of aromatic compounds on polyethylene as a membrane material.* Journal of Applied Polymer Science, 1999. **74**(5): p. 1037-1043.
27. Donnet, J.B., et al., *Characterisation of a precipitated silica surface by inverse liquid chromatography Part I.* Kautschuk Gummi Kunststoffe, 2004. **57**(4): p. 151-159.
28. Maafa, D., H. Balard, and J.B. Donnet, *The study of adsorption of iodine on carbon black by inverse liquid chromatography.* Rubber Chemistry and Technology, 2007. **80**(5): p. 895-906.
29. Antworth, C.P., R.R. Yates, and W.T. Cooper, *Applications of inverse chromatography in organic geochemistry—I. Characterization of polar solute-soil organic matter interactions by high performance liquid chromatography.* Organic Geochemistry, 1989. **14**(2): p. 157-164.
30. Southworth, D., *Solubility of Pollen Exines.* American Journal of Botany, 1974. **61**(1): p. 36-44.
31. Wang, Y., et al., *Carbon Microspheres with Supported Silver Nanoparticles Prepared from Pollen Grains.* Langmuir, 2005. **21**(23): p. 10846-10849.
32. Poletto, M., A.J. Zattera, and V. Pistor, *Structural Characteristics and Thermal Properties of Native Cellulose*. Cellulose - Fundamental Aspects. 2013.
33. Semsarilar, M., et al., *Supramolecular hybrids of cellulose and synthetic polymers.* Polymer Chemistry, 2012. **3**(12): p. 3266-3275.
34. LIU, Y., et al., *GRAFTING OF METHYL ACRYLATE ONTO CARBON BLACK SURFACE INITIATED BY POTASSIUM DIPERIODATOCUPRATE (III).* IRANIAN POLYMER JOURNAL (ENGLISH), 2005.
35. Hemsley, A.R. and I. Poole, *The Evolution of Plant Physiology*. 2004: Elsevier Science.
36. Lee, J.Y., et al., *Observations related to tetrahydrofuran and methane hydrates for laboratory studies of hydrate-bearing sediments.* Geochemistry, Geophysics, Geosystems, 2007. **8**(6): p. Q06003.
37. Nadykto, A.B. and F. Yu, *Uptake of neutral polar vapor molecules by charged clusters/particles: Enhancement due to dipole-charge interaction.* Journal of Geophysical Research: Atmospheres, 2003. **108**(D23): p. 4717.
38. Blum, L. and W.R. Fawcett. *A Simple Model for the Dielectric Behavior of Polar Solvents in the Mean Spherical Approximation*. 1993; Available from: http://handle.dtic.mil/100.2/ADA260283.
39. Herber, R.H. and Y. Maeda, *Intercalation compounds of iron(III) oxychloride: systematics of nitrogen-containing Lewis base intercalants.* Inorganic Chemistry, 1981. **20**(5): p. 1409-1415.
40. Domínguez, E., et al., *Isolation of intact pollen exine using anhydrous hydrogen fluoride.* Grana, 1998. **37**(2): p. 93-96.
41. Shaw, G. and D.C. Apperley, *13C-NMR spectra of Lycopodium clavatum sporopollenin and oxidatively polymerised β-carotene.* Grana, 1996. **35**(2): p. 125-127.
42. Fowkes, F.M., *Role of acid-base interfacial bonding in adhesion.* Journal of Adhesion Science and Technology, 1987. **1**(1): p. 7-27.
43. Fowkes, F.M., et al., *Acid–base complexes of polymers.* Journal of Polymer Science: Polymer Chemistry Edition, 1984. **22**(3): p. 547-566.

44. Parida, S.K., et al., *Adsorption of organic molecules on silica surface.* Advances in Colloid and Interface Science, 2006. **121**(1–3): p. 77-110.
45. R.H. Dowdy, M.M.M., *ALCOHOL-WATER INTERACTIONS ON MONTMORILLONITE SURFACES. I. ETHANOL*, in *Clays and Clay Minerals. Proceedings of the Fifteenth Conference*. 1967, Oxford. p. 259-271.
46. Kazakevich, Y.V. and R. LoBrutto, *HPLC for Pharmaceutical Scientists*. 2007: Wiley.
47. Kiso, Y. and T. Kitao, *Elution characteristics of polymeric solutes and inorganic salts in HPLC on a cellulose acetate column.* Chromatographia, 1986. **22**(7-12): p. 341-344.

CHAPTER 3

EXAMINING POLLEN AS A FILLER IN POLYVINYL ACETATE MATRICES

This chapter was published in part in *J. Mater. Chem. A,* 2014, 2, 17031-17040, and is reproduced here with permission.

3.1 Overview

Pollen grains have the potential to be effective plant-based biorenewable reinforcing fillers for polymers due to their high mechanical strength, chemical stability, and unique micro- and nano-structured surfaces. Pollen–polymer composites could form the basis for a new class of light-weight, high strength sustainable materials if compatible polymer–filler systems can be engineered. The exine shell of pollen, composed of sporopollenin, offers opportunities for surface functionalization to provide for compatibility between the pollen and the polymer matrix, but this idea has been previously unexplored. We present the first demonstration of surface functionalization of sporopollenin to enable incorporation of pollen as a reinforcing filler, using ragweed pollen in poly(vinyl acetate) (PVAc). Composites prepared with 'as received', untreated ragweed pollen displayed interfacial voids, degraded mechanical properties, and a decreased glass transition width with increased pollen loading, relative to neat PVAc. Composites prepared with pollen treated *via* an acid–base surface preparation displayed improved interfacial morphology and increasing modulus with pollen loading (29% increase). Interfacial adhesion was optimal for pollen functionalized with vinyltrimethoxysilane (VTMS), followed by in situ free radical polymerization of PVAc. In situ polymerization of functionalized pollen resulted in simultaneous stiffening and strengthening of composites (80% increase in tensile strength). Films containing treated and functionalized pollen also displayed a wider glass transition regions in the presence of pollen filler relative to neat PVAc.

3.2 Introduction

Particulate fillers are often incorporated into polymers in order to improve their mechanical, thermal, and optical properties, to name a few [1-4]. Many studies have demonstrated the successful use of non-biological materials ranging from inorganic particles, such as calcium carbonate, to carbon organic materials including carbon blacks and nanotubes as reinforcing fillers in fabricating polymer composites [5-8]. Many particulates are denser than the polymer, or are derived in a non-sustainable manner, and there is interest in finding lower density, sustainably sourced alternatives. In addition, most fillers are spherical or irregular spheroids, without significant capability to alter the particle fine surface features or geometry.

In contrast, pollen has the potential to be an effective biorenewable filler due to its high strength, chemical stability, low density and the unique architecture of its outer shell [9-13]. Besides being used directly as fillers, biological particulates such as pollen grains, bacteria, and viruses have attracted much research interest as templates for fabricating synthetic inorganic mimics that preserve their unique surface architectures [9-11, 14-16]. These inorganic mimics may also function as fillers that combine biological architecture with synthetic chemistry. While some studies have investigated pollen grains, only one study has reported utilization of pollen as a filler [17]. Furthermore, pollens from sources such as ragweed plants are ubiquitous and inexpensive natural materials that are based on sustainable, non-food resources.

Pollen grains are the carrier of the male gametes for plant reproduction. A pollen grain is composed of an outer layer (exine) and an inner layer (intine) [18, 19]. The exine is composed of sporopollenin, a highly crosslinked organic substance consisting of fatty acids, phenylpropanoids, and phenolics [20, 21]. Figure 1.4 displays monomer and macromer components that have been confirmed in sporopollenin, such as long aliphatic chains, aromatic

cross-linkers (mainly cinnamic acids), ether cross-linkages and ester functions [22]. The exine's chemical composition suggests compatibility with polymers capable of polar interactions. Underneath the exine layer, not exposed to the outer surface, lies the intine which is rich in cellulose and hemicelluloses. The cellular material carried within the grain is easily extracted using well known techniques, leaving behind a hollow, strong shell.

To date, the one known study that explored pollen grains as reinforcing fillers of polymers used solution casting of native, untreated ragweed pollen in polystyrene and polycaprolactone [17]. Interfacial voids between the polymer and pollen filler were reported to result in only small improvements in strain at break at low pollen loadings. One may expect that utilization of more polar polymers, as well as polymerizing monomer *in situ* in the presence of functionalized pollen may enhance interfacial compatibility. This can be rationalized by expected increased adhesion due to covalent binding of chains to the pollen surface as well as a decreased viscosity of the initial reaction mixture (relative to a solvent-casting solution).

To explore these ideas, in the present study pollen fillers were incorporated into a more polar matrix polymer than those previously explored, poly(vinyl acetate) (PVAc), by both solution casting and *in situ* free radical polymerization of vinyl acetate monomer (VAM). Short ragweed pollen (*A. artemisiifolia*) was selected as a model pollen grain because of its natural abundance, unique 'spiny' echinate surface morphology, and previously published adhesion data.[23, 24]As received pollen was compared to pollen modified by two treatments: acid-base hydrolysis and functionalization with an organosilane. The effectiveness of pollen as a reinforcing and strengthening filler in PVAc was characterized by mechanical properties, interfacial morphology, and glass transition temperature of pollen-polymer composites as a function of pollen loading, processing method, and pollen treatment.

3.3 Experimental

3.3.1 Materials

Defatted Short ragweed (D, A. artemisiifolia, Greer Laboratories) pollen grains were stored at 4 °C prior to use. VAM (Sigma Aldrich) was filtered through aluminum silicate to remove hydroquinone inhibitor. Azobisisobutyronitrile (AIBN, Sigma Aldrich) was of reagent grade and absolute ethanol was used as solvent. Potassium hydroxide (KOH, EMD Millipore) and phosphoric acid (H_3PO_4, BDH chemicals) were used for pollen treatment. Vinyltrimethoxysilane (VTMS, Sigma Aldrich) was used to functionalize the pollen surface. For solution processing, dichloromethane (DCM, Sigma Aldrich) was used as a solvent for PVAc (Sigma Aldrich, M_w = 500,000).

3.3.2 Solution Processing of Pollen-PVAc Composites

A measured mass of pollen was dispersed in DCM and sonicated for uniform dispersion. The desired mass of polymer was then added step wise to the solvent to make a 15 vol% PVAc solution. The mixtures were agitated on a rotational stirrer for 24 h. The solutions were cast on glass plates with a doctor blade, and slowly dried under a solvent saturated environment for 24 h. The films were dried under vacuum for 24 h at 90 °C. Samples were slowly cooled down to room temperature before peeling the films from the plates using a razor. Average film thicknesses were 130 μm ± 20 μm.

3.3.3 *In situ* Polymerization of Pollen-PVAc Composites

AIBN (0.0135 g) was added to VAM (32.66 g) in a round bottom flask. After the AIBN dissolved, 15 mL of ethanol were also added to the flask. For composites, a measured mass of pollen grains (for composites containing 1-15 vol% of pollen) was dispersed in the ethanol and sonicated prior to addition to the flask, to ensure pollen dispersion. The flask was purged with

nitrogen and the mixture was stirred at 75 °C for 2.5 h. The resulting solution mixtures were cast on glass plates with a doctor blade, and slowly dried under a solvent saturated environment for 24 h. The films were dried under vacuum for 24 h at 90 °C. Samples were slowly cooled down to room temperature before peeling the films from the plates using a razor.

3.3.4 Extraction of Pollen Cellular Material

An acid-base treatment (hereafter labeled as AB) was used to clean and isolate the exine shell for incorporation in polymer films as well as to prepare them for further functionalization [19, 25]. Briefly, pollen was dispersed in 6w/v% KOH solution for 24 hours while stirring. After washing the pollen with hot water, ethanol, and drying the pollen, it was dispersed in 85% H_3PO_4 for 7 days. This pollen was dried after washing with hot water, acetone, and ethanol. This process caused the pollen grains to lose ~80% of their original weight. AB pollen was incorporated in polymer films via the *in situ* polymerization mentioned above. Figure 3.1 shows D pollen with intracellular material intact versus hollow AB pollen.

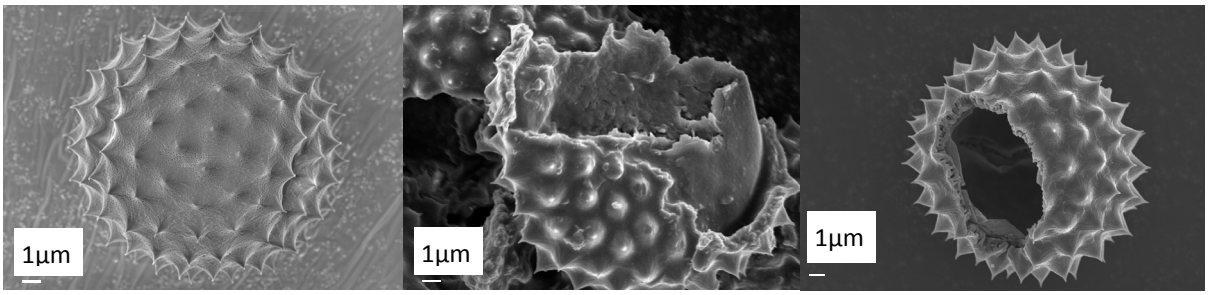

Figure 3.1: Native D pollen (left), D Pollen crushed exposing intracellular material (middle), and hollow AB pollen (right).

3.3.5 Silane Functionalization of Pollen Grains

AB pollen was used as the starting point for functionalization with VTMS (hereafter referred to as ABV) to enable grafting of polymer chains to the pollen surface. AB pollen was heated under vacuum at 100 °C to remove adsorbed water then dispersed in toluene and sonicated. This solution was purged under nitrogen for 30 minutes while stirring. VTMS was

added to the flask with a syringe through a rubber stopper. This solution was heated overnight and pollen was recovered after washing with toluene, hexane, and ethanol. ABV pollen was incorporated in polymer films via the *in situ* polymerization mentioned above. Figure 3.2 shows a schematic for the reaction of VTMS with pollen hydroxyl groups and functionalized pollen's copolymerization with vinyl acetate monomer. Average film thicknesses were 160 μm ± 10 μm.

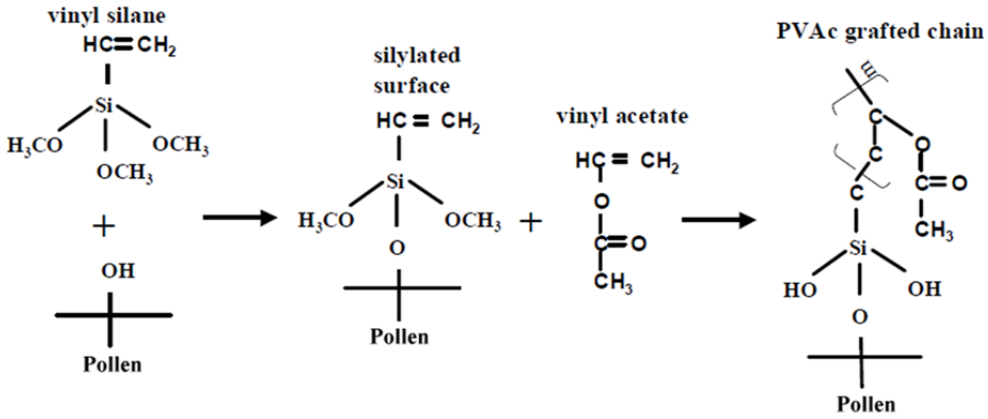

Figure 3.2: Schematic of pollen surface functionalization and copolymerization of functionalized pollen with monomer (adapted from [26]).

3.3.6 Sample Types

The composite processing methods and pollen treatments explained above were combined into four different sample types that were characterized in this study. These samples were as follows: solution processed PVAc with native defatted pollen (S-D), polymerized PVAc with native defatted pollen (P-D), polymerized PVAc with acid-base pollen (P-AB), and polymerized PVAc with silane functionalized AB pollen (P-ABV).

3.3.7 Characterization

FTIR spectra were obtained on a Thermo Scientific spectrophotometer from 4000 cm^{-1} to 400 cm^{-1}. Pollen received as is, acid treated, and functionalized with VTMS were mixed with KBr powders and pressed in pellets for measurement. A high-throughput mechanical characterization (HTMECH) apparatus was used to measure mechanical properties including tensile strength,

elastic modulus, and toughness, as described previously [27]. Briefly, the polymer films were mounted on a steel grid and contacted with a steel pin with a 1.5 mm diameter hemispherical cap at a constant strain rate (0.5mm/s). The pin is oriented normal to the film surface, resulting in equi-biaxial deformation. For each sample, an average thickness was obtained using 9 measurements with a micrometer, 9 stress–strain profiles were measured to failure, and mechanical properties of the films were obtained. All mechanical tests were performed under ambient conditions. Scanning electron microscopy (SEM) was performed with a Zeiss Ultra-60 FE-SEM instrument to examine the interfacial morphology of both freeze fractured and HTMECH fracture surfaces of the composites. Molecular weights of polymerized samples were measured by GPC. A Shimadzu liquid chromatograph was used with THF as the eluent. One Phenogel 5 mm linear column and one Phenogel 5 mm mixed bed column were calibrated with 10 PS standards samples from 500 to 1.2×10^{-6} g mol^{-1}. A Netzsch STA409PG was used for simultaneous thermogravimetric analysis (TGA) and differential scanning calorimetry (DSC) of pollen samples after treatment steps. Approximately 8 mg of pollen (D, AB, ABV, or AB-PVAc) were used for each experiment. A heating rate of 10 K/min was used up to 900 °C under a mixed gas stream of nitrogen and air. Differential scanning calorimetry (DSC) measurements were performed on composite samples with a TA Instruments DSC Q200 in a nitrogen atmosphere, using specimens of 8–9mg cut from films and sealed in aluminum pans with lids. Samples were heated from 10 to 80 °C, above T_g of the pure PVAc, at 20 °C/min, kept isothermal for 1 min, cooled down to 10 °C at 20 °C/min, and held isothermal for 1 min again. This cycle was repeated twice. T_g values were taken from the second cycle from the onset value of the tangents on the heat flow curves. The width of the glass transition region, ΔT_g, was taken as the difference between the endpoint and the onset temperatures. The density of materials was assessed by

pycnometry in a 25 ml specific gravity bottle. Ethanol was used to determine the density of D and AB pollen and water was used to determine the density of neat PVAc and pollen-PVAc composites. A known mass of material, m_s, was added to the bottle of known mass (m_0). The liquid of known density was then added to bottle and the total mass, m_T, is measured. The density of the solid is given by:

$$\rho_s = m_s \Big/ \left(V - \frac{m_T - m_0 - m_s}{\rho_{H2O}} \right) \tag{3.1}$$

where V is the volume of the flask.

3.4 Results and Discussion

3.4.1 FTIR Analysis

Figure 3.3 shows the FTIR spectra of native pollen and pollen recovered following each chemical modification (D, AB, ABV, and AB-PVAc). The cellulose fingerprint in D pollen appears in the 1100 to 900 cm^{-1} region, due to the presence of polysaccharide material in the pollen intine [21, 28]. The spectrum for AB pollen shows an important lack of peaks associated with polysaccharides in this range, indicating the full or partial dissolution the intine [29, 30]. Additionally, D pollen displays a very broad band at 3375 cm^{-1} due to O-H stretching, having a stronger intensity than the –CH stretches of $–CH_2$ groups at 2910 and 2840 cm^{-1}. In contrast, AB pollen displays a more narrow –OH band with a smaller intensity than the $–CH_2$ peaks. AB pollen's OH band is also shifted to higher wavenumbers around 3450 cm^{-1}, indicating increased fractions of free hydroxyls. The C=O stretch of carboxyl groups also shifts from 1672 cm^{-1} to 1707 cm^{-1} in D and AB pollen, respectively. The acid-base hydrolysis decreases the ratio of hydroxyl to methylene groups, likely due to the dissolution of the strongly H-bonded cellulosic intine and results in higher fractions of free hydroxyl (not associated with the cellulose) and

carboxyl groups in the sporopollenin, which would be more accessible for surface interactions with a composite matrix phase.

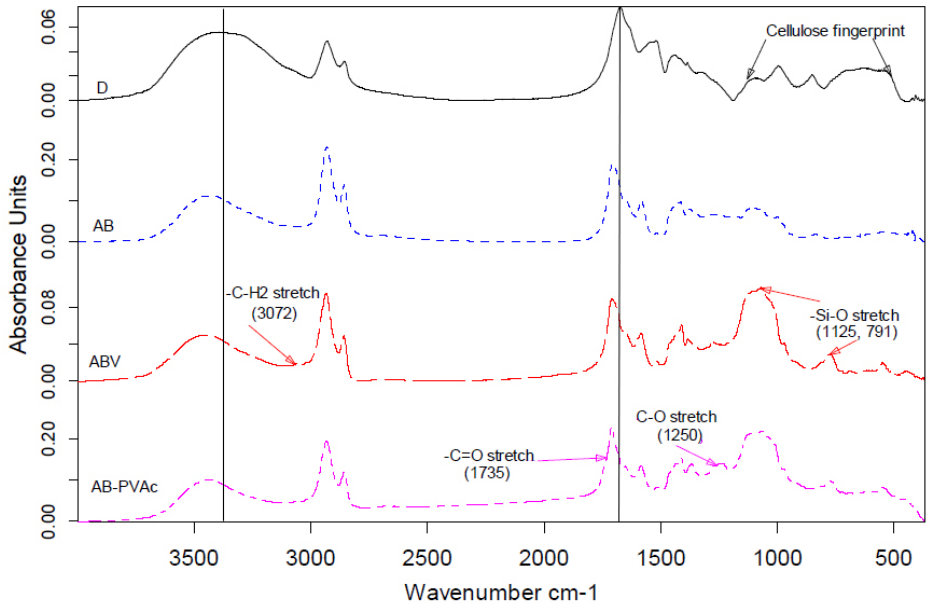

Figure 3.3: FTIR spectra of pollen treatment steps.

Silane functionalized pollen (ABV) spectra displayed a large band at 1125 cm^{-1} and a peak at 791 cm^{-1}, which are assigned to stretching vibration of Si-O-Si bonds [31, 32]. There is an additional small peak at 3072 cm^{-1} assigned to the vinyl acetate groups on the silane [33]. These peaks indicate the successful attachment of silane to the pollen surface. Finally, pollen recovered from the copolymerization of ABV pollen with monomers displayed a peaks characteristic of PVAc at 1250 cm^{-1} and a shoulder peak at 1735 cm^{-1} assigned to stretching vibrations of C-O and C=O bonds, respectively [34]. These peaks confirm the successful functionalization of pollen with VTMS and the grafting of polymer chains to the pollen surface (AB-PVAc) following *in situ* vinyl acetate polymerization.

3.4.2 Interfacial Morphology

Figure 3.4 to Figure 3.7 present the SEM images of freeze fractured and HTMECH fracture surfaces of pollen-PVAc composites. Figure 3.4 shows the fracture surfaces for S-D

films. Freeze fracture samples (Figure 3.4a and Figure 3.4b) reveal the presence of interfacial voids between native D pollen and the polymer matrix. These voids appear smaller than the voids observed in our previous work utilizing less polar polystyrene and polycaprolactone, but are still present [17]. Thin polymer bridges at the pollen-polymer interface (Figure 3.4b) can be observed where the matrix has pulled away from the pollen surface. HTMECH fracture surfaces (Figure 3.4c and Figure 3.4d) reveal that the pollen lies in void pockets of the polymer matrix and the pollen simply introduces voids in the material.

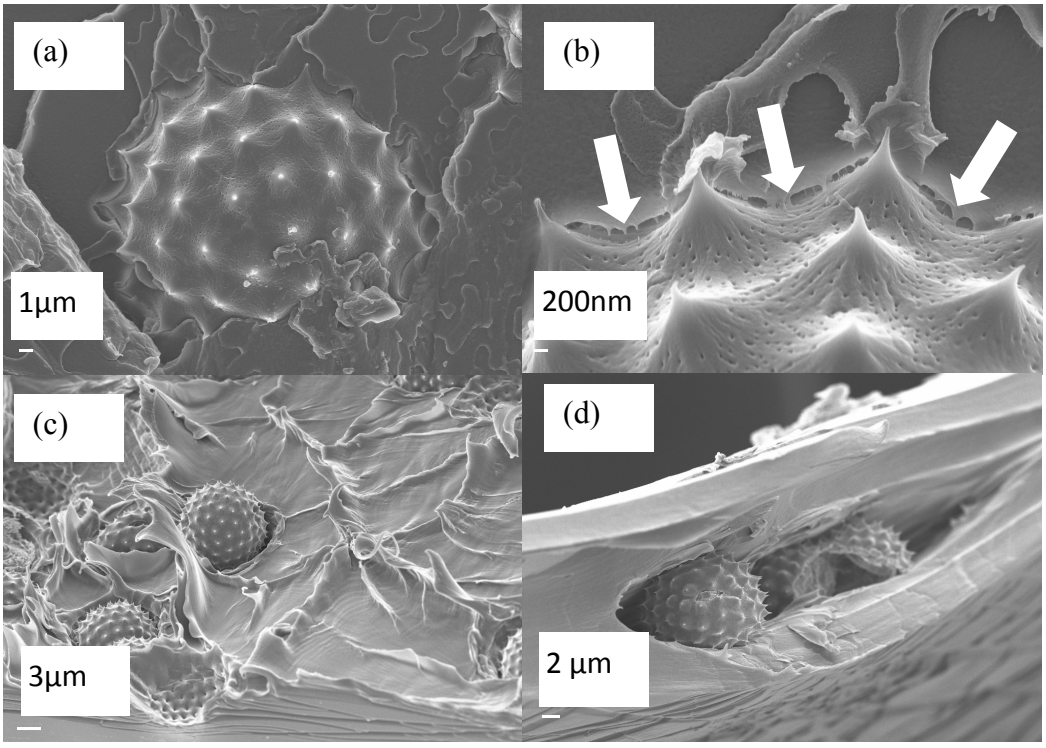

Figure 3.4: S-D fracture surfaces. Freeze fractured cross sections (a and b) and HTMECH fracture surfaces (c and d). Arrows indicate polymer bridging.

Figure 3.5 shows similar results for P-D films. Freeze fracture samples still reveal voids surrounding some of the pollen grains (Figure 3.5a). However, some better adhered interfaces are present (Figure 3.5b). HTMECH fracture surfaces (Figure 3.5c and Figure 3.5d) still show void pockets surrounding pollen grains and significant separation at the interface. The pockets are not as large as in the solution processed films (Figure 3.4). However, polymerized films fractured at

much lower stresses than solution processed films, so the smaller void pockets may be due to the smaller magnitudes of stress and deformation.

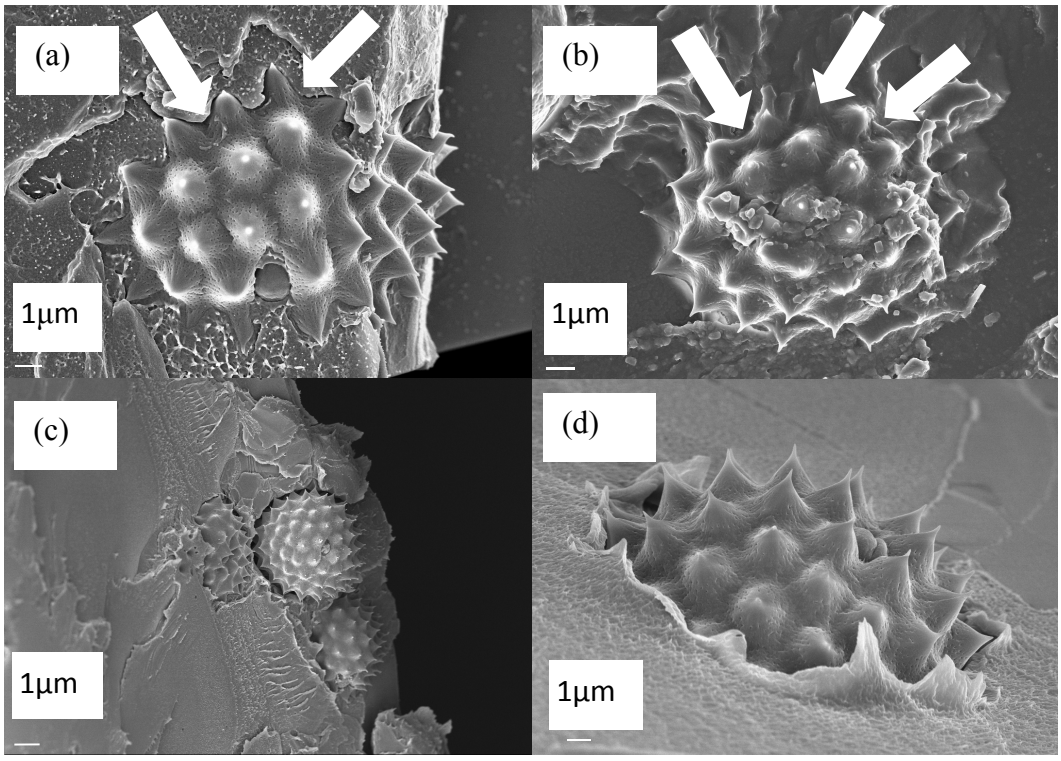

Figure 3.5: P-D fracture surfaces. Freeze fractured cross sections (a and b). 6a arrows indicate voids and 6b arrows indicate better adhered interfaces. HTMECH fracture surfaces (c and d).

Figure 3.6 shows the fracture surfaces for P-AB films. Freeze fracture samples (Figure 3.6a and Figure 3.6b) show an optimized interface for P-AB films versus S-D and P-D films, with a continuous interface between polymer matrix and pollen grains. No polymer bridging or interfacial voids are present surrounding pollen grains. HTMECH fracture surfaces (Figure 3.6c and Figure 3.6d) further establish the optimized interface. Void pockets are no longer present with AB pollen that were present in films with D pollen. The optimized interface of P-AB films is likely due to increased specific interactions between the pollen surface and the polymer matrix. The acid-base treatment eliminates intracellular material (Figure 3.1) that may block pollen surface hydroxyl and carboxyl groups. These exposed –OH and C=O functional groups

likely increase hydrogen bonding (-OH) or dipole-dipole and van der Waals interactions with PVAc's carbonyls [35, 36]. Additionally, additional hydroxyl groups may be generated on the pollen surface due to phosphorylation of hydroxyls and/or carboxyls, [30] thus increasing opportunities for adhesive interactions between pollen and the polymer matrix.

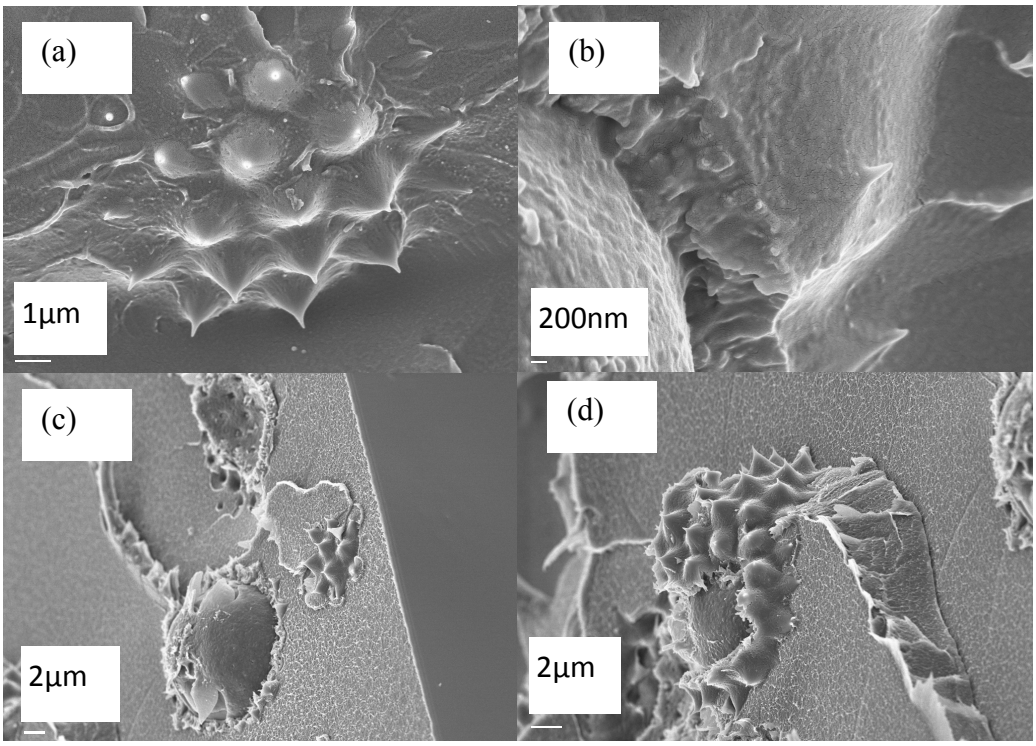

Figure 3.6: P-AB fracture surfaces. Freeze fractured cross sections (a and b) and HTMECH fracture surfaces (c and d).

Figure 3.7 shows the fracture surfaces for P-ABV films. Freeze fractured samples (Figure 3.7a and Figure 3.7b) indicate that polymer coats the pollen surface and the pores of the pollen surface are less visible than previously observed due to this coating (Figure 3.7b). HTMECH fracture surfaces (Figure 3.7b and Figure 3.7d) indicate the presence of deformed polymer that is still attached to the pollen after fracture. These images suggest that polymer is strongly attached to the pollen surface, possibly an indicator of successful grafting.

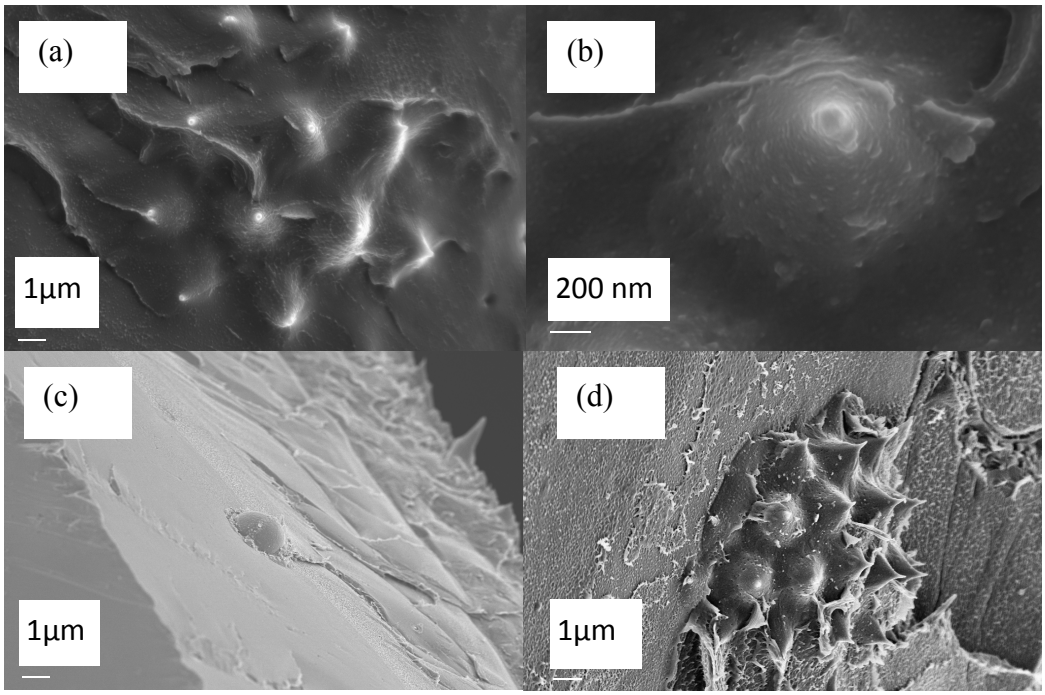

Figure 3.7: P-ABV fracture surfaces. Freeze fractured cross sections (a and b) and HTMECH fracture surfaces (c and d).

3.4.3 Mechanical Properties

Figure 3.8 to Figure 3.11 show the mechanical properties obtained for the various pollen-PVAc composites. Figure 3.8 shows properties for S-D films. Elastic modulus decreased continuously with increased pollen loading. Tensile strength and strain at break both increased slightly at low pollen loadings and then decreased continuously with increased pollen loading. The mechanical properties measured for S-D films are comparable to mechanical properties of PVAc and PVAc-zeolite composites previously measured with the HTMECH [37]. The properties of PVAc and PVAc-zeolite measured with HTMECH were also found to match properties measured with conventional tensile testing of the same films.

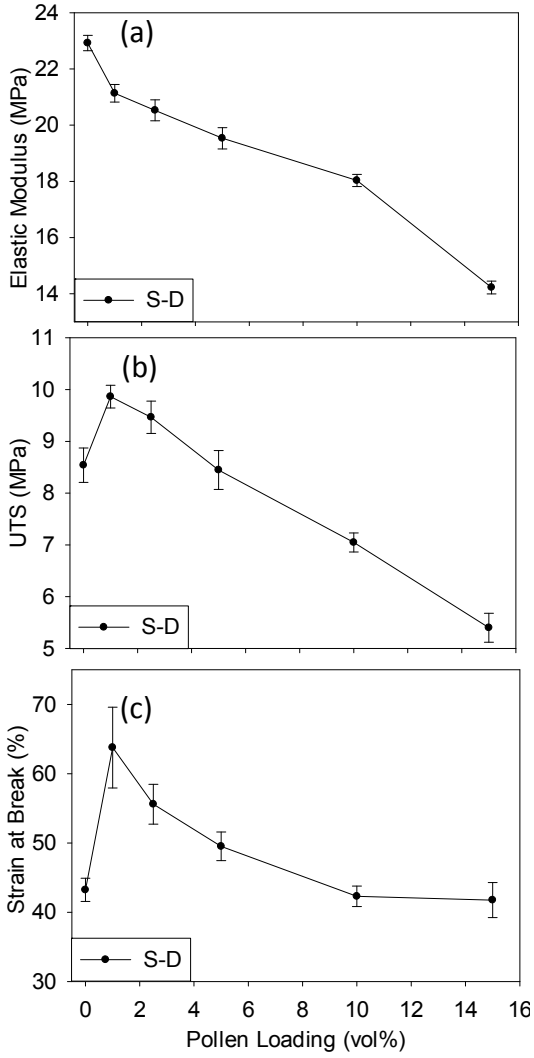

Figure 3.8: Elastic modulus (a), UTS (b), and strain at break (c) of S-D composites. The error bars are 95% confidence intervals.

Figure 3.9 shows similar trends in the properties for P-D films. The elastic modulus trend is slightly different than that of S-D films, with a possible small increase at low pollen loadings and a more gradual decline as pollen content increases further. Again, tensile strength and strain at break both increased slightly at low pollen loadings and then decreased continuously with increased pollen loading. The larger mechanical property values of S-D films versus polymerized films are due to the higher molecular weight of solution cast films (500,000 g/mol). The molecular weight of polymerized films was ~78,000 g/mol measured by gel permeation chromatography.

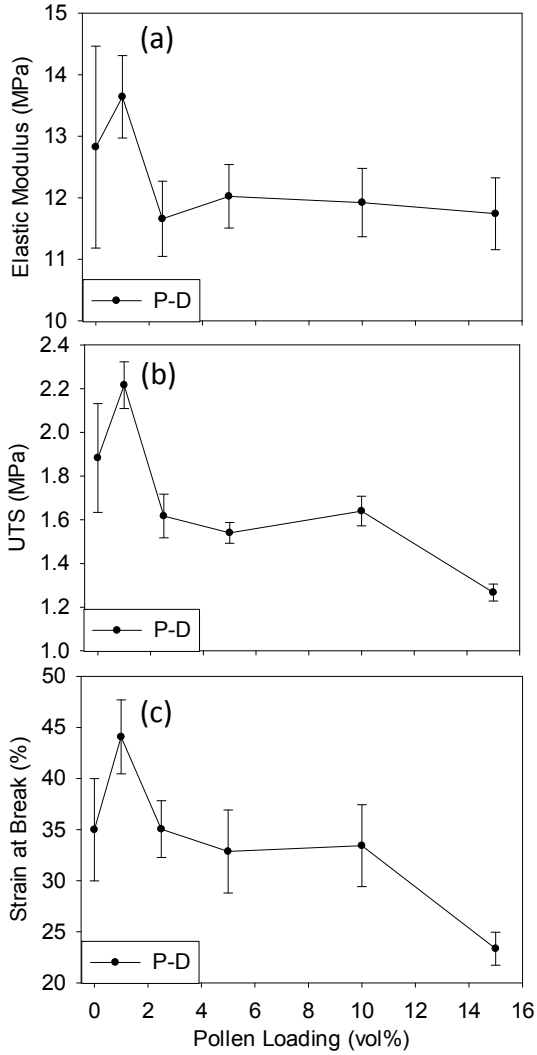

Figure 3.9: Elastic modulus (a), UTS (b), and strain at break (c) of P-D composites. The error bars are 95% confidence intervals.

Properties for P-AB films are shown in Figure 3.10. In contrast to S-D and P-D films, here, the elastic modulus increases with increasing loading. It is well-known that elastic modulus is independent of interfacial adhesion when it is measured at low deformations where interfacial separation does not occur [3]. As seen in Figure 3.4 and Figure 3.5, films with D pollen that display decreasing modulus also contain interfacial voids after preparation. Thus, an increasing loading of D pollen increases the amount of interfacial voids, decreasing the stiffness of the material [38]. On the other hand, films with AB pollen, which show increasing modulus, lack interfacial voids after preparation (Figure 3.6). Thus, incorporation of AB pollen eliminates

interfacial voids associated with untreated D pollen, which corresponds with increased material stiffness. Additionally, small increases in tensile strength and strain at break at low pollen loadings are absent. The continual decrease in these properties, as well as the lack of a toughening effect at low pollen loadings, further suggests the absence of interfacial voids. However, the decrease in tensile strength and strain at break with pollen loading indicate that the degree of adhesion between the phases is still low, although interfacial voids are not obvious in the SEM.

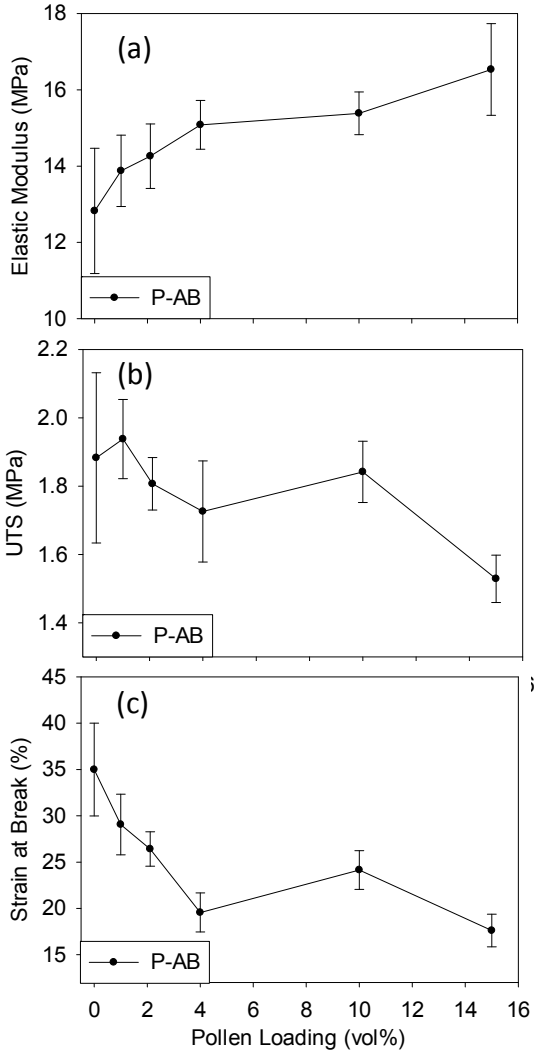

Figure 3.10: Elastic modulus (a), UTS (b), and strain at break (c) of P-AB composites. The error bars are 95% confidence intervals.

Figure 3.11 shows the properties of P-ABV films. Again, elastic modulus increases with increased pollen loading, similar to P-AB. In contrast with all other films, the tensile strength and strain at break of P-ABV films increase continually with increased pollen loading. This suggests that grafted polymer chains that are covalently bonded to the pollen surface are entangled with the chains of the polymer matrix. These mechanical observations and the proposed covalent-derived adhesion are consistent with the SEM evidence of strongly attached residual polymer at fracture surfaces (Figure 3.7).

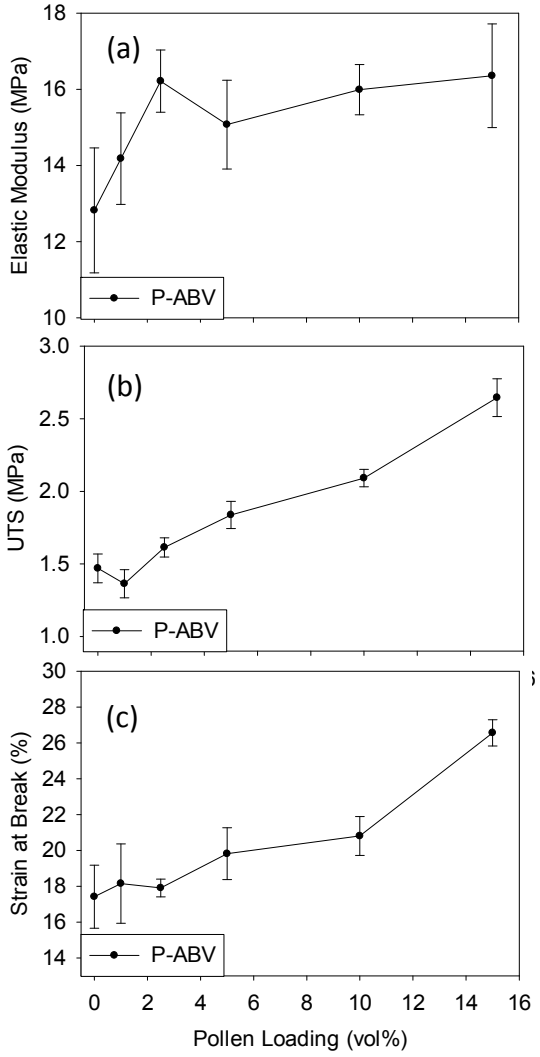

Figure 3.11: Elastic modulus (a), UTS (b), and strain at break (c) of P-ABV. The error bars are 95% confidence intervals.

The stiffening effects observed in P-AB and P-ABV (Figure 3.10a and Figure 3.11a) films indicate that the pollen exine shell has a higher inherent modulus than the polymer matrix, although independent measurements of exine tensile modulus are not available. Both curves appear to approach a plateau at higher pollen loadings. A plateau is sometimes indicative of particle-particle interactions and agglomeration, [3] although this was not evident from the SEM images. Although the pollen is micron sized, it introduces nanoscale spine features in the composite, which may allow particle-particle interactions at distances greater than expected based on the nominal particle diameter. There has been only one other study that reports a pollen modulus. This study reports the E_h (the product of a compressive elastic modulus and wall thickness) of desiccated ragweed pollen as 1653 N/m via micromanipulation techniques [12]. This results in a compressive modulus of 1653 MPa, using an approximate wall thickness of 1 micron for ragweed pollen. This value was used to compare the experimental modulus data to a lower bound model [3, 39-41] for elastic modulus as shown in Figure 3.12. The Reuss lower bound assuming iso-stress is given by the inverse rule of mixtures:

$$E_C^{lower} = E_f E_m / \left[E_f \left(1 - V_f\right) + E_m V_f \right] \tag{3.2}$$

where E_c^{lower}, E_f and E_m are the modulus of the composite, the filler, and the neat matrix respectively. V_f is the volume fraction of the filler. Figure 3.12 shows that the experimental data for both P-AB and P-ABV films fall within the lower bound, when using the compressive pollen modulus of 1653 MPa. Although not shown here, the data also fell well into the Voigt upper bound, based on the rule of mixtures. Two models, Halpin-Tsai and Counto, which fall above the lower bounds, were fit to the experimental data in order to estimate the modulus of pollen. The Halpin-Tsai semi-empirical model is shown in Equation 3.3:

$$E_c = E_m \left(\frac{1 + \eta \zeta V_f}{1 - \eta V_f} \right) \tag{3.3}$$

ζ and η are expressed as:

$$\zeta=2+40V_f^{10} \tag{3.4}$$

$$\eta=\left(\frac{E_f}{E_m}-1\right)/\left(\frac{E_f}{E_m}+\zeta\right) \tag{3.5}$$

The Halpin-Tsai model [3, 40-42] predicted a modulus of 67.3 MPa for AB pollen and 62 MPa for ABV pollen versus the measured 12.8 MPa of the neat polymer. The largest percent errors were 8.8% and 17.5% for P-AB and P-ABV respectively. The Counto model, [3, 43, 44] shown in Equation 3.6, is a model for two phase particulate composites assuming a perfect bonding between filler and matrix and gives predictions in good agreement with a wide range of test data.

$$E_c=E_m\left[1+V_f/\left(\sqrt{V_f}-V_f+\frac{E_m}{E_f-E_m}\right)\right] \tag{3.6}$$

As shown in Figure 3.12, the Counto model, which is non-linear, provides a slightly better fit. The model predicted a modulus of 68.2 MPa for AB pollen and 69.8 MPa for ABV pollen versus the measured 12.8 MPa of the neat polymer. The largest percent errors were 6.3% and 15.4% for P-AB and P-ABV respectively. As expected, the predicted moduli of AB and ABV pollen are comparable for both models because elastic modulus is independent of interfacial adhesion when it is measured at low deformations where interfacial separation does not occur [3]. The data is found to still fall above the lower bound when the estimates of pollen modulus from the Halpin-Tsai and Counto models are used as E_f. Additional models were considered such as the Takayanagi I, [45] which can account for decrease in reinforcement efficiency due to filler aggregation above percolation. However, in this case, pollen loadings are below percolation if they are considered as hard spheres (V_f = .18), so this model is not appropriate. Thus, the

modeling shown here may overestimate the modulus of the pollen somewhat but is still useful due to the challenge of fitting data the displays plateauing behavior.

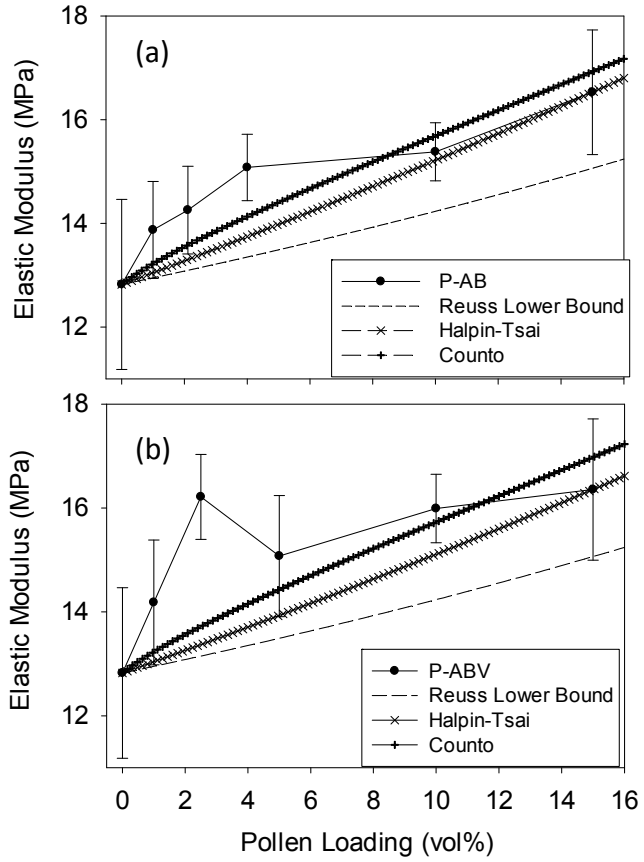

Figure 3.12: Experimental data versus theories for elastic modulus: a) P-AB and b) P-ABV experimental modulus data.

3.4.4 Thermal Properties

Figure 3.13 shows both the percent weight loss and heat flow of both D, AB, ABV, and AB-PVAc pollen. In Chapter 2, weight loss and heat flow behavior for D and AB pollen were discussed. Briefly, weight loss occurred up to ~500 °C for D pollen and ~560 °C for AB pollen. Two weight loss events correspond with first the burning off of components intracellular material, cellulose, and hemicellulose (200 – 400 ˚C) and the second weight loss event corresponds with the decomposition of higher molecular sporopollenin, 400 – 550 ˚C). The temperature of the first event shifts from 333 ˚C to 344 ˚C for D and AB pollen respectively due

to more thermally resistant crystalline cellulose burning off as opposed to amorphous cellulose (dissolved in acid-base treatment). The heat flow plots also reveals that the temperature of the second event shifts from 483 ˚C to 503 ˚C for D and AB pollen respectively due to decomposition of a more pure sporopollenin. Finally, the residual masses are .48% and .94% D and AB respectively.

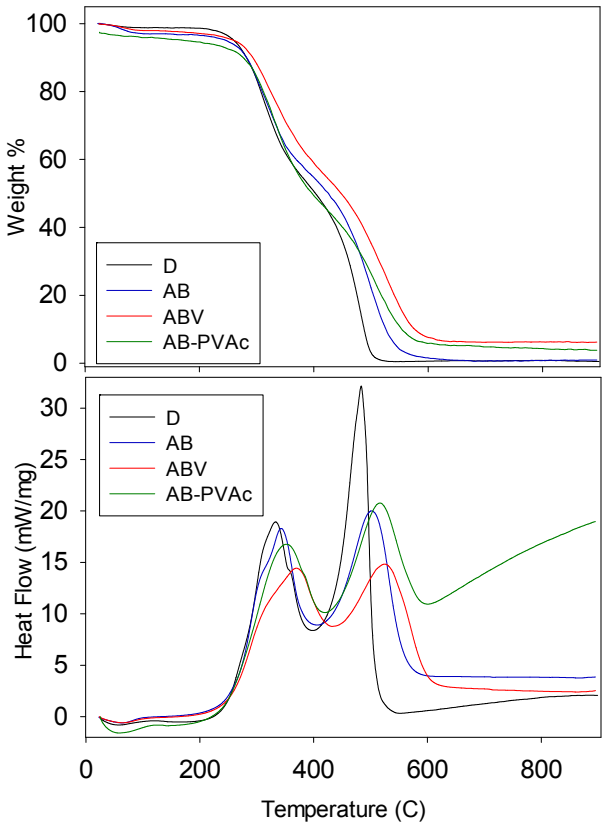

Figure 3.13: Percent weight loss and heat flow for both D, AB, ABV, and AB-PVAc pollen.

Weight loss occurred for ABV up to ~ 600 °C. Heat flow plots reveal that the temperatures of the first and second event shift to their highest temperatures of 371 °C and 527 °C, respectively. Finally, the residual mass of ABV pollen is 6.2%. This means the grafting ratio of VTMS (grafting ratio = residual mass % ABV – residual mass % AB) on the surface is 5.3%. These results provide further indication of the successful functionalization of the pollen surface. Both decomposition peaks shift to higher temperatures due to the presence of additional

functional groups and organics on the pollen surface protecting the surface and making it more thermally stable. Additionally, the increased residual mass is likely due to the oxidation of Si in air, resulting in oxide residue from SiO_2 from the silane coating.

Weight loss for AB-PVAc occurred up to ~ 570 °C. The heat flow plot reveals the temperature of the first and second event occurred at 355 °C and 517 °C, respectively. The residual mass is 3.8%. This means the grafting ratio of PVAc (grafting ratio = residual mass % ABV – residual mass % AB-PVAc) is 2.4%. These results also provide further indication of the successful attachment of PVAc to the pollen surface. Both decomposition peaks occur at higher temperatures than AB pollen, but lower temperatures than ABV pollen. A PVAc coating improves thermal stability versus AB pollen, but is not as thermally stable as ABV pollen because of the silane coatings oxidation to SiO_2, which is more thermally resistant than PVAc. Also, the residual mass is smaller than that of ABV because of the addition of a PVAc coating, reducing the contribution of the SiO_2 to the residual mass.

Glass transition behavior was measured for the four different sample types as a function of pollen loading (0, 5, and 15 vol%). Little dependence was found of T_g values on pollen loading. However, the width of the glass transition region appears to correlate with the observed interfacial and mechanical properties. Table 3.1 reports the width of the glass transition region, ΔT_g, for the four different composites. Both S-D and P-D films display decreasing ΔT_g with increased pollen loading. The polymer chains at the polymer-pollen interface of these composites exhibit faster relaxation dynamics due to increased mobility of chains at the interfacial voids observed with SEM. Thus they display a decreasing trend in the width of the glass transition region. P-AB and P-ABV films display larger ΔT_g in the presence of pollen versus neat polymer. Here, the polymer chains at the polymer-pollen interface exhibit slower relaxation dynamics due

to decreased mobility of chains at the interface.[46, 47] This corresponds with the optimized interface (Figure 3.6 and Figure 3.7) and improved mechanical properties of these composites (Figure 3.10 and Figure 3.11). Polymer chains may show improved interactions with the AB pollen surface versus the D pollen surface due to increased specific interactions and/or improved Van der Waals based compatibility, resulting in a larger width of the glass transition region in the presence of pollen filler. A similar result with ABV pollen is likely due to improved interactions of grafted polymer chains covalently bonded to the pollen surface that are able to entangle with the chains of the polymer matrix. Also, ΔT_g for P-AB and P-ABV films initially increase at lower loadings and then decrease at higher loadings, but still remain higher than the ΔT_g of the neat polymer. This may indicate an optimum loading exists where pollen filler has its maximum effect on ΔT_g. At higher loadings, particle-particle interactions become more likely which could decrease pollens overall effect on ΔT_g because of a reduction in pollen-PVAc interface. This may also play a role in the plateauing behavior observed for P-AB and P-ABV modulus. At higher loadings, the contribution of the pollen-PVAc interface to increased modulus may be lessened compared to the contribution at lower loadings where particle-particle interactions do not reduce the pollen-PVAc interfacial area.

Table 3.1: Width of glass transition regions (ΔT_g) of pollen-PVAc composites.

Pollen Loading (vol %)	S-D ΔT_g (°C)	P-D ΔT_g (°C)	P-AB ΔT_g (°C)	P-ABV ΔT_g (°C)
0	8.81	6.44	6.44	6.44
5	6.44	6.33	8.12	7.83
15	4.57	5.06	7.03	7.37

3.4.5 Density of Materials

Using pycnometry, the density of D was measured as 1.305 g/cm^3, while the density of AB pollen was measured as 1.165 g/cm^3. The intracellular material present in D pollen makes it denser than the hollow AB pollen as seen in Figure 3.1. The native D pollen is much less dense than widely used fillers in industry, such as talc (ρ = 2.75 g/cm^3) and calcium carbonate (ρ = 2.71 g/cm^3), and has a density comparable to advanced fillers such as carbon nanotubes (ρ = 1.3-1.4 g/cm^3), cellulose (ρ = 1.5g/cm^3) and starch (ρ = 1.5 g/cm^3). Interestingly, the hollow shells of AB pollen have a density that is lower than all of these fillers. Figure 3.14 shows AB and D pollen dispersed in a PVAc-ethanol solution. D pollen settles out of solution in a matter of days. However, AB pollen remains well dispersed in solution for several months, further indicating the decreased density of AB pollen versus D Pollen.

Figure 3.14: AB pollen dispersed in PVAc solution after several months (left) and D pollen settled out of PVAc.

Pycnometry was also used to determine the densities of the neat PVAc and pollen-PVAc composites. Neat PVAc's density was measured as 1.195 g/cm^3, matching its reported value of 1.19 g/cm^3. P-D and P-AB film densities were measured as 1.269 g/cm^3 and 1.183 g/cm^3, respectively. AB pollen decreased the material density by 1.04% at 15 vol% pollen loading versus neat PVAc. Thus, unlike many other fillers would, pollen did not significantly impact the

low density of the PVAc matrix. Also, interesting future work may involve sealing AB pollen and trapping air within the shells, which would allow for larger density reductions.

3.4.6 Comparison to Previous Study

An initial study that explored pollen as reinforcing filler of polymers used solution casting of native non-deffatted (ND) ragweed pollen in polystyrene (PS) and polycaprolactone (PCL) [17]. Figure 3.15 and Figure 3.16 display the interfacial morphology of these composites.

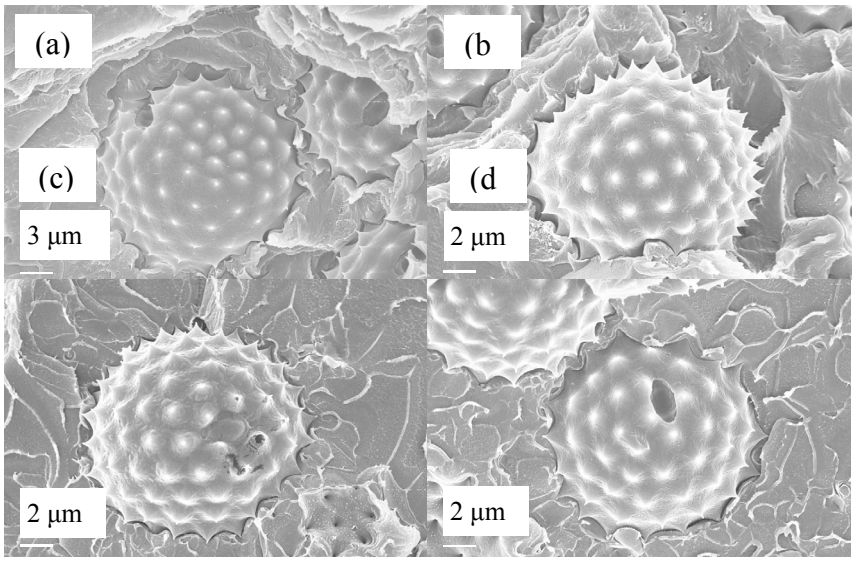

Figure 3.15: Freeze fracture surfaces of ND pollen in PS.

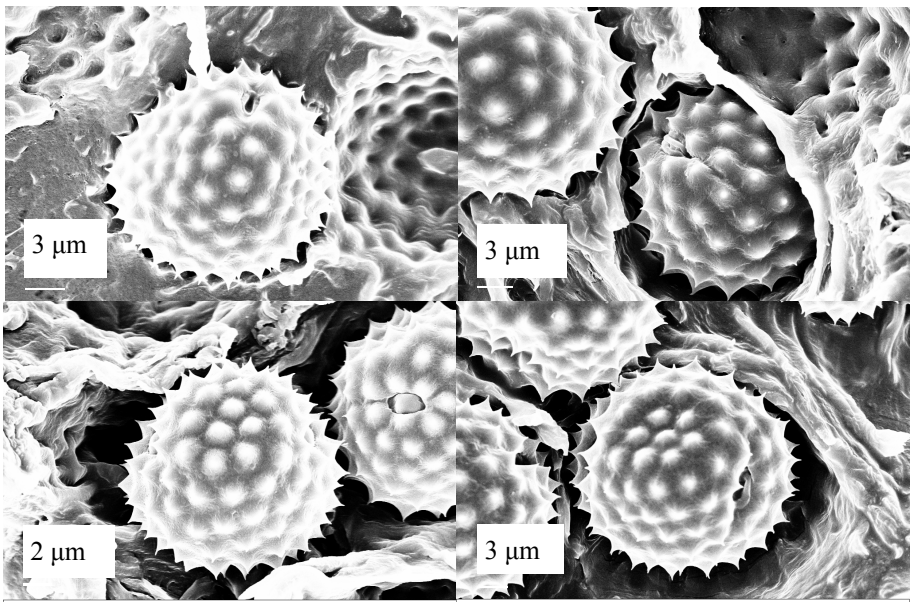

Figure 3.16: Freeze fracture surfaces of ND pollen in PCL.

The work presented in this chapter utilized as received defatted pollen grains as opposed to non-defatted pollen grains, which still have some pollen coat present. One may expect this additional impurity to impact composite properties. The pollen coat may remain on the pollen surface decreasing adhesion between the exine surface and the polymer matrix or it may impact polymer properties if dispersed throughout the polymer solution. However, as Figure 3.4, Figure 3.5, Figure 3.15, and Figure 3.16 show, interfacial voids are present in both cases of ND and D pollen.

PS is an aromatic polymer with a T_g of 100 °C, PCL is a biodegradable semi-crystalline polymer with a T_g of -60 °C and T_m of 60 °C, and PVAc is a rubbery polymer with a T_g of 30 °C. Despite the various differences in polymer type and properties, interfacial voids were present in all systems. However, the size of the interfacial voids varied to some degree. The largest voids were present in PCL, as shown in Figure 3.16. The pollen surface is known to be composed of primarily fatty acids, a smaller fraction of aromatic moieties, and including ester and hydroxyl groups. Based on functionalities, it was expected the PCL may display favorable interactions with the pollen surface due to the polymers methylene and ester groups. However, the presence of these large interfacial voids were attributed to the hindrance of interactions of polymer chains with spiked, convex surface features due to the ordered crystalline regions of PCL. PS composites displayed smaller interfacial voids and partial wetting of pollen grains (Figure 3.15). Based on functionalities, it was not expected that PS (aromatic) would display enhanced interactions with pollen relative to PCL. Thus, smaller voids and partial wetting with PS was attributed to the amorphous nature of PS, which would facilitate interaction of polymer chains with spiked, convex surface features of pollen. The voids in PVAc composites appear even smaller, but are still present. PVAc contains ester groups and is amorphous, which play a role in

PVAc composites displaying the smallest voids with native pollen grains. Considering these results, polymer thermal properties may not play a major role in the wetting of pollen grains. Interfacial voids existed for a PCL, PVAc, and PS despite their T_g being well below room temperature, near room temperature, and well above room temperature respectively.

Figure 3.17 and Figure 3.18 display reanalyzed mechanical properties measured with the HTMECH of PS and PCL composites respectively. The initial analysis of mechanical properties was obtained with an automatic method in the HTMECH software. During the PVAc work it was discovered that this method gave erroneous results, especially in elastic modulus and strain at break measurements. This was solved by simply using a manual method in the HTMECH software, which allowed for selecting the appropriate analysis range of stress strain curves and the appropriate region for elastic modulus measurement for each grid test point. This decreased error at each data point and resulted in more realistic values. Thus, the original data for PS and PCL composites was reanalyzed using this manual method and are presented here.

The mechanical properties are similar to those measured in the PVAc work when incorporating D pollen. In general, PS properties degraded with increased loading of ND pollen (Figure 3.17). With the original analysis, small increases in elongation at pollen loadings were observed and attributed to a synergistic effect between addition of tough filler and inefficient stress transfer. After reanalysis, these small improvements are less apparent and less significant. In PCL composites, mechanical properties degraded with increased pollen loading in both original and reanalyzed data.

Both the interfacial morphologies and the reanalyzed mechanical properties of initial work with non-defatted pollen in PS and PCL seem to corroborate and support the data and conclusions of the PVAc work. Despite differences in pollen type and polymers matrices, similar

results were obtained. Interfacial voids were present in using both forms of as received untreated pollen grains and mechanical properties were degraded at higher more relevant pollen loadings. These results further support the importance of the acid-base hydrolysis treatment of as received pollen grains to tune surface interactions, eliminate interfacial voids, and render pollen a reinforcing and light-weighting filler.

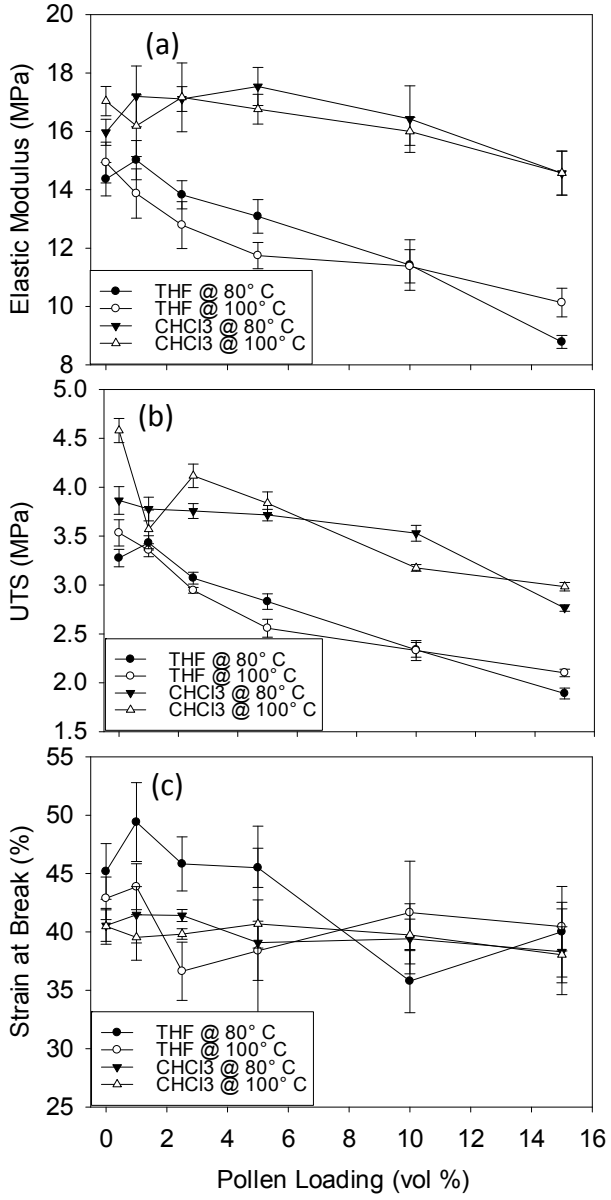

Figure 3.17: Elastic modulus (a), UTS (b), and strain at break (c) of pollen grain filled PS composites prepared with different solvents (THF and $CHCl_3$) and annealing conditions (80 and 100 °C for 24 h, respectively). The error bars are 95% confidence intervals.

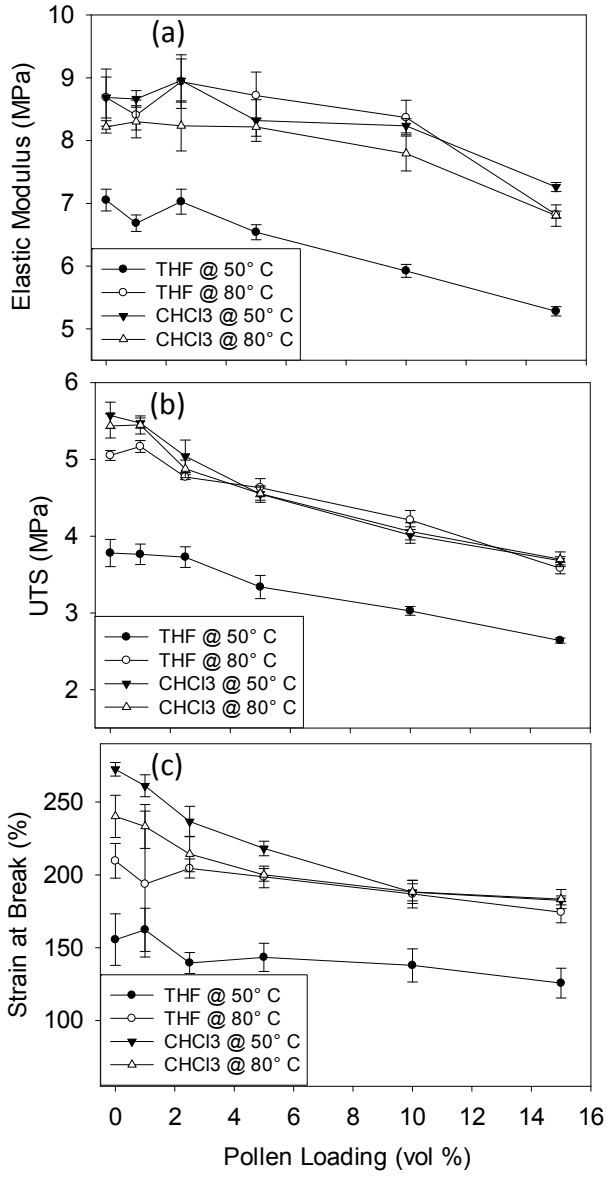

Figure 3.18: Elastic modulus (a), UTS (b), and strain at break (c) of pollen grain filled PCL composites prepared with different solvents (THF and $CHCl_3$) and annealing conditions (50 and 80 °C for 24 h, respectively). The error bars are 95% confidence intervals.

3.5 Conclusions

In this study, the effect of ragweed pollen loading on the mechanical, interfacial, and thermal properties of PVAc composites prepared by a solution processing and free radical polymerization casting method was investigated. Native pollen (D) was observed to introduce interfacial voids in both solution processed and polymerized composites. These interfacial voids resulted in degraded mechanical properties at high pollen loadings and a decreasing width of the

glass transition region. Treatment of pollen via an acid-base hydrolysis method (AB) improved the interfacial adhesion relative to D pollen, likely the result of improved interactions between AB pollen and the PVAc matrix. Eliminating interfacial voids resulted in stiffening of the composite due to the addition of pollen filler, indicating that pollen has a relatively higher elastic modulus than the PVAc matrix. However, the degree of adhesion between AB pollen and PVAc matrix was still too low to allow for strengthening, indicated by decreasing material strength with increased pollen loading. Interfacial adhesion was further improved by functionalizing AB pollen with a vinyl silane in order to graft polymer chains on the pollen surface. Tensile strength and strain at break of films prepared with P-ABV increased with increased pollen loading, indicating a higher degree of adhesion than P-AB. Composites with both AB and ABV pollen displayed a wider glass transition region in the presence of pollen filler, compared to D pollen. These results indicate that pollen is a promising plant-based filler for reinforcing polymers, but that surface functionalization is a likely necessity to achieve significant improvements. Because functionalization appears to be an effective strategy, it would also be interesting to investigate other polymers that are reactive with hydroxyl groups, e.g., urethanes and epoxies. In addition, the unique variety of nano- and micro-structures on pollens (as a function of plant species) creates an opportunity to use pollen as a model particulate to elucidate the effect of complex filler geometries on the wetting and adhesion of fillers.

3.6 References

1. Limited, R.T., *High Performance Fillers 2005: Cologne, Germany, 8-9 March 2005*. 2005: Rapra.
2. Wypych, G., *Handbook of Fillers, 3e*. 2010: ChemTec Publishing.
3. Fu, S.-Y., et al., *Effects of particle size, particle/matrix interface adhesion and particle loading on mechanical properties of particulate–polymer composites.* Composites Part B: Engineering, 2008. **39**(6): p. 933-961.
4. Ash, B.J., et al., *Mechanical properties of Al2O3/polymethylmethacrylate nanocomposites.* Polymer Composites, 2002. **23**(6): p. 1014-1025.

5. Lučić, S., V. Kovačević, and D. Hace, *Mechanical properties of adhesive thin films.* International Journal of Adhesion and Adhesives, 1998. **18**(2): p. 115-123.
6. Spitalsky, Z., et al., *Carbon nanotube–polymer composites: Chemistry, processing, mechanical and electrical properties.* Progress in Polymer Science, 2010. **35**(3): p. 357-401.
7. Vollenberg, P.H.T. and D. Heikens, *The mechanical properties of chalk-filled polypropylene: a preliminary investigation.* Journal of Materials Science, 1990. **25**(7): p. 3089-3095.
8. Wang, W., et al., *Effective reinforcement in carbon nanotube–polymer composites.* Philosophical Transactions of the Royal Society A: Mathematical, Physical and Engineering Sciences, 2008. **366**(1870): p. 1613-1626.
9. Hall, S.R., H. Bolger, and S. Mann, *Morphosynthesis of complex inorganic forms using pollen grain templates.* Chemical Communications, 2003(22): p. 2784-2785.
10. Hall, S.R., et al., *Fabrication of Porous Titania (Brookite) Microparticles with Complex Morphology by Sol−Gel Replication of Pollen Grains.* Chemistry of Materials, 2006. **18**(3): p. 598-600.
11. Jenik, M., et al., *Pollen-imprinted polyurethanes for QCM allergen sensors.* Analytical and Bioanalytical Chemistry, 2009. **394**(2): p. 523-528.
12. Liu, T. and Z. Zhang, *Mechanical properties of desiccated ragweed pollen grains determined by micromanipulation and theoretical modelling.* Biotechnology and Bioengineering, 2004. **85**(7): p. 770-775.
13. Thio, B.J.R., J.-H. Lee, and J.C. Meredith, *Characterization of Ragweed Pollen Adhesion to Polyamides and Polystyrene Using Atomic Force Microscopy.* Environmental Science & Technology, 2009. **43**(12): p. 4308-4313.
14. Feng, C. and L. Dong-Xu, *Morphology-controlled synthesis of SiO 2 hollow microspheres using pollen grain as a biotemplate.* Biomedical Materials, 2009. **4**(2): p. 025009.
15. Wang, Y., et al., *Carbon Microspheres with Supported Silver Nanoparticles Prepared from Pollen Grains.* Langmuir, 2005. **21**(23): p. 10846-10849.
16. Wang, Y., et al., *Replication of biological organizations through a supercritical fluid route.* Chemical Communications, 2005(23): p. 2948-2950.
17. Lee, J.H., et al., *Pollen: A Novel, Biorenewable Filler for Polymer Composites.* Macromolecular Materials and Engineering, 2011. **296**(11): p. 1055-1062.
18. Piffanelli, P., J.H.E. Ross, and D.J. Murphy, *Biogenesis and function of the lipidic structures of pollen grains.* Sexual Plant Reproduction, 1998. **11**(2): p. 65-80.
19. Wiermann, R. and S. Gubatz, *POLLEN WALL AND SPOROPOLLENIN.* International Review of Cytology-a Survey of Cell Biology, 1992. **140**: p. 35-72.
20. Blackmore, S., et al., *Pollen wall development in flowering plants.* New Phytologist, 2007. **174**(3): p. 483-498.
21. Dominguez, E., et al., *Pollen sporopollenin: degradation and structural elucidation.* Sexual Plant Reproduction, 1999. **12**(3): p. 171-178.
22. Hemsley, A.R. and I. Poole, *The Evolution of Plant Physiology*. 2004: Elsevier Science.
23. Thio, B.J.R., J.H. Lee, and J.C. Meredith, *Characterization of Ragweed Pollen Adhesion to Polyamides and Polystyrene Using Atomic Force Microscopy.* Environmental Science & Technology, 2009. **43**(12): p. 4308-4313.

24. Lin, H., I. Gomez, and J.C. Meredith, *Pollenkitt Wetting Mechanism Enables Species-Specific Tunable Pollen Adhesion.* Langmuir, 2013. **29**(9): p. 3012-3023.
25. Southworth, D., *Solubility of Pollen Exines.* American Journal of Botany, 1974. **61**(1): p. 36-44.
26. Cohen, Y., *Novel ceramic-polymer composite membranes for the separation of liquid waste. Annual progress report, September 15, 1996--September 14, 1997*. 1997. p. Medium: ED; Size: 12 pages.
27. Sormana, J.-L., S. Chattopadhyay, and J.C. Meredith, *High-throughput mechanical characterization of free-standing polymer films.* Review of Scientific Instruments, 2005. **76**(6): p. 062214-9.
28. Domínguez, E., et al., *Isolation of intact pollen exine using anhydrous hydrogen fluoride.* Grana, 1998. **37**(2): p. 93-96.
29. Shaw, G. and D.C. Apperley, *13C-NMR spectra of Lycopodium clavatum sporopollenin and oxidatively polymerised β-carotene.* Grana, 1996. **35**(2): p. 125-127.
30. Barrier, S., *Physical and chemical properties of sporopollenin exine particles*, in *Chemistry*. 2008, The University of Hull.
31. Blagojević, S.L., et al., *Silane pre-treatment of calcium carbonate nanofillers for polyurethane composites.* Issues, 2013. **13**.
32. He, J., et al., *Tailoring the performance of polymer composites via altering the properties of the intrapore polymers of MCM-48 nanocomposites as fillers.* Composites Part A: Applied Science and Manufacturing, 2006. **37**(3): p. 379-384.
33. Di Maggio, R., et al., *Hybrid organic–inorganic materials using zirconium based NBBs and vinyl trimethoxysilane: Effect of pre-hydrolysis of silane.* Polymer, 2010. **51**(4): p. 832-841.
34. Leskovac, M., et al., *Pre-treatment of CaCO3 nanofiller by irradiation in the presence of vinyl monomers for the preparation of poly(vinyl acetate) composites*, in *e-Polymers*. 2004. p. 348.
35. Fowkes, F.M., *Role of acid-base interfacial bonding in adhesion.* Journal of Adhesion Science and Technology, 1987. **1**(1): p. 7-27.
36. Fowkes, F.M., et al., *Acid–base complexes of polymers.* Journal of Polymer Science: Polymer Chemistry Edition, 1984. **22**(3): p. 547-566.
37. Lee, J.-H., et al., *Effect of nanowhisker-modified zeolites on mechanical and thermal properties of poly(vinyl acetate) composites with pure-silica MFI.* Polymer, 2010. **51**(24): p. 5744-5755.
38. Liu, L., et al., *Effects of cure cycles on void content and mechanical properties of composite laminates.* Composite Structures, 2006. **73**(3): p. 303-309.
39. Bergström, J.S. and M.C. Boyce, *Mechanical Behavior of Particle Filled Elastomers.* Rubber Chemistry and Technology, 1999. **72**(4): p. 633-656.
40. Delawa, U., *Delaware Composites Design Encyc: Micromechanical Materials Model*. 1990: Taylor & Francis.
41. Islam, M.A. and K. Begum, *Prediction Models for the Elastic Modulus of Fiber-reinforced Polymer Composites: An Analysis*. 2011. Vol. 3. 2011.
42. Wu, Y.-P., et al., *Modeling Young's modulus of rubber–clay nanocomposites using composite theories.* Polymer Testing, 2004. **23**(8): p. 903-909.
43. Bakker, R.F.M., *PERMEABILITY OF BLENDED CEMENT CONCRETES.* Journal of the American Concrete Institute, 1983. **80**(4): p. 345-345.

44. Yoshitake, I.e.a., *A Prediction Method of Tensile Young's Modulus of Concrete at Early Age.* Advances in Civil Engineering, 2012. **2012**.
45. Loos, M.R. and I. Manas-Zloczower, *Reinforcement Efficiency of Carbon Nanotubes – Myth and Reality.* Macromolecular Theory and Simulations, 2012. **21**(2): p. 130-137.
46. Fragiadakis, D., L. Bokobza, and P. Pissis, *Dynamics near the filler surface in natural rubber-silica nanocomposites.* Polymer, 2011. **52**(14): p. 3175-3182.
47. Robertson, C.G. and C.M. Roland, *Glass Transition and Interfacial Segmental Dynamics in Polymer-Particle Composites.* Rubber Chemistry and Technology, 2008. **81**(3): p. 506-522.

CHAPTER 4

EXAMINING POLLEN AS A FILLER IN WATERBORNE EPOXY MATRICES

This chapter is in preparation for publication.

4.1 Overview

Pollen grains have the potential to be effective plant-based biorenewable fillers in polymer matrices due to their high mechanical strength, chemical stability, and unique architectures. For this reason, pollen-polymer composites are attractive because they could form the basis for a new class of light-weight, high strength sustainable materials. Pollen, being a microparticle that possesses a rich variety of surface nanoscale topography and features, also provides a unique way to study how filler fine-surface structure affects interphase adhesion and mechanical reinforcement. In this work, we present evidence for the effectiveness of pollen as a reinforcing filler in waterborne epoxy resin matrices, characterized as a function of pollen loading and surface treatment. Composites prepared with as received ragweed pollen (D) displayed decreased mechanical properties and increasing glass transition temperatures (T_g) with increasing pollen loading. A soft interphase forms around native pollen due to selective binding of amine crosslinker to intracellular material. Pollen treated via an acid-base (AB) surface preparation becomes a load bearing filler in composites, displaying simultaneous stiffening and strengthening, improved interfacial morphology (absence of the soft interphase), and increasing T_g with increasing pollen loading. AB pollen interacts more strongly with the epoxy matrix than D pollen due to either strong hydrogen bonding or covalent bonds with polar functional groups (hydroxyls or carboxyls). This may be due to higher exposure of –OH groups on AB pollen than

D pollen or a higher number of –OH groups on AB pollen and elimination of intracellular material.

4.2 Introduction

Particulate fillers are often incorporated into polymers in order to improve their physical and/or chemical properties. Fillers can alter mechanical, thermal, and optical properties, to name a few [1-4]. Many studies have demonstrated the successful use of non-biological materials ranging from inorganic particles, such as calcium carbonate, to carbon organic materials including carbon blacks and nanotubes as reinforcing fillers in fabricating polymer composites [5-8]. Many particulates are denser than the polymer, or are derived in a non-sustainable manner, and there is interest in finding lower density, sustainably sourced alternatives. In addition, most fillers are spherical or irregular spheroids, without significant capability to alter the particle fine surface features or geometry.

In contrast, pollen has the potential to be an effective biorenewable filler due to its high strength, chemical stability, low density and the unique architecture of its outer shell [9-13]. Besides being used directly as a filler, biological particulates such as pollen grains, bacteria, and viruses have attracted much research interest as templates for fabricating synthetic inorganic mimics that preserve their unique surface architectures [9-11, 14-16]. These inorganic mimics may also function as fillers that combine biological architecture with synthetic chemistry. While some studies have investigated pollen grains, only two studies has reported utilization of pollen as a filler [17, 18]. Furthermore, pollens from sources such as the ragweed plants are ubiquitous and inexpensive natural materials that are based on sustainable, non-food plant resources.

Pollen grains are the carrier of the male gametes for plant reproduction. A pollen grain is composed of an outer layer (exine) and an inner layer (intine) [19, 20]. The exine is composed of

sporopollenin, a highly crosslinked organic substance consisting of fatty acids, phenylpropanoids, and phenolics [21, 22]. Figure 1.4 displays monomer and macromer components that have been confirmed in sporopollenin, such as long aliphatic chains, aromatic cross-linkers (mainly cinnamic acids), ether cross-linkages and ester functions [23]. The exine's chemical composition suggests compatibility with polymers capable of polar interactions. Underneath the exine layer, not exposed to the outer surface, lies the intine, which is rich in cellulose and hemicelluloses. The cellular material carried within the grain is easily extracted using well known techniques, leaving behind a hollow, strong shell.

Only two studies have explored pollen grains as reinforcing filler in thermoplastics polystyrene, polycaprolactone, and polyvinyl acetate [17, 18]. These studies showed that surface treatment and surface functionalization of pollen was critical in tuning interfacial adhesion and mechanical properties of pollen-polymer composites, in order to make pollen an effective load bearing filler. To date, the effectiveness of pollen fillers in thermosetting polymers has remained unexplored. Epoxy resins are widely used in adhesives, coatings, composites, electric systems, and aerospace applications [24]. Epoxy resins can be crosslinked with curing agents such as amines, hydroxyls, and carboxyls in order to form flexible or rigid materials. Due to increased legislative restrictions on organic solvent emissions, waterborne epoxy resins are becoming increasingly important [25]. Additionally, waterborne and water-soluble matrices should display a high level of compatibility with water-dispersible fillers, reducing or eliminating the need for chemical functionalization of the filler. In this work, we demonstrate for the first time the successful incorporation of pollen in waterborne epoxy matrices. Short ragweed pollen (*A. artemisiifolia*) is selected as a model pollen grain because of its natural abundance, unique 'spiny' echinate surface morphology, and previously-published studies on plastic composites and

adhesion data [26, 27]. As received pollen is compared to pollen modified by an acid-base hydrolysis. The effectiveness of pollen as a reinforcing and strengthening filler in epoxy is characterized by mechanical properties, interfacial morphology, and glass transition temperature of pollen-polymer composites as a function of pollen loading and pollen treatment.

4.3 Experimental

4.3.1 Materials

Defatted Short ragweed (D, A. artemisiifolia, Greer Laboratories) pollen grains were stored at 4 °C prior to use. Potassium hydroxide (KOH, EMD Millipore) and phosphoric acid (H_3PO_4, BDH chemicals) were used pollen treatment. Epoxy resin (diglycidyl ether of bisphenol-A (DGEBA), Air Products and Chemicals Inc., Ancarez AR555, 55 wt.% solid epoxy emulsion in water stabilized by a nonionic surfactant with D_{50} = 0.5 mm, epoxy equivalent weight (EEW) = 550) was used as received. Amine (polyoxypropylenediamine, Air Products and Chemicals Inc., Anquamine 401, 70 wt.% solute content in water solution, amine hydrogen equivalent weight (AHEW) = 200) was diluted with approximately equal weight of DI water to reduce the viscosity. The final solute content in the amine/water solution was approximately 35 wt%.

4.3.2 Extraction of Pollen Cellular Material

An acid-base treatment (hereafter labeled as AB) was used to clean and isolate the exine shell for incorporation in polymer films as well as to prepare them for further functionalization [20, 28]. Briefly, pollen was dispersed in 6w/v% KOH solution for 24 hours while stirring. After washing the pollen with hot water, ethanol, and drying the pollen, it was dispersed in 85% H_3PO_4 for 7 days. This pollen was dried after washing with hot water, acetone, and ethanol. This process caused the pollen grains too lose ~80% of their original weight. Figure 3.1 shows D pollen (both intact and crushed) and AB pollen.

4.3.3 Pollen-Epoxy Composite Film Preparation

Stoichiometric amounts of epoxy and amine were mixed at room temperature with the desired amount of D or AB pollen suspended in water in order to form composites of 0-15 wt% pollen loading. The mixture was magnetically stirred for 1-5 h depending on pollen concentration, with higher concentrations mixed for longer times. The mixtures were then precured for 0.5-2 h at room temperature until the viscosity of the mixture was suitable for casting. Precuring times were determined by visual inspection and increased with pollen concentration because greater amounts of water (introduced with the pollen suspension) were present at higher pollen concentration, diluting the reactive epoxy. The mixture was cast on glass plates with a doctor blade and allowed to dry in air for a short time until the mixture is not able to flow on the substrate. Then, films were then cured for ~22 min at 100 °C. Samples were peeled off the substrates using a razor. Neat epoxy was prepared using the same protocol. Both D and AB pollen were incorporated into epoxy matrices. Hereafter, the samples are labeled as follows: Epoxy with native defatted pollen (E-D) and epoxy with acid-base treated pollen (E-AB).

4.3.4 Characterization

FTIR spectra were obtained on a Thermo Scientific spectrophotometer from 4000 cm^{-1} to 400 cm^{-1}. Pollen received as is, acid-base treated, and recovered from epoxy solution were mixed with KBr powders and pressed in pellets for measurement. A high-throughput mechanical characterization (HTMECH) apparatus was used to measure mechanical properties including tensile strength, elastic modulus, and toughness, as described previously [29]. Briefly, the polymer films were mounted on a steel grid and contacted with a steel pin with a 1.5 mm diameter hemispherical cap at a constant strain rate (0.5mm/s). The pin is oriented normal to the

film surface, resulting in equi-biaxial deformation. For each sample, an average thickness was obtained using 9 measurements with a micrometer, 9 stress–strain profiles were measured to failure, and mechanical of the films were obtained. Uniaxial tensile testing was also performed using an Instron 5566. AFM contact mode and force-modulation scans of composite cross sections were made with a Veeco AFM Dimension 3100. The samples were prepared by laser cutting films into 100 mm x 80 mm strips, a gage length of 80 mm was utilized, and a strain rate of 8 mm/min was used strips in an effort to maintain sample ratios from ASTM D882-10 to determine elastic modulus. Sample slippage was mitigated by covering the ends of samples in kapton tape grips. A minimum of four samples were tested for each material composition where possible, and the average values were reported. All mechanical tests were performed under ambient conditions. Scanning electron microscopy (SEM) was performed with a Zeiss Ultra-60 FE-SEM instrument to examine the interfacial morphology of both freeze fractured and HTMECH fracture surfaces of the composites. Differential scanning calorimetry (DSC) measurements were performed with a TA Instruments DSC Q200 in a nitrogen atmosphere, using specimens of 8–9mg cut from films and sealed in aluminum pans with lids. Samples were heated from 10 to 150 °C, above T_g of the neat epoxy, at 20 °C/min, kept isothermal for 1 min, cooled down to 10 °C at 20 °C/min, and held isothermal for 1 min again. This cycle was repeated twice. T_g values were taken from the second cycle from the onset value of the tangents on the heat flow curves. The density of materials was assessed by pycnometry in a 25 ml specific gravity bottle. Ethanol was used to determine the density of D pollen, AB pollen, neat epoxy, and composites. A known mass of material, m_s, was added to the volumetric flask of known mass (m_0). The liquid of known density was then added to the flask up to the graduation marking and the total mass, m_T, is measured. The density of the solid is given by:

$$\rho_s = m_s / \left(V - \frac{m_T - m_0 - m_s}{\rho_{H2O}} \right) \quad (4.1)$$

where V is the volume of the flask.

4.4 Results and Discussion

4.4.1 FTIR Analysis

Figure 4.1 shows the FTIR spectra of native pollen, native pollen recovered from epoxy solution, acid-base pollen, and acid-base pollen recovered from solution following each chemical modification (D, D-Epoxy, AB, AB-Epoxy). The cellulose fingerprint in D pollen appears in the 1100 to 900 cm^{-1} region, due to the presence of polysaccharide material in the pollen intine [22, 30]. The spectrum for AB pollen shows an important lack of peaks associated with polysaccharides in this range, indicating the full or partial dissolution the intine [31, 32]. Additionally, D pollen displays a very broad band at 3393 cm^{-1} due to O-H stretching that shows a stronger intensity than the –CH stretches of $–CH_2$ groups at 2930 and 2855 cm^{-1}. In contrast, AB pollen displays a more narrow –OH band with a smaller intensity than the $–CH_2$ peaks. AB pollen's OH band is also shifted to higher wavenumbers around 3433 cm^{-1}, indicating increased fractions of free hydroxyls. The C=O stretch of carboxyl groups also shifts from 1674 cm^{-1} to 1706 cm^{-1} in D and AB pollen, respectively. Therefore, the acid-base hydrolysis decreases the ratio of hydroxyl to methylene groups due to the dissolution of the strongly H-bonded cellulosic intine and results in higher fractions of free hydroxyl and carboxyl groups more accessible for surface interactions. Additionally, additional hydroxyl groups may be generated on the pollen surface due to phosphorylation of hydroxyls and/or carboxyls [32].

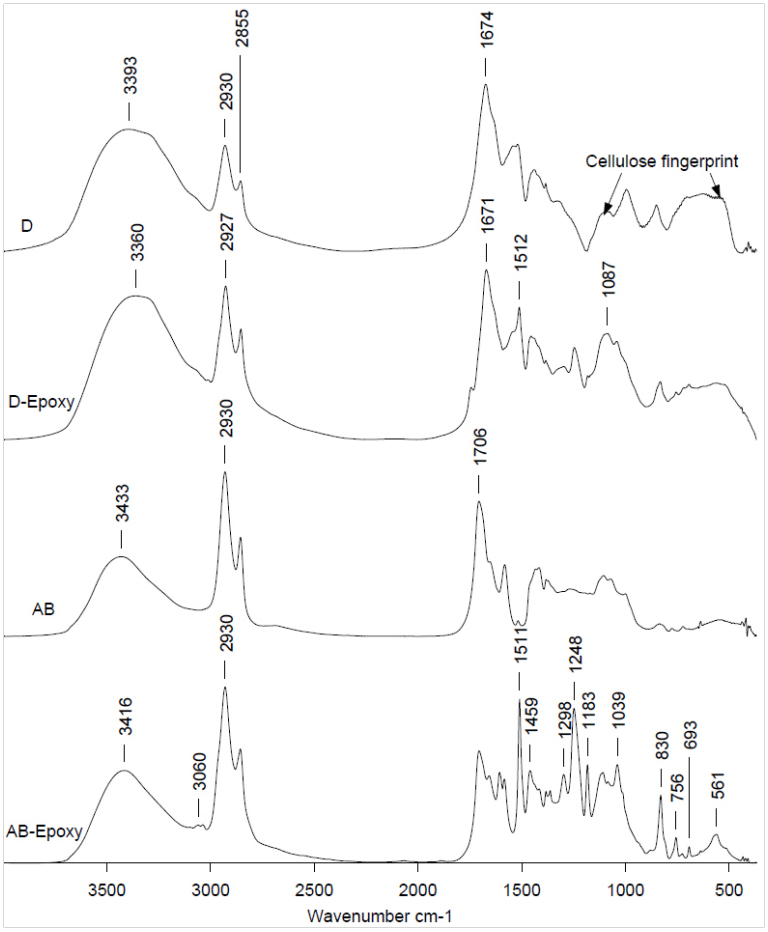

Figure 4.1: FTIR spectra D and AB pollen as well as both recovered from epoxy solution.

AB-Epoxy displays several additional peaks versus AB pollen, indicating the strong interactions between AB pollen and epoxy. Peaks associated with the epoxide group appear at 3060 cm^{-1} due to C-H stretching and at 830 cm^{-1} C-O-C stretching [33]. C-H stretches of aromatic groups in the epoxy molecules appear as a shoulder peak at 2925 cm^{-1} [33-35]. The C-C stretching of aromatics also appears at 1511 cm^{-1} and the C=C stretching of aromatic groups appears at 1459 cm^{-1} [33, 34, 36]. C-O-C stretching of epoxy ether groups appear at 1248 cm^{-1} and 1039 cm^{-1} [33-35]. Many of these peaks are lacking on D-Epoxy and where new peaks are visible (1511 cm^{-1} and 1246 cm^{-1}), they are weak signals. The higher intensity of peaks and presence of numerous new peaks on AB-Epoxy versus D-Epoxy may be due to higher fractions of free hydroxyl and carboxyl groups more accessible for surface interactions on AB pollen

versus D pollen, allowing for a greater degree of hydrogen bonding between epoxy molecules and AB pollen. Epoxy is known to crosslink with a hydroxyl and carboxyl functionalities [37-40], so it is possible that the epoxide molecules react with pollen surface hydroxyls or carboxyls and form covalent linkages between the pollen and the epoxy matrix. Figure 4.1 shows that between AB and AB-Epoxy the ratio of –OH (~3400 cm^{-1}) groups to -CH_2 (2930 cm^{-1}) is unchanged, while ratio of –COOH (1706 cm^{-1}), to both –OH and –CH_2, decreases. This may indicate the consumption of carboxyl groups due to reaction with epoxides.

Figure 4.2 shows displays an AB pollen grain and its clean, clear surface. D pollen is similar in the clearness of its surface as seen in Figure 2.5. Figure 4.3 displays the recovered D-Epoxy grains which also correspond with the spectra in Figure 4.1. It is clear that epoxy has been thickly coated on the D pollen surface. This also corresponds with the new FTIR peaks for D-Epoxy versus D pollen. Figure 4.4 displays AB-epoxy which corresponds with the AB-Epoxy spectra in Figure 4.1. It is clear that epoxy has been coated on the AB pollen outer and inner surfaces. The inner surface of pollen grains is heavily coated with epoxy spheres. The outer surface however is not as thickly coated as D pollen. This seems counterintuitive to the stronger FTIR peaks on AB-Epoxy spectra versus D-Epoxy spectra.

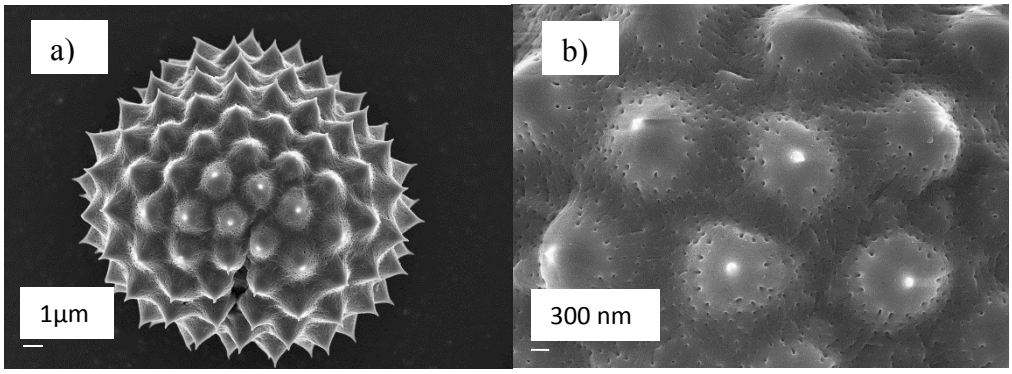

Figure 4.2: AB pollen with clear surfaces.

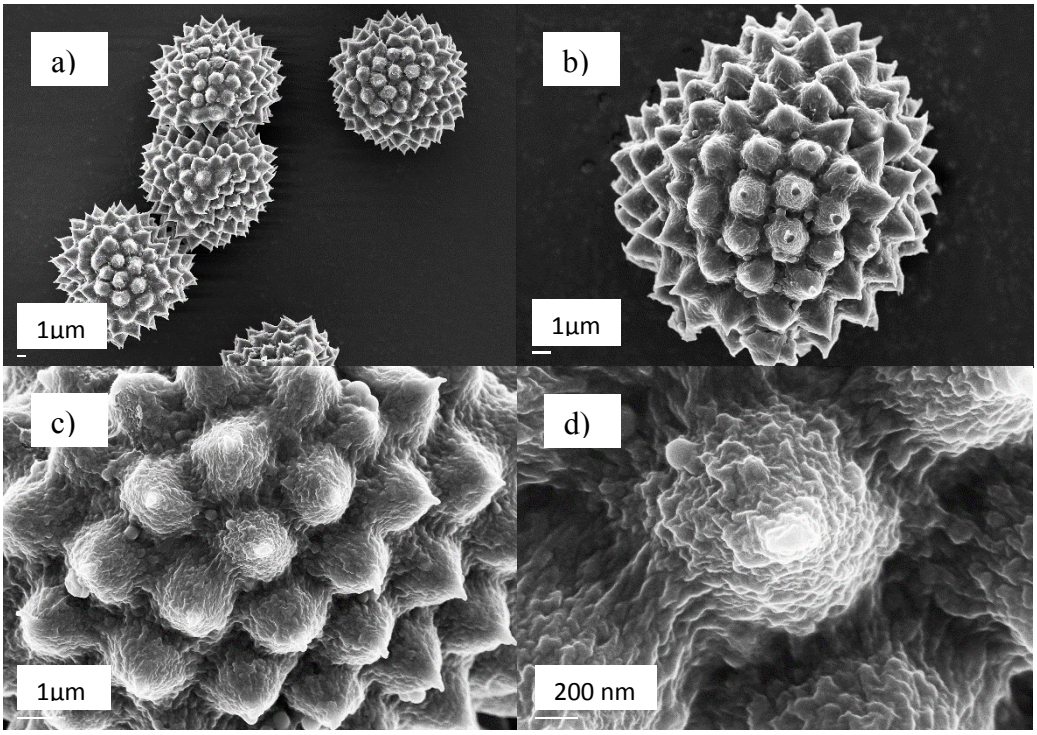

Figure 4.3: Recovered D-Epoxy pollen.

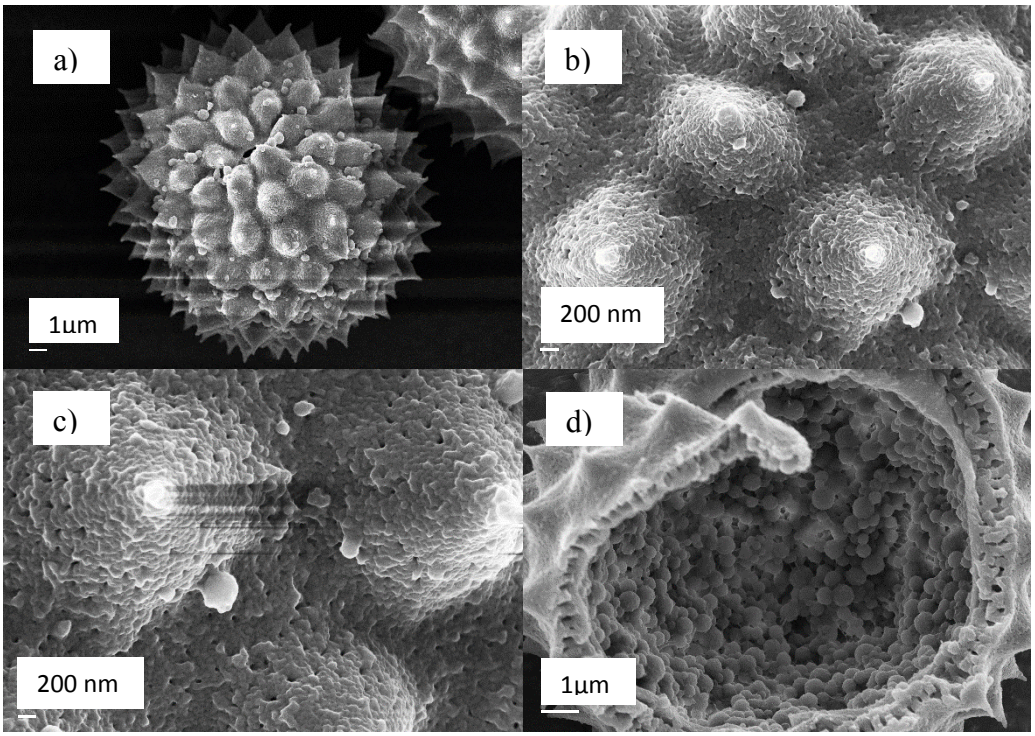

Figure 4.4: Recovered AB-Epoxy pollen:

4.4.2 Interfacial Morphology

Figure 4.5 presents the SEM images of freeze fractured and HTMECH fracture surfaces of E-D films. Both freeze fracture (Figure 4.5a and Figure 4.5b) and HTMECH fracture surfaces (Figure 4.5f-Figure 4.5h) show intimate contact between the pollen and the epoxy matrix in general. However, a visible interphase ~1 μm in thickness can be seen surrounding the D pollen cross sections. Where intact D Pollen grains can be found (Figure 4.5c-Figure 4.5e), interfacial voids are present. It can also be observed that small amounts of epoxy attach to the surface and pores of D pollen, but the surface remains mostly clear (indicated by the visibility of pollen pores). With both fracture surfaces the majority of D pollen grains are broken within the exine shell structure, indicating some degree of adhesion between the two phases. This thick interphase may correspond with the thick coating of epoxy observed on recovered D-Epoxy molecules. The coating observed on D-Epoxy (Figure 4.3) appeared smooth just like the thick interphase, as opposed to rough spheres displayed in the bulk matrix.

Figure 4.6 presents the SEM images of freeze fractured and HTMECH fracture surfaces of E-AB films. Both freeze fracture (Figure 4.6a-Figure 4.6f) and HTMECH fracture surfaces (Figure 4.6g and Figure 4.6h) reveal intimate contact between pollen grains and the epoxy matrix. Additionally, E-AB films lack the visible interphases that were present with E-D films. Also in contrast to D pollen, where intact AB pollen can be found (Figure 4.6b-Figure 4.6e), its surface is clearly coated with layers of epoxy, making the pollen surface and pores no longer visible. The interface between the pollen outer surface and the epoxy matrix is virtually indistinguishable. Again, the pollen grains that are visible are almost always broken cross sections of AB pollen due to some degree of adhesion between the epoxy matrix and AB pollen outer surface. This corresponds with the recovered AB-Epoxy grain images. As opposed to the

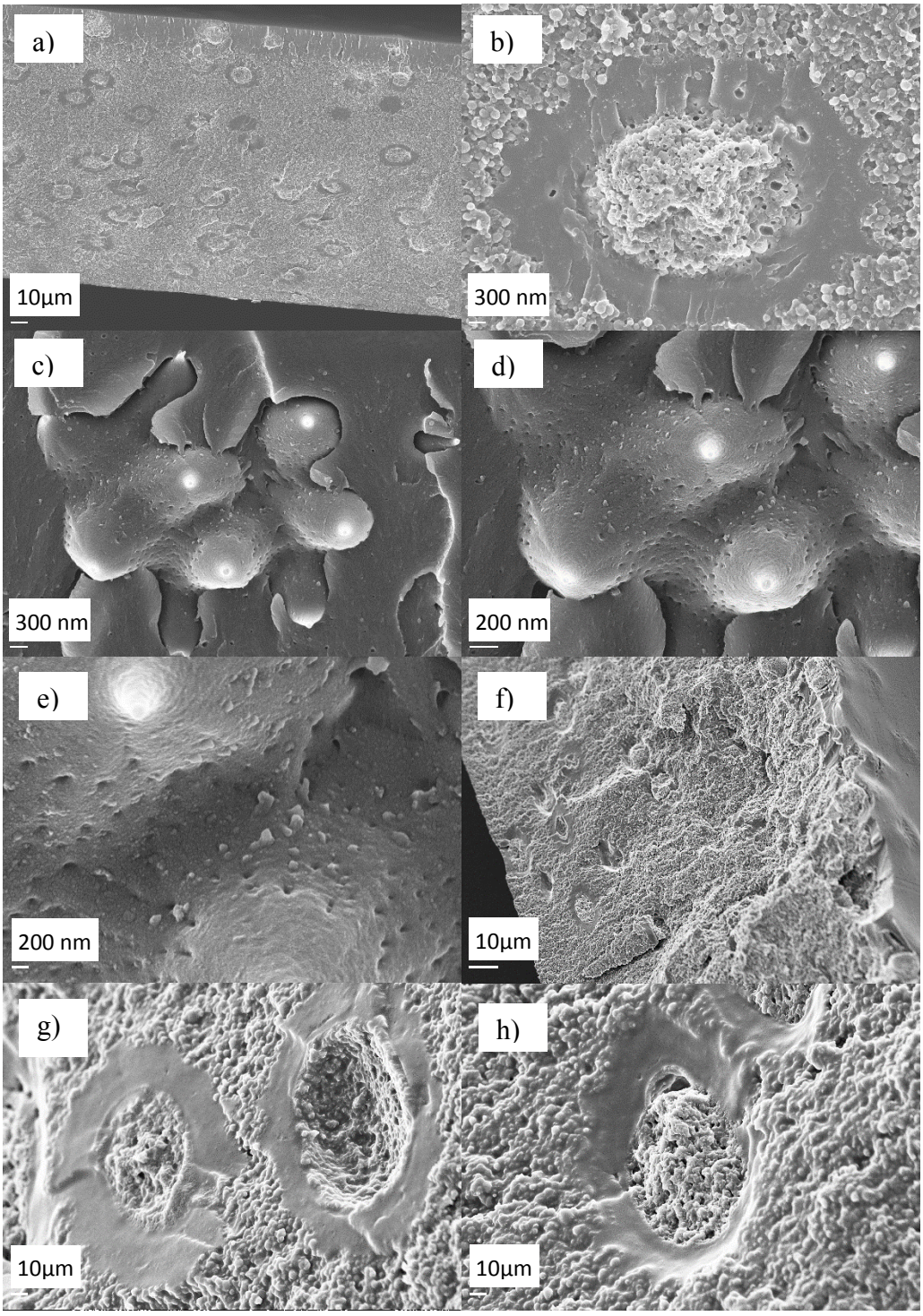

Figure 4.5: E-D fracture surfaces. Freeze fractured cross sections (a-e) and HTMECH fracture surfaces (f-h).

thick, smooth coating of D-Epoxy, AB-epoxy had a thinner, rougher coating with more epoxy spheres, more similar to the bulk matrix in fracture surfaces. On AB-Epoxy (Figure 4.4d), the

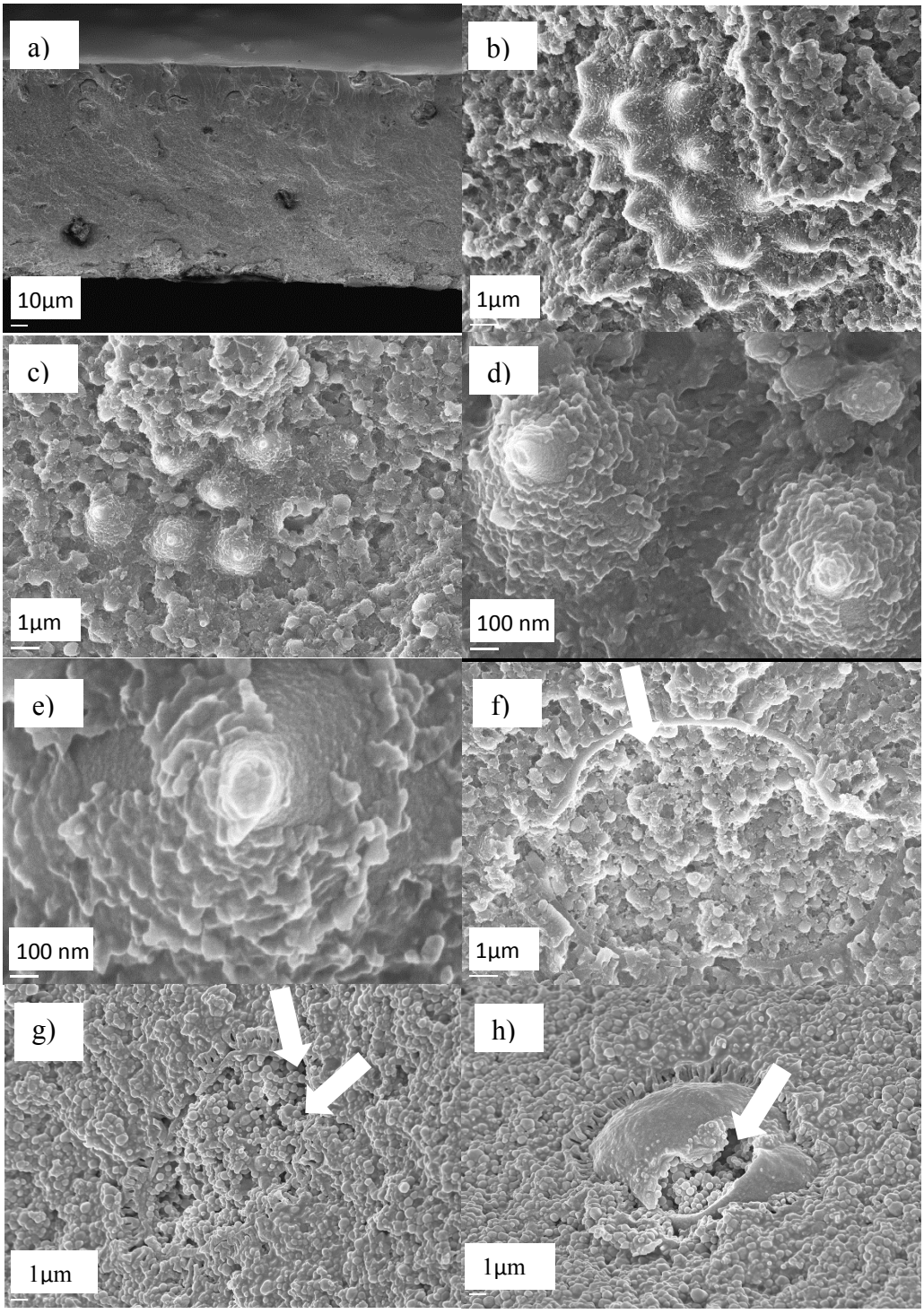

Figure 4.6: E-AB fracture surfaces. Freeze fractured cross sections (a-f) and HTMECH fracture surfaces (g and h). Arrows indicate epoxy within pollen grains and additional air gaps.

inner surface morphology (inside the pollen grain) reflects that of the bulk matrix of fracture surfaces even more clearly. Finally, the fact that epoxy enters the hollow shells (arrows in Figure

4.6f-Figure 4.6h) may have two interesting outcomes. First, this epoxy may be shielded from stresses experienced outside the grain during deformation. This is referred to as “occluded polymer”. Second, it is evident that the epoxy within the shells displays more air gaps than that of the matrix arrows in (Figure 4.6g-Figure 4.6h). Thus, AB pollen introduces a greater amount of air into the final material than D pollen or the unfilled epoxy. AB pollen is already more lightweight than the epoxy matrix, but the integration of air within the pollen shells will further reduce the weight of the final material.Selective binding of epoxy reaction components may cause the formation of the thick interphase that occurs with D pollen that is absent with AB pollen. It is well known that amines can strongly bind to lipid structures, such as phospholipids, and cellulose, which are present in D pollen intracellular material within the D pollen [41-43]. This was investigated by mixing both D and AB pollen in dilute amine-water solutions.

Figure 4.7 shows pure polyoxypropylenediamine-water solutions and the supernatants of pollens mixed in polyoxypropylenediamine-water solutions at several time steps. The supernatant of amine-water solutions mixed with D pollen display a strong color shift, becoming dark yellow even after 15 minutes. In the AB pollen mixtures, where intracellular material is absent, no color shift occurs. D pollen mixed with only water (not shown in Figure 4.7) extracted some intracellular material, but still remained essentially clear, so extracted intracellular material alone does not account for the strong color shift. One explanation is that the intracellular material is released from the within the pollen grain and strongly binds with the amine crosslinker. This may explain why interphases are formed in E-D films. Intracellular material may diffuse out of the D pollen core and bind with amine outside of the shell, preventing the amine from crosslinking epoxide molecules and creating a zone which is depleted of amine. Also, if this zone is depleted of amine and the epoxide is not fully crosslinked during curing, this zone may be

softer than the bulk matrix. This depleted zone that is not fully crosslinked may be evidenced on recovered D-Epoxy pollen grains (Figure 4.3), which are coated with a layer of partially cured epoxy that is smooth in appearance. In contrast to D pollen, the AB pollen lacks intracellular material, therefore no selective binding of amine will occur and epoxy is able to cure full and interact with the pollen surface. This is also reflected in the SEM images of recovered AB-Epoxy pollen grains (Figure 4.4). The surface of these grains is no longer coated with a thick partially cured epoxy (as in the case of D-pollen) because of the absence of selective amine binding with intracellular material. Also, the coatings the inner and outer pollen exine surfaces more clearly mirror the morphology of the crosslinked bulk matrix of fractured surfaces (Figure 4.6). In addition, AB pollen likely displays increased hydrogen bonding versus D pollen due to the exposure and/or increase of hydroxyl groups on the pollen surface after treatment, further improving interfacial adhesion. These results also corroborate the FTIR spectra which displayed additional and stronger absorbances for epoxy functional groups on AB pollen versus D pollen recovered from epoxy solution.

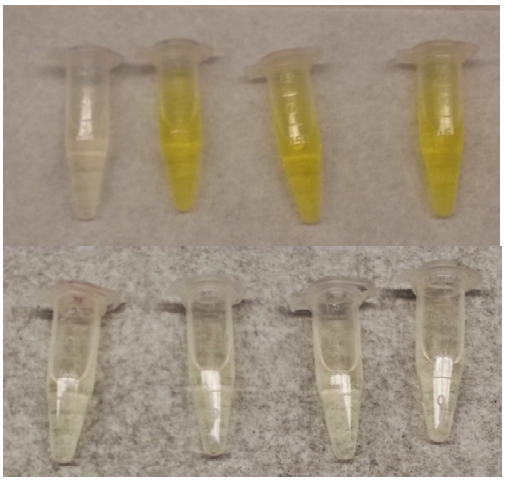

Figure 4.7: Supernatant extracts of D (top) and AB pollen (bottom) mixed with dilute amine-water solution. Left to right: initial amine-water solution, followed by the supernatant after 15, 30, and 45 minutes, of contact with D or AB pollen.

4.4.3 Mechanical Properties

Figure 4.8 shows the mechanical properties obtained for both E-D and E-AB films with HTMECH. The error bars are 95% confidence intervals. Elastic modulus, tensile strength, and strain at break all decreased continuously with the increased loading of D pollen. Considering the interfacial morphology of E-D films, this may be due to the visible interphase present in these films. The interphase may not be fully crosslinked due to depletion of amine, making it softer than the bulk matrix. Thus, with increasing pollen loading, the material is increasingly softened and efficient stress transfer between the phases is impaired, effectively decreasing material stiffness and strength with increased pollen loading. In contrast, elastic modulus, tensile strength, and strain at break all simultaneously increase with the increased loading of AB pollen. Versus neat epoxy, composites containing AB pollen showed increased modulus (~17% increase), tensile strength (86% increase), and strain at break (73% increase). As discussed above, E-AB films did not display a visible interphase, attributed to uncured epoxy in D pollen. Thus AB pollen likely forms a stronger more interconnected interphase with epoxy than D pollen, which is capable of interacting strongly with AB pollen surface (through hydrogen bonding or covalent bonding). The mechanical results suggest that there is a high degree of adhesion between the AB pollen and the epoxy matrix, resulting in efficient stress transfer between the phases, further supporting the presence of strong physical interactions between AB pollen and epoxy. Epoxy chains that are strongly interacting with the pollen surface are chemically incorporated into the epoxy matrix. These mechanical observations and the proposed strong physical interactions driving adhesion are also consistent with the SEM evidence of strongly attached epoxy to the AB pollen surface (Figure 4.6b-Figure 4.6e). In our previous study with polyvinyl acetate, an additional surface functionalization with an organosilane coupling agent was required to

optimize interfacial adhesion and achieve simultaneous increases in all mechanical properties. Strong hydrogen bonding between AB pollen, and possibly the formation of covalent bonds between surface –OH groups and the epoxide and the epoxy matrix eliminates the need for an additional functionalization step. These results indicate that pollen is more compatible with epoxy materials than previous thermoplastics that were studied.

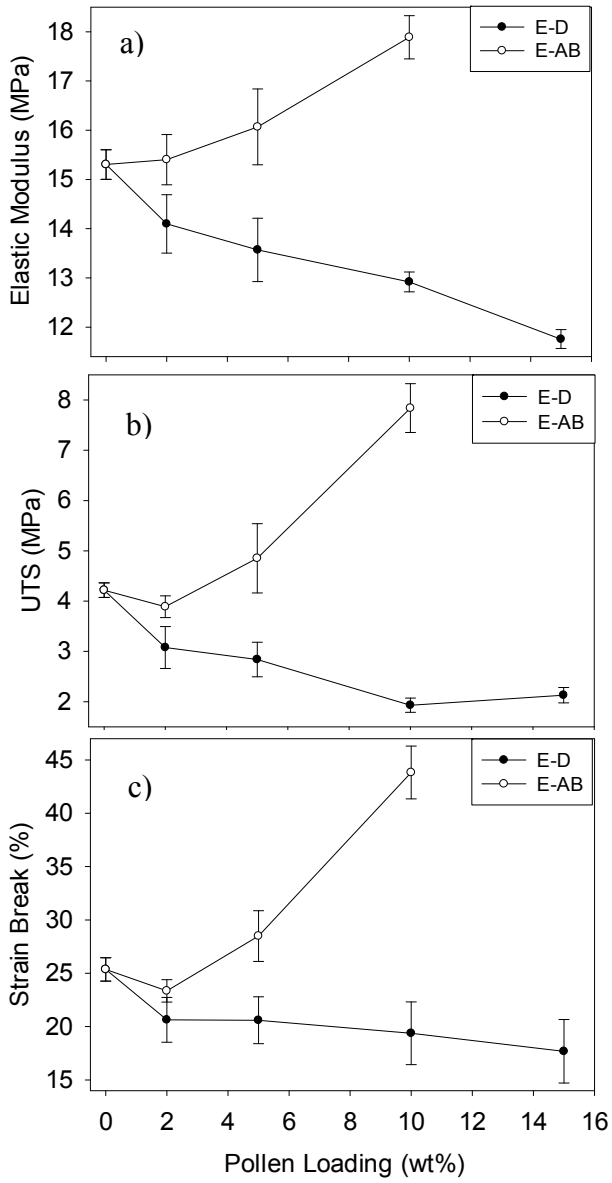

Figure 4.8: Elastic modulus (a), UTS (b), and strain at break (c) of both E-D and E-AB composites measured with HTMECH under biaxial tension. The error bars are 95% confidence intervals.

Figure 4.9 shows the elastic modulus obtained for both E-D and E-AB with standard tensile testing on an Instron. It is clear that the general trends of elastic modulus match well on both instruments (decreasing stiffness with increased D pollen loading and increasing stiffness

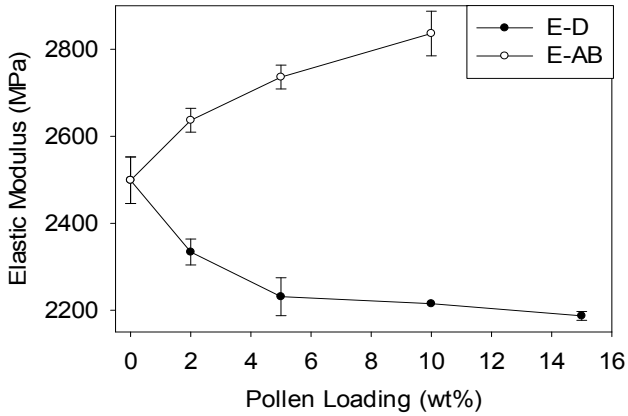

Figure 4.9: Elastic modulus of both E-D and E-AB composites measured under uniaxial tension. The error bars are 95% confidence intervals.

with increased AB pollen loading). However, the magnitudes of elastic modulus are very different. For example, for neat epoxy, the HTMECH (biaxial) modulus was 15.3 MPa, compared to the Instron (uniaxial) modulus of 2499 MPa. This difference may arise for several different reasons. First, the strain rates utilized with the two instruments are slightly different (HTMECH: .5 mm/s, Instron: .13 mm/s). However, this likely does not play a role because the faster strain rate of the HTMECH would be expected to result in a higher elastic modulus, which is the opposite of what is observed. Previously, a correlation between elastic moduli measured for highly elastic poly(urethane ureas) on both HTMECH and Instron was demonstrated [44]. A strong linear correlation was found between HTMECH and uniaxial results, with a coefficient of $E_{HTMECH} = 1.35E_{UNIAXIAL}$, in agreement with elastic membrane theory. However, tensile (in-plane) strain dominates in these low-modulus elastomer films in HTMECH biaxial tests resulting in elastic modulus magnitudes that are similar to uniaxial tests for which in-plane tension is the only stress. However, differences can appear when comparing biaxial to uniaxial measurements

for materials with higher modulus, higher thickness, and plastic deformation. In thicker, or higher modulus films, bending contributions to the overall stress can be significant and even dominant. This is likely the case with the stiffer epoxy materials where biaxial loading from the center of the film (as in HTMECH) leads to bending stresses that can become significant in addition to tensile (in plane) stresses, decreasing the magnitude of the observed elastic modulus on the HTMECH.

AFM contact mode and force modulation scans of E-D cross sections are shown in Figure 4.10. The scans correspond with the interphases observed in Figure 4.5. These scans were made

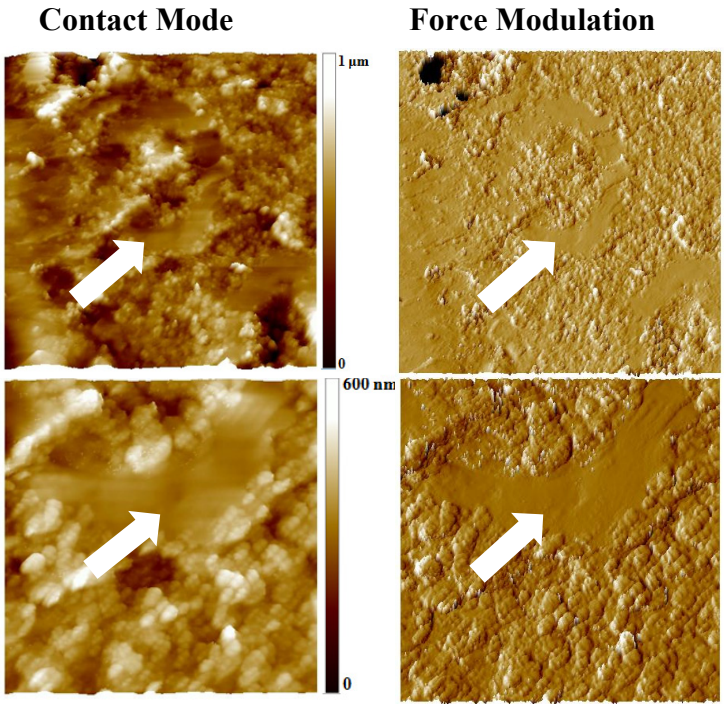

Figure 4.10: Contact mode topography (left) and force modulation image (right) of E-D film. 40 µm scan (top row) and15 µm scan (bottom row). Arrows indicate identical interphase area in each mode.

in attempts to show evidence of a softer interphase versus a harder bulk matrix. The brighter regions of the force modulation scans, which occur primarily in the bulk matrix of the film indicate that the bulk matrix is indeed harder than the interphase (Figure 4.10 arrows), which shows up darker. This however may result from the roughness difference between the interphase

and the bulk. Further work must be done in order to fully accept these preliminary results. Perhaps using a harder tip, the roughness difference effect may be diminished. Even when pushing the tip directly into the different regions (bulk versus interphase) in order to quantify any elastic modulus differences, there was no indication of significant modulus difference between the interphase and the bulk matrix. Again, the roughness of the surrounding epoxy matrix compared to the interphase, raises difficulties in interpreting the data.

The stiffening effects observed in E-AB films (Figure 4.8 and Figure 4.9) indicate that the pollen exine shell has a higher inherent modulus than the epoxy matrix, although independent measurements of exine modulus are not available. There has been only one other study that reported the E_h (the product of a compressive elastic modulus and wall thickness) of dessicated

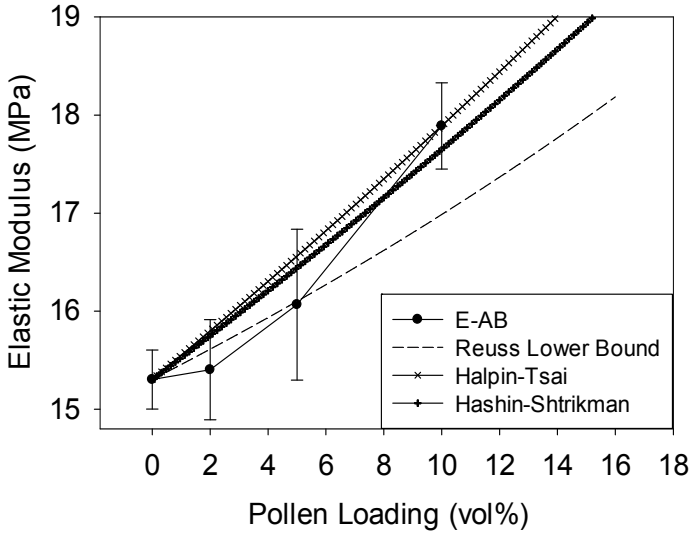

Figure 4.11: Experimental data versus theories for elastic modulus E-AB experimental modulus data from HTMECH data.

ragweed pollen as 1653 N/m via micromanipulation techniques [12]. This results in a compressive modulus of 1653 MPa, using an approximate wall thickness of 1 micron for ragweed pollen. This value was used to compare the experimental HTMECH modulus data with a lower bound model [3, 45-47] for elastic modulus as shown in Figure 4.11. The Reuss lower bound assuming iso-stress is given by the inverse rule of mixtures:

$$E_C^{lower} = E_f E_m / \left[E_f \left(1 - V_f\right) + E_m V_f \right] \tag{4.2}$$

where E_c^{lower}, E_f and E_m are the modulus of the composite, the filler, and the neat matrix respectively. V_f is the volume fraction of the filler. Figure 4.11 shows that the experimental data above 10% pollen loading falls above the lower bound, when using the pollen modulus of 1653 MPa. Two models that fall above the lower bound were fit to the experimental data in order to estimate the modulus of pollen. The Halpin-Tsai model, the most popular semi-empirical model, is shown in Equation 4.3.

$$E_c = E_m \left(\frac{1 + \eta \zeta V_f}{1 - \eta V_f} \right) \tag{4.3}$$

ζ and η are expressed as:

$$\zeta = 2 + 40 V_f^{10} \tag{4.4}$$

$$\eta = \frac{\frac{E_f}{E_m} - 1}{\frac{E_f}{E_m} + \zeta} \tag{4.5}$$

The Halpin-Tsai model [3, 46-48] predicted a modulus of 67.8 MPa for AB pollen versus the measured 15.3 MPa of the neat epoxy. The largest percent error was 3%. The Hashin-Shtrikman model [45, 49, 50], shown in Equation 4.6, is a model for stiff and almost incompressible particles.

$$E_c = E_m \left(\frac{3E_m + 2E_f + 3V_f\left(E_f - E_m\right)}{3E_m + 2E_f - 2V_f\left(E_f - E_m\right)} \right) \tag{4.6}$$

The model predicted a modulus of 67.7 MPa for AB pollen versus 15.3 MPa of the neat epoxy. The largest percent error were 2%. The data remains above the lower bounds (Equation 4.2) when the estimates of pollen modulus from the Halpin-Tsai and Hashin-Shtrikman models are used as E_f. Experimental Instron modulus data was also compared with a lower bound model as shown in Figure 4.12. In addition to the Halpin-Tsai model, the Counto model was used to fit the Instron experimental data. The Counto model, [3, 51, 52] shown in Equation 4.7, is a model for

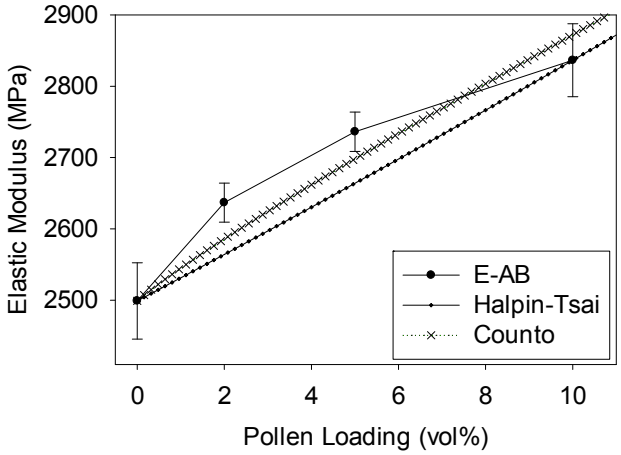

Figure 4.12: Experimental data versus theories for elastic modulus E-AB experimental modulus data with Instron data.

two phase particulate composites assuming a perfect bonding between filler and matrix and gives predictions in good agreement with a wide range of test data.

$$E_c = E_m \left[1 + V_f \Big/ \left(\sqrt{V_f} - V_f + \frac{E_m}{E_f - E_m} \right) \right] \tag{4.7}$$

As shown in Figure 4.12, the Counto model, which is non-linear, provides a slightly better fit. The Halpin-Tsai model predicted a modulus of 8169 MPa and the Counto model predicted a modulus of 8005 MPa for AB pollen versus the measured 2499 MPa of the neat epoxy polymer. The largest percent errors were 2.7% and 1.8% for the Halpin-Tsai and the Counto model respectively. Thus, modeling predicts that pollen is about 4 times harder than the epoxy matrix from HTMECH data and 3 times harder than the epoxy matrix from Instron data.

4.4.4 Thermal Properties

Glass transition behavior was measured for the two different sample types as a function of pollen loading, as seen in Figure 4.13 and Table 4.1. It is clear that in both E-D and E-AB films, the T_g increases with increased pollen loading, suggesting restriction of epoxy chains surrounding pollen surfaces [53, 54]. This correlates with the observed interfacial and mechanical properties observed in the films. Comparing E-D and E-AB films, it is observed that

T_g values in E-AB films are higher than T_g values in E-D films at similar pollen loadings. For example, at 10 wt% pollen loading, E-D film displays a T_g of 65.4 °C and E-AB displays a T_g of 69.1 °C. This suggests a higher restriction of epoxy chains in E-AB films. The soft interphase that is not fully crosslinked likely causes the depressed T_g value. Due to lack of a soft interphase in D pollen composites and stronger interactions with epoxy, AB pollen is able to elevate the T_g more significantly. These results correspond well with FTIR peaks of higher intensity on AB pollen recovered from epoxy solution than D pollen and improved mechanical properties of E-AB films. Again, these results indicate that pollens-filled epoxies show improved compatibility versus previous thermoplastics [17, 18]. Previously, T_g of polyvinyl acetate was not altered significantly with increased pollen loading, even after surface treatment and functionalization. However, with epoxy, even prior to any surface treatments D pollen is able to elevate T_g, indicating improved matrix compatibility.

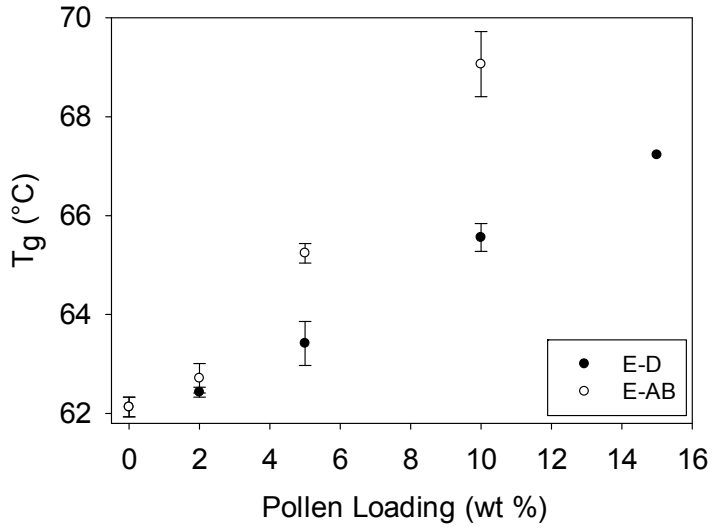

Figure 4.13: Glass trasition (T_g) of pollen-epoxy composites as a function of pollen loading.

Table 4.1: Glass trasition (T_g) of pollen-epoxy composites as a function of pollen loading.

Pollen Loading (wt %)	E-D T_g (°C)	E-AB T_g (°C)
0	62.13	62.13
2	62.36	62.71
5	63.1	65.24
10	65.36	69.07
15	67.23	--

4.4.5 Density of Materials

Using pycnometry, the density of D pollen was measured to be 1.305 g/cm^3, while the density of AB pollen was measured to be 1.165 g/cm^3. The intracellular material present in D pollen makes it denser than the hollow AB pollen, as seen in Figure 3.1. The native D pollen is much less dense than widely used mineral fillers, such as talc (ρ = 2.75 g/cm^3) and calcium carbonate (ρ = 2.71 g/cm^3), and has a density comparable to such as carbon nanotubes (ρ = 1.3-1.4 g/cm^3), cellulose (ρ = 1.5 g/cm^3) and starch (ρ = 1.5 g/cm^3). Interestingly, the hollow shells of AB pollen have a density that is lower than all of these fillers.

Pycnometry was also used to determine the densities of the neat epoxy and pollen-epoxy composites. Neat epoxy's density was measured as 1.214g/cm^3, comparable to previously measured densities of epoxy [55, 56]. E-D and E-AB film densities were measured as 1.208g/cm^3 and 1.221 g/cm^3, respectively. Thus, unlike many other fillers would have done, pollen did not significantly increase the density of the epoxy matrix. AB pollen decreased the material density by ~.5% at a 10 wt% loading versus neat epoxy. However, E-AB mechanical properties appear to still be increasing at 10 wt% pollen loading. Thus, it is likely that further decreases in density are possible while still enhancing the mechanical properties of the cured epoxy. Also, interesting future work may involve sealing AB pollen and trapping air within the shells, which would allow for larger density reductions.

4.5 Conclusions

In this study, the effect of ragweed pollen loading on the mechanical, interfacial, and thermal properties of epoxy composites was investigated. Composites prepared with as received ragweed pollen (D) displayed decreased mechanical properties with increasing pollen loading due to the presence of a soft interphase. This interphase was formed due to the strong selective binding of amine crosslinker to D pollen intracellular material, resulting in an amine depleted zone of epoxide that did not fully crosslink. However, D pollen composites still showed increased glass transition temperatures (T_g) with increasing pollen loading. Pollen treated via an acid-base (AB) surface preparation becomes a load bearing filler in epoxy, displaying simultaneous stiffening and strengthening coupled with an improved interfacial morphology and increased T_g with increasing pollen loading. AB does not selectively bind amine due to the absence of intracellular material, and interacts more strongly with the epoxy matrix than D pollen due to epxposed and/or generated polar functional groups (hydroxyls and carboxyls) on AB pollen versus D pollen. Pollen displayed higher compatibility with epoxy than the thermoplastics previously studied (polystyrene, polycaprolactone, and polyvinyl acetate). This was clearly indicated by elimination of an additional functionalization step to optimize adhesion, elevated glass transition temperatures, and improved interfacial morphology. Finally, pollen was found to have no significant effect on the low epoxy density. These results indicate that pollen is a promising filler for creating high strength, light-weight polymer composites and merits further study. For example, investigating additional matrices with potential compatibility with pollen or incorporating pollen of different species in polymers in order to elucidate the effect of filler microstructure on the wetting and adhesion of fillers.

4.6 References

1. Limited, R.T., *High Performance Fillers 2005: Cologne, Germany, 8-9 March 2005*. 2005: Rapra.
2. Wypych, G., *Handbook of Fillers, 3e*. 2010: ChemTec Publishing.
3. Fu, S.-Y., et al., *Effects of particle size, particle/matrix interface adhesion and particle loading on mechanical properties of particulate–polymer composites.* Composites Part B: Engineering, 2008. **39**(6): p. 933-961.
4. Ash, B.J., et al., *Mechanical properties of Al2O3/polymethylmethacrylate nanocomposites.* Polymer Composites, 2002. **23**(6): p. 1014-1025.
5. Lučić, S., V. Kovačević, and D. Hace, *Mechanical properties of adhesive thin films.* International Journal of Adhesion and Adhesives, 1998. **18**(2): p. 115-123.
6. Spitalsky, Z., et al., *Carbon nanotube–polymer composites: Chemistry, processing, mechanical and electrical properties.* Progress in Polymer Science, 2010. **35**(3): p. 357-401.
7. Vollenberg, P.H.T. and D. Heikens, *The mechanical properties of chalk-filled polypropylene: a preliminary investigation.* Journal of Materials Science, 1990. **25**(7): p. 3089-3095.
8. Wang, W., et al., *Effective reinforcement in carbon nanotube–polymer composites.* Philosophical Transactions of the Royal Society A: Mathematical, Physical and Engineering Sciences, 2008. **366**(1870): p. 1613-1626.
9. Hall, S.R., H. Bolger, and S. Mann, *Morphosynthesis of complex inorganic forms using pollen grain templates.* Chemical Communications, 2003(22): p. 2784-2785.
10. Hall, S.R., et al., *Fabrication of Porous Titania (Brookite) Microparticles with Complex Morphology by Sol−Gel Replication of Pollen Grains.* Chemistry of Materials, 2006. **18**(3): p. 598-600.
11. Jenik, M., et al., *Pollen-imprinted polyurethanes for QCM allergen sensors.* Analytical and Bioanalytical Chemistry, 2009. **394**(2): p. 523-528.
12. Liu, T. and Z. Zhang, *Mechanical properties of desiccated ragweed pollen grains determined by micromanipulation and theoretical modelling.* Biotechnology and Bioengineering, 2004. **85**(7): p. 770-775.
13. Thio, B.J.R., J.-H. Lee, and J.C. Meredith, *Characterization of Ragweed Pollen Adhesion to Polyamides and Polystyrene Using Atomic Force Microscopy.* Environmental Science & Technology, 2009. **43**(12): p. 4308-4313.
14. Feng, C. and L. Dong-Xu, *Morphology-controlled synthesis of SiO 2 hollow microspheres using pollen grain as a biotemplate.* Biomedical Materials, 2009. **4**(2): p. 025009.
15. Wang, Y., et al., *Carbon Microspheres with Supported Silver Nanoparticles Prepared from Pollen Grains.* Langmuir, 2005. **21**(23): p. 10846-10849.
16. Wang, Y., et al., *Replication of biological organizations through a supercritical fluid route.* Chemical Communications, 2005(23): p. 2948-2950.
17. Lee, J.H., et al., *Pollen: A Novel, Biorenewable Filler for Polymer Composites.* Macromolecular Materials and Engineering, 2011. **296**(11): p. 1055-1062.
18. Fadiran, O.O. and J.C. Meredith, *Surface treated pollen performance as a renewable reinforcing filler for poly(vinyl acetate).* Journal of Materials Chemistry A, 2014. **2**(40): p. 17031-17040.

19. Piffanelli, P., J.H.E. Ross, and D.J. Murphy, *Biogenesis and function of the lipidic structures of pollen grains.* Sexual Plant Reproduction, 1998. **11**(2): p. 65-80.
20. Wiermann, R. and S. Gubatz, *POLLEN WALL AND SPOROPOLLENIN.* International Review of Cytology-a Survey of Cell Biology, 1992. **140**: p. 35-72.
21. Blackmore, S., et al., *Pollen wall development in flowering plants.* New Phytologist, 2007. **174**(3): p. 483-498.
22. Dominguez, E., et al., *Pollen sporopollenin: degradation and structural elucidation.* Sexual Plant Reproduction, 1999. **12**(3): p. 171-178.
23. Hemsley, A.R. and I. Poole, *The Evolution of Plant Physiology*. 2004: Elsevier Science.
24. Tesoro, G., *Epoxy resins-chemistry and technology, 2nd Edition, Clayton A. May, Ed., Marcel Dekker, New York, 1988, 1,288 pp. Price: $195.00.* Journal of Polymer Science Part C: Polymer Letters, 1988. **26**(12): p. 539-539.
25. Petrie, E.M., *Epoxy adhesive formulations*. 2006, McGraw-Hill: New York.
26. Thio, B.J.R., J.H. Lee, and J.C. Meredith, *Characterization of Ragweed Pollen Adhesion to Polyamides and Polystyrene Using Atomic Force Microscopy.* Environmental Science & Technology, 2009. **43**(12): p. 4308-4313.
27. Lin, H., I. Gomez, and J.C. Meredith, *Pollenkitt Wetting Mechanism Enables Species-Specific Tunable Pollen Adhesion.* Langmuir, 2013. **29**(9): p. 3012-3023.
28. Southworth, D., *Solubility of Pollen Exines.* American Journal of Botany, 1974. **61**(1): p. 36-44.
29. Sormana, J.-L., S. Chattopadhyay, and J.C. Meredith, *High-throughput mechanical characterization of free-standing polymer films.* Review of Scientific Instruments, 2005. **76**(6): p. 062214-9.
30. Domínguez, E., et al., *Isolation of intact pollen exine using anhydrous hydrogen fluoride.* Grana, 1998. **37**(2): p. 93-96.
31. Shaw, G. and D.C. Apperley, *13C-NMR spectra of Lycopodium clavatum sporopollenin and oxidatively polymerised β-carotene.* Grana, 1996. **35**(2): p. 125-127.
32. Barrier, S., *Physical and chemical properties of sporopollenin exine particles*, in *Chemistry*. 2008, The University of Hull.
33. María González González, J.C.C.a.J.B., *Applications of FTIR on Epoxy Resins - Identification, Monitoring the Curing Process, Phase Separation and Water Uptake*, in *Infrared Spectroscopy - Materials Science, Engineering and Technology*, P.T. Theophile, Editor. 2012, InTech.
34. Cecen, V., et al., *FTIR and SEM analysis of polyester- and epoxy-based composites manufactured by VARTM process.* Journal of Applied Polymer Science, 2008. **108**(4): p. 2163-2170.
35. Xu, S., et al., *Mechanical and thermal properties of waterborne epoxy composites containing cellulose nanocrystals.* Polymer, 2013. **54**(24): p. 6589-6598.
36. Yang, J.I., *PART I: SYNTHESIS OF AROMATIC POLYKETONES VIA SOLUBLE PRECURSORS DERIVED FROM BIS(A-AMININITRILE)S PART II: MODIFICATIONS OF EPOXY RESINS WITH FUNCTIONAL HYPERBRANCHED POLY(ARYLENE ESTER)S*, in *Chemistry*. 1998, Virginia Tech.
37. Ansari, F., et al., *Cellulose nanofiber network for moisture stable, strong and ductile biocomposites and increased epoxy curing rate.* Composites Part A: Applied Science and Manufacturing, 2014. **63**(0): p. 35-44.

38. Han, S.O. and L.T. Drzal, *Curing characteristics of carboxyl functionalized glucose resin and epoxy resin.* European Polymer Journal, 2003. **39**(7): p. 1377-1384.
39. Liu, F., et al., *Curing of diglycidyl ether of bisphenol-A epoxy resin using a poly(aryl ether ketone) bearing pendant carboxyl groups as macromolecular curing agent.* Polymer International, 2009. **58**(8): p. 912-918.
40. Wu, S. and M.D. Soucek, *Kinetic modelling of crosslinking reactions for cycloaliphatic epoxides with hydroxyl- and carboxyl-functionalized acrylic copolymers: 1. pH and temperature effects.* Polymer, 1998. **39**(23): p. 5747-5759.
41. Ma, J.Y., J.K. Ma, and K.C. Weber, *Fluorescence studies of the binding of amphiphilic amines with phospholipids.* Journal of Lipid Research, 1985. **26**(6): p. 735-44.
42. Tadolini, B. and G. Hakim, *Interaction of Polyamines with Phospholipids: Spermine and Ca2+ Competition for Phosphatidylserine Containing Liposomes*, in *Progress in Polyamine Research*, V. Zappia and A. Pegg, Editors. 1988, Springer US. p. 481-490.
43. Amato, M., et al., *Interactions between Amines and Phospholipids: A Chromatographic Study on Immobilized Artificial Membrane (IAM) Stationary Phases at Various pH Values.* Helvetica Chimica Acta, 2000. **83**(10): p. 2836-2847.
44. Sormana, J.-L. and J.C. Meredith, *High-Throughput Discovery of Structure−Mechanical Property Relationships for Segmented Poly(urethane−urea)s.* Macromolecules, 2004. **37**(6): p. 2186-2195.
45. Bergström, J.S. and M.C. Boyce, *Mechanical Behavior of Particle Filled Elastomers.* Rubber Chemistry and Technology, 1999. **72**(4): p. 633-656.
46. Delawa, U., *Delaware Composites Design Encyc: Micromechanical Materials Model*. 1990: Taylor & Francis.
47. Islam, M.A. and K. Begum, *Prediction Models for the Elastic Modulus of Fiber-reinforced Polymer Composites: An Analysis*. 2011. Vol. 3. 2011.
48. Wu, Y.-P., et al., *Modeling Young's modulus of rubber–clay nanocomposites using composite theories.* Polymer Testing, 2004. **23**(8): p. 903-909.
49. Hashin, Z., *Analysis of Composite Materials—A Survey.* Journal of Applied Mechanics, 1983. **50**(3): p. 481-505.
50. Hashin, Z. and S. Shtrikman, *A variational approach to the theory of the elastic behaviour of multiphase materials.* Journal of the Mechanics and Physics of Solids, 1963. **11**(2): p. 127-140.
51. Bakker, R.F.M., *PERMEABILITY OF BLENDED CEMENT CONCRETES.* Journal of the American Concrete Institute, 1983. **80**(4): p. 345-345.
52. Yoshitake, I.e.a., *A Prediction Method of Tensile Young's Modulus of Concrete at Early Age.* Advances in Civil Engineering, 2012. **2012**.
53. Yim, A., R.S. Chahal, and L.E.S. Pierre, *The effect of polymer—filler interaction energy on the T'g of filled polymers.* Journal of Colloid and Interface Science, 1973. **43**(3): p. 583-590.
54. Lu, H. and S. Nutt, *Restricted Relaxation in Polymer Nanocomposites near the Glass Transition.* Macromolecules, 2003. **36**(11): p. 4010-4016.
55. Sharma, K. and M. Shukla, *Three-Phase Carbon Fiber Amine Functionalized Carbon Nanotubes Epoxy Composite: Processing, Characterisation, and Multiscale Modeling.* Journal of Nanomaterials, 2014. **2014**: p. 10.
56. Yasmin, A., J.L. Abot, and I.M. Daniel, *Processing of clay/epoxy nanocomposites by shear mixing.* Scripta Materialia, 2003. **49**(1): p. 81-86.

CHAPTER 5

EXPLORING THE EFFECTS OF POLLEN SURFACE MICROSTRUCTURES ON ADHESION AND COMPOSITE PROPERTIES

5.1 Overview

Pollen grains have the potential to be effective plant-based biorenewable reinforcing fillers for polymers due to their high mechanical strength, chemical stability, and unique micro- and nano-structured surfaces. Pollen–polymer composites could form the basis for a new class of light-weight, high strength sustainable materials if compatible polymer–filler systems can be engineered. Pollen, being a microparticle that possesses a rich variety of surface nanoscale topography and features, also provides a unique way to study how filler fine-surface structure affects wetting, interphase adhesion, and mechanical reinforcement. In this work, the effect of the size of surface microstructures on wetting, interphase adhesion, and mechanical properties of pollen-polymer composites is explored. First, interfacial morphology and mechanical properties of polyvinyl acetate (PVAc) composites highly loaded with silane functionalized ragweed pollen and silane functionalized silica particles are compared in order to examine the effect of the presence of surface structural features. Silane-treated pollen-PVAc composites had higher tensile strength and strain at break than silanated silica particles. SEM images revealed voids at the silica-PVAc interface that were not observed with pollen grains. Thus, pollen shape (nanopores) and roughness may enhance wetting and adhesion at the interface when compared to a smooth spherical particle. Finally, the species of pollen incorporated in PVAc matrices was varied in order determine the effect of the size of surface nano- and micro- structures on wetting, adhesion, and composite properties. Pollen with smaller surface structures were wetted more effectively by PVAc than pollen with larger structures. However, mechanical properties were not

significantly different between composites with the different species of pollen. The results of this work highlight the potential of utilizing pollen as a probe to study how fine surface structures on particles can affect wetting and adhesion of polymers.

5.2 Introduction

Particulate fillers are often incorporated into polymers in order to improve their physical and/or chemical properties. Fillers can alter mechanical, thermal, and optical properties, to name a few [1-4]. Many studies have demonstrated the successful use of non-biological materials ranging from inorganic particles, such as calcium carbonate, to carbon organic materials including carbon blacks and nanotubes as reinforcing fillers in fabricating polymer composites [5-8]. Many particulates are denser than the polymer, or are derived in a non-sustainable manner, and there is interest in finding lower density, sustainably sourced alternatives. Most fillers are spherical or irregular spheroids, without significant capability to alter the particle fine surface features or geometry.

In contrast, pollen has the potential to be an effective biorenewable filler with a variety of unique architectures of its outer shell [9-13]. Besides being used directly as a filler, biological particulates such as pollen grains, bacteria, and viruses have attracted much research interest as templates for fabricating synthetic inorganic mimics that preserve their unique surface architectures [9-11, 14-16]. In these studies, particles such as pollen grains can be coated through various methods (i.e. sol-gel processes) and then burned off in order to obtain micro- or nanoparticles with unique morphologies otherwise unachievable. These inorganic mimics may also function as fillers that combine biological architecture with synthetic chemistry. While some studies have investigated pollen grains, only two studies have reported utilization of pollen as a filler [17, 18].

Pollen grains are the carrier of the male gametes for plant reproduction. A pollen grain is composed of an outer layer (exine) and an inner layer (intine) [19, 20]. The exine is composed of sporopollenin, a highly crosslinked organic substance consisting of fatty acids, phenylpropanoids, and phenolics [21, 22]. Monomer and macromer components that have been confirmed in sporopollenin, include long aliphatic chains, aromatic cross-linkers (mainly cinnamic acids), ether cross-linkages and ester functions [23]. The exine's chemical composition suggests compatibility with polymers capable of polar interactions. Underneath the exine layer, not exposed to the outer surface, lies the intine, which is rich in cellulose and hemicelluloses. The cellular material carried within the grain is easily extracted using well known techniques, leaving behind a hollow, strong shell.

Thus, pollen being a microparticle that possesses a rich variety of surface nanoscale topography and features, provides a unique way to study how filler fine-surface structure affects wetting, interphase adhesion, and mechanical reinforcement. In this work, the effect of the size of surface microstructures on wetting, interphase, adhesion, and mechanical properties was explored. First, interfacial morphology and mechanical properties of poly(vinyl acetate) (PVAc) composites highly loaded with silane functionalized short ragweed pollen (*A. artemisiifolia*) and silane functionalized silica particles were compared in order to examine the effects 'rough' particle versus a completely smooth spherical particle. Finally, several species of pollen were incorporated in PVAc in order determine the effect of the size of surface nano- and micro-structures on wetting, adhesion, and composite properties. Short ragweed pollen, Kentucky Blue/June (*Poa pratensis*), and Dog Fennel (*Eupatorium capillifolium*), were incorporated in PVAc matrices. The results of this work highlight the potential of utilizing pollen as a probe to study how fine surface structures on particles can affect wetting and adhesion of polymers.

5.3 Experimental

5.3.1 Materials

Defatted types of Short ragweed (*A. artemisiifolia*), Kentucky Blue/June (*Poa pratensis*), and Dog Fennel (*Eupatorium capillifolium*) were purchased from Greer Laboratories and stored at 4 °C prior to use. Potassium hydroxide (KOH, EMD Millipore) and phosphoric acid (H_3PO_4, BDH chemicals) were used for pollen treatment. 20 micron (average particle size) silica gel (VWR) was also incorporated in PVAc. VAM (Sigma Aldrich) was filtered through aluminum silicate to remove hydroquinone inhibitor. Azobisisobutyronitrile (AIBN, Sigma Aldrich) was of reagent grade and absolute ethanol was used as solvent. Vinyltrimethoxysilane (VTMS, Sigma Aldrich) was used to functionalize pollen and silica surfaces.

5.3.2 Extraction of Pollen Cellular Material

An acid-base treatment (hereafter labeled as AB) was used to clean and isolate the exine shell for incorporation in polymer films as well as to prepare them for further functionalization [20, 24]. Briefly, pollen was dispersed in 6w/v% KOH solution for 24 hours while stirring. After washing the pollen with hot water, ethanol, and drying the pollen, it was dispersed in 85% H_3PO_4 for 7 days. This pollen was dried after washing with hot water, acetone, and ethanol. This process caused the pollen grains to lose ~80% of their original weight. This treatment was used for all three pollen types and these are labelled ABR (ragweed), ABK (Kentucky), and ABD (dog fennel). AB pollens were incorporated in polymer films via the *in situ* polymerization.

5.3.3 Silane Functionalization of Particles

AB pollen was used as the starting point for functionalization with VTMS (hereafter referred to as ABV) to enable grafting of polymer chains to the pollen surface. AB pollen was heated under vacuum at 100 °C to remove adsorbed water then dispersed in toluene and

sonicated. This solution was purged under nitrogen for 30 minutes while stirring. VTMS was added to the flask with a syringe through a rubber stopper. This solution was heated overnight and pollen was recovered after washing with toluene, hexane, and ethanol. Silica was functionalized with the same procedure. ABV pollen and silica was incorporated in polymer films via the *in situ* polymerization.

5.3.4 *In situ* Polymerization of PVAc Composites

AIBN (0.0135 g) was added to VAM (32.66 g) in a round bottom flask. After the AIBN dissolved, 15 mL of ethanol were also added to the flask. For composites, a measured mass of pollen grains or silica particles (for composites containing 1-15 vol%) was dispersed in the ethanol and sonicated prior to addition to the flask, to ensure pollen dispersion. The flask was purged with nitrogen and the mixture was stirred at 75 °C for 2.5 h. The resulting solution mixtures were cast on glass plates with a doctor blade, and slowly dried under a solvent saturated environment for 24 h. The films were dried under vacuum for 24 h at 90 °C. Samples were slowly cooled down to room temperature before peeling the films from the plates using a razor.

5.3.5 Characterization

FTIR spectra were obtained on a Thermo Scientific spectrophotometer from 4000 cm^{-1} to 400 cm^{-1}. A high-throughput mechanical characterization (HTMECH) apparatus was used to measure mechanical properties including tensile strength, elastic modulus, and toughness, as described previously [25]. Briefly, the polymer films were mounted on a steel grid and contacted with a steel pin with a 1.5 mm diameter hemispherical cap at a constant strain rate (0.5mm/s). The pin is oriented normal to the film surface, resulting in equi-biaxial deformation. For each sample, an average thickness was obtained using 9 measurements with a micrometer, 9 stress–strain profiles were measured to failure, and mechanical properties of the films were obtained.

All mechanical tests were performed under ambient conditions. Scanning electron microscopy (SEM) was performed with a Zeiss Ultra-60 FE-SEM instrument to examine the interfacial morphology of both freeze fractured and HTMECH fracture surfaces of the composites.

5.4 Results and Discussion

5.4.1 Pollen versus Smooth Silica Particles

In chapter 3, Figure 3.7 displayed the freeze fracture and HTMECH fracture surfaces of ABV pollen in polymerized PVAc. ABV pollen displayed optimal interfacial adhesion in that study, relative to other functionalizations, due to the grafting of polymer chains on the pollen surface which are able to entangle with the chains of the polymer matrix, resulting in adhesion between the phases. Here, silica particles were also functionalized with VTMS, in order to minimize differences in adhesion arising from differences in surface chemistry so that the smooth spherical silica particle can be compared to the more complex spiny pollen grain as a filler. Figure 5.1 displays silica particles utilized and the freeze fracture and HTMECH fracture surfaces of functionalized silica in polymerized PVAc. Freeze fracture surfaces display good adherence of the PVAc matrix to silica surfaces. Arrows in Figure 5.1c show areas where PVAc remained strongly attached to the otherwise exposed surface of silica particles. HTMECH fracture surfaces (Figure 5.1b to Figure 5.1d) reveal small amounts of residual polymer attached to the silica surface after fracture, but also that the PVAc often separates from the silica surface after testing (indicated by arrows). This interfacial separation was not observed in HTMECH fracture surfaces with ABV incorporated in PVAc (Figure 3.7). Pollen shape factors, such as pollen pores,

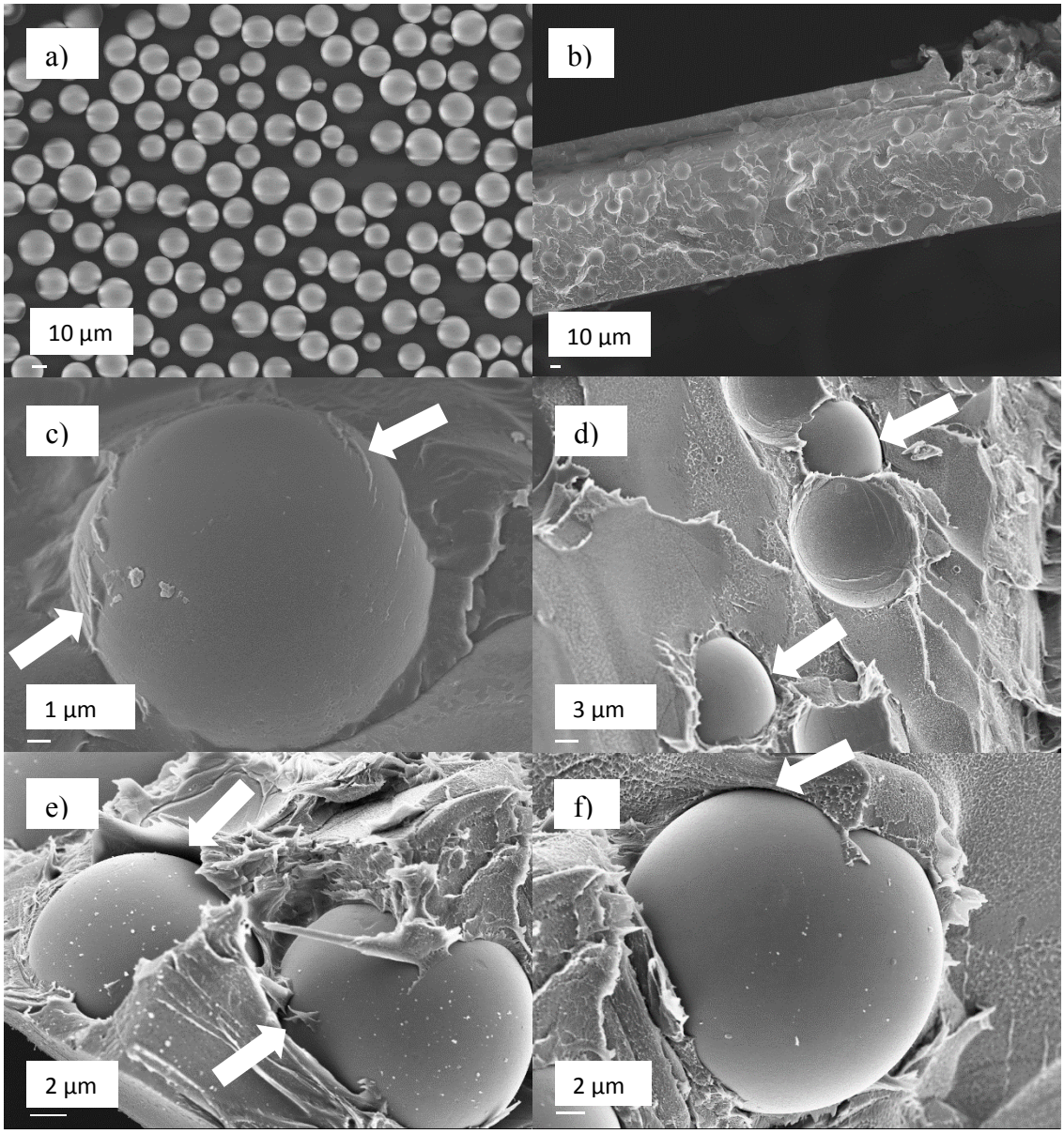

Figure 5.1: Functionalized silica (a) incorporated in PVAc fracture surfaces. Freeze fractured cross sections (b and c) and HTMECH fracture surfaces (d and f).

apertures, and hollowness may also play a role in enhanced adhesion and lack of interfacial separation. Polymer chains are grafted on both the inside and outside of pollen grain due to their hollow shape. Chains of the bulk matrix may also be able to interlock with the surface of the pollen surface. This additional mechanical interlocking of polymer chains with the pollen surface may diminish interfacial separation versus a non-hollow silica particle.

Figure 5.2 displays the mechanical properties of highly loaded composites with ABV

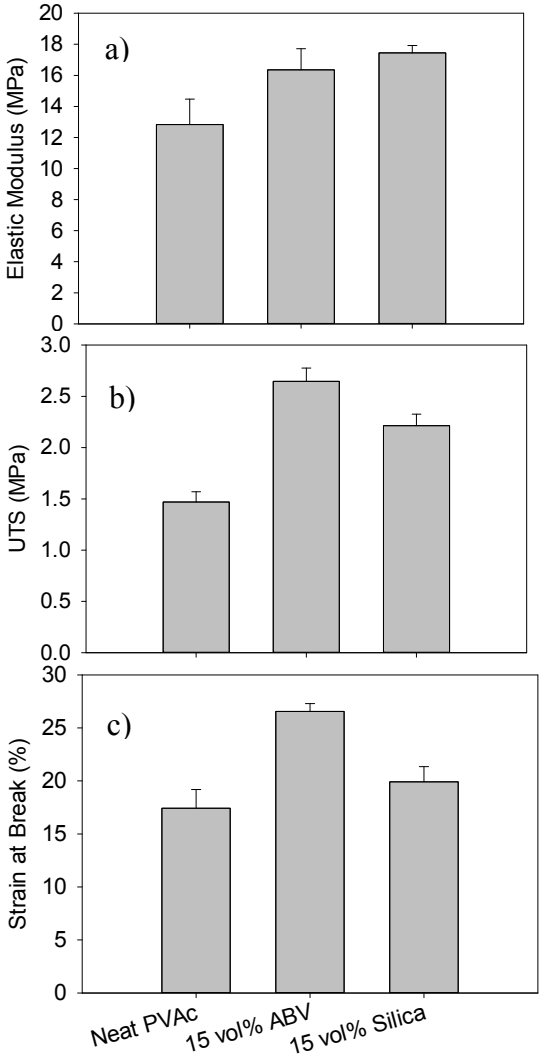

Figure 5.2: Elastic modulus (a), UTS (b), and strain at break (c) of neat PVAc and highly loaded PVAc composites with ABV and silca, measured with HTMECH. The error bars are 95% confidence intervals.

pollen and silica versus neat polymer. Silica appears to follow the same trends as PVAc-ABV composites. At the highest loading, functionalized silica increased elastic modulus, UTS, and strain at break. This is attributed to the addition of stiffer silica particles in the matrix as well as interfacial adhesion due to the grafting of polymer chains on the silica surface. Comparing, high loadings of ABV and silica, silica imparts higher stiffness to the PVAc matrix. ABV pollen is estimated to be stiffer than various polymers (Chapter 3 and 4), however it is not as stiff as silica and thus does not stiffen the matrix to the same degree. As stated in Chapters 3

4, a previous study estimated ragweed's compressive modulus to be about 1653 MPa [12]. A similar micromanipulation study of silica particles estimated a compressive modulus of 30.8 GPa [26]. It is clear however that at similar loadings, ABV pollen imparts higher tensile strength and strain at break on PVAc than silica particles. Degree of adhesion is vital for effective stress transfer from the matrix to filler particle surface, resulting in reinforcement. Thus, the larger magnitude of tensile strength in ABV composites versus silica composites may indicate a higher degree of adhesion between PVAc and ABV pollen than with silica. This is consistent with the observed lack of interfacial separation evidenced in SEM images with ABV versus silica fillers (Figure 5.1). Again, pollen shape may also play a role in in the lack of separation due to additional interlocking of polymer with the pollen surface. Finally, pollen grains may be more flexible than silica particles as indicated by modulus measurements from previous micromanipulation studies [12, 26]. Ragweed was determined to behave purely elastically in the deformation range studied (up to 17% deformation and with average fracture forces of 1.2 mN). In the silica study, microspheres transitioned from elastic to elastic-plastic at deformations of 8.5% and fracture forces of ~.3mN. Thus pollen's enhanced flexibility versus silica may lead to improvements in the strain at break of the PVAc matrix with pollen filler.

5.4.2 Effect of Surface Feature Sizes

Figure 5.3 displays the three different pollen species chosen for investigating the effects of the size of pollen surface features on wetting and adhesion of the polymer matrix. The various characteristics of the pollen grains are summarized in Table 5.1. ABK is the "smoothest" grain chosen, with the smallest and most closely-spaced features.

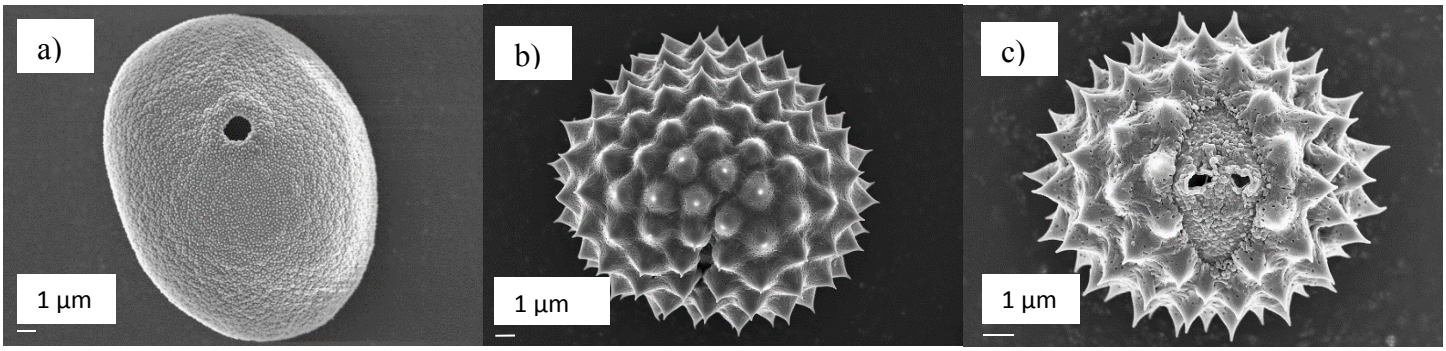

Figure 5.3: ABK (a), ABR (b), and ABD (c) pollen grains.

Table 5.1: Characteristics of chosen pollen grains for microstructure investigations.

Species	Shape	Diameter	Diamter (tip to tip)	Feature Height	Feature Base	Base Spacing	Pores
ABK	Spheroidal/ Ovulate	~19-27 µm	~19-27 µm	~90-150 nm	~90-150 nm	~100-270 nm	--
ABR	Spheroidal	~15 µm	~18 µm	~1.5 µm	~1.4-1.7 µm	~2-2.8 µm	~20-70 nm
ABD	Spheroidal	~12 µm	~15 µm	~1.5 µm	~1.4-1.7 µm	~2-2.8 µm	~100-166 nm

Also, ABK possesses only one aperture (large opening shown in Figure 5.3a) and has no pores visible with SEM. The exine shell in ABK is much thinner than that of the other species chosen. Compared to ABK, ABR possesses larger spine features, 3 apertures, and nano sized pores on the surface. Finally, ABD possesses spines that are similar in size to ABR spines, but larger relative to the diameter of the ABD pollen. ABD also possesses 3 apertures, which are more opened than ABR pollen's apertures, and nano sized pores that are larger than ABR pollen's pores.

In Chapter 3 it was shown that in the absence of the acid-base hydrolysis treatment there was little to no adhesion between ragweed pollen grains and the PVAc matrix, resulting in interfacial voids (Figure 3.4). As received, untreated defatted blue june pollen was incorporated in polymerized PVAc to explore whether the absence of AB treatment results in poor adhesion

for pollens other than ragweed. Figure 5.4 shows both freeze fractured and HTMECH fracture surfaces of these composites, where arrows indicate interfacial voids are clearly present. Thus, in order to probe wetting and adhesion of varied microstructures, it is ideal to treat all of the pollen surfaces to promote uniform adhesion. The chosen pollen species were all subjected to the acid-base hydrolysis before incorporation in polymerized PVAc. Figure 5.5 shows the similar FTIR spectra of ABR, ABK, and ABD pollens. Characteristic peaks such as the –OH stretch (~3400 cm^{-1}), –CH stretches of $–CH_2$ groups (2940 and 2855 cm^{-1}), and C=O stretch of carboxyl groups (~1706 cm^{-1}) peaks occur at generally the same wavenumbers. However, compared to both ABR and ABD pollens, ABK pollen appears to have a higher ratio of CH_2 groups to both hydroxyl and carboxyl groups, indicated by peak intensities. Thus, with the similarities in sporopollenin chemistry across species, it is plausible rule-out chemical differences as a cause for any differences in interfacial morphology or mechanical properties of composites.

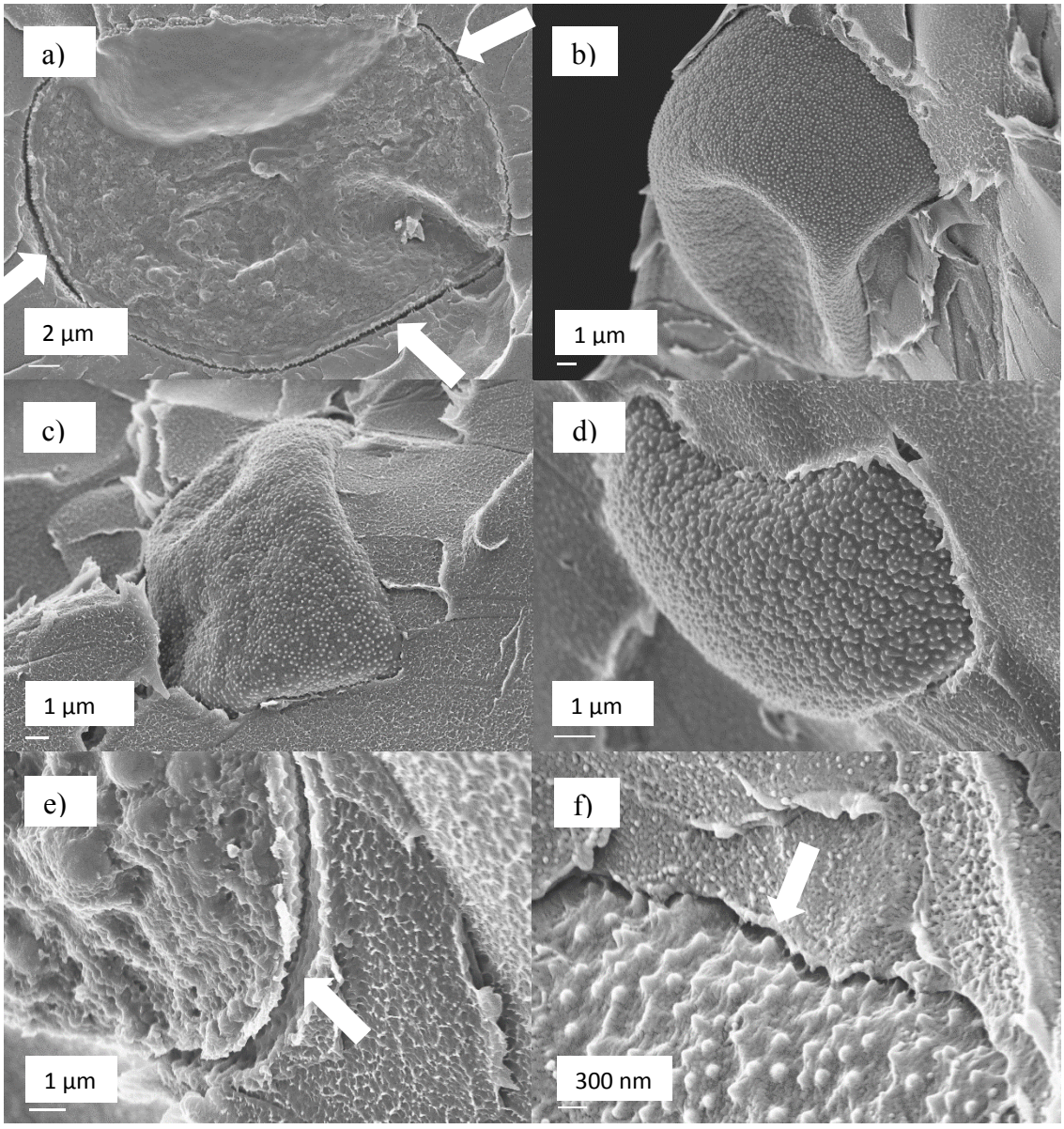

Figure 5.4: As received, defatted blue june pollen in PVAc. Freeze fractured cross sections (a) and HTMECH fracture surfaces (b to f). Arrows indicate interfacial voids.

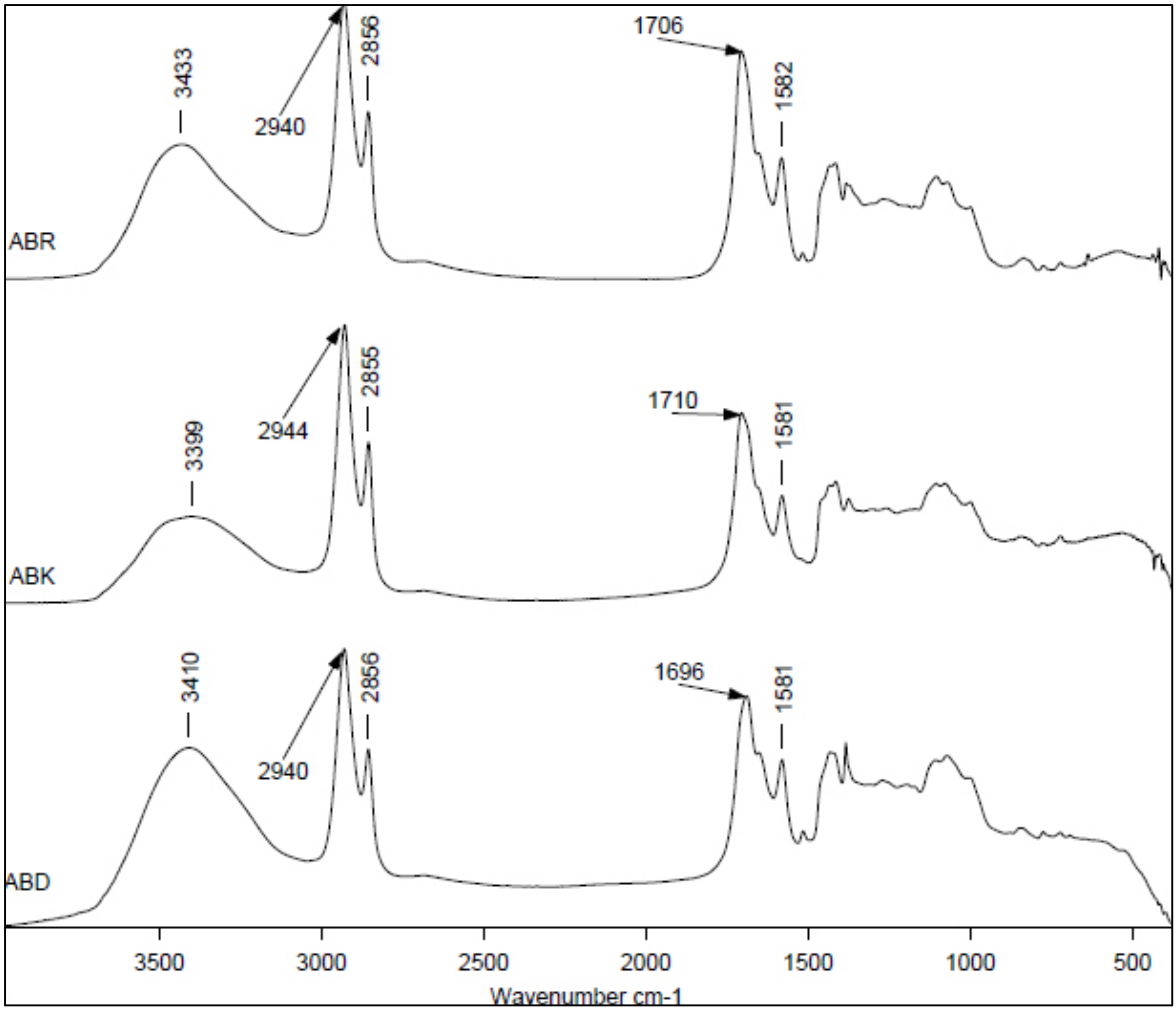

Figure 5.5: FTIR spectra of three pollen species after acid-base treatment.

Figure 5.6 shows freeze fractured surfaces of ABK pollen incorporated in PVAc. Again, as observed in the work from Chapters 2 and 3, acid-base hydrolysis of pollen eliminated interfacial voids due to exposed and/or generated polar functional groups on the pollen surface,

resulting in specific interactions and enhanced adhesion. Figure 5.6a shows a large number of broken cross sections of ABK pollen grains. This may indicate strong adhesion between the matrix and the ABK surface, which lead to cohesive failure in the exine shell. However, as mentioned previously the exine shell of ABK is thinner than the other species probed. Where ABK pollen is easily found in the images, one can observe areas where PVAc covered and remained strongly to the ABK surface. As,

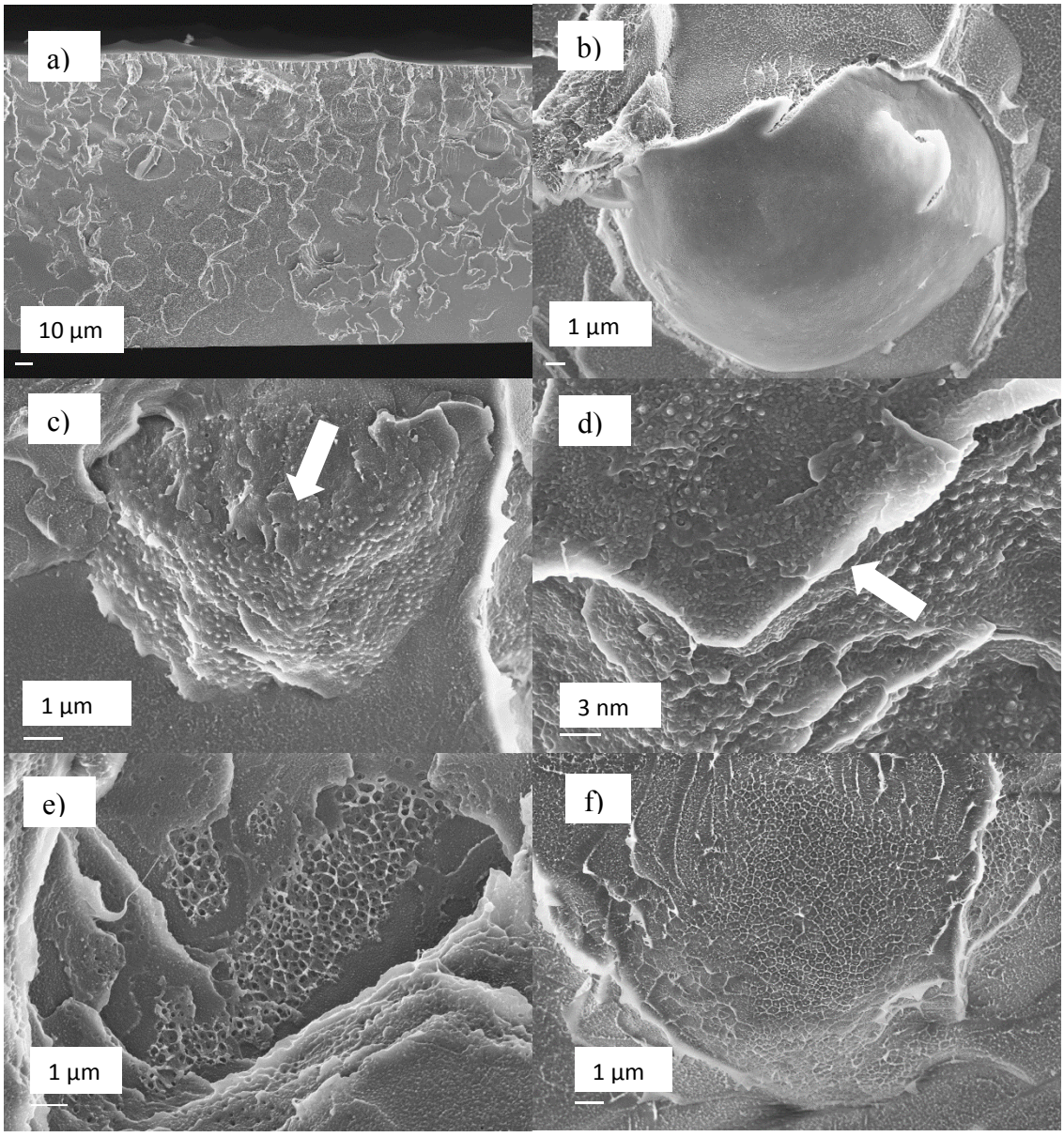

Figure 5.6: Freeze fractured cross sections of ABK pollen in PVAc.

opposed to work with ABR in Chapter 3 (Figure 3.6), and even silica surfaces (Figure 5.1), the surface of ABK is rarely ever completely exposed and always retains some adherent PVAc. Figure 5.6e shows the imprint where an ABK pollen grain was originally present and Figure 5.6f shows a commonly found, deeply imbedded ABK grain in the matrix with the same webbing pattern shown in Figure 5.6e. This pattern is caused by the polymer matrix intimately filling the spaces between the ABK nano features. Figure 5.7 shows the HTMECH fracture surfaces of ABK in PVAc. Again, Figure 5.7a and

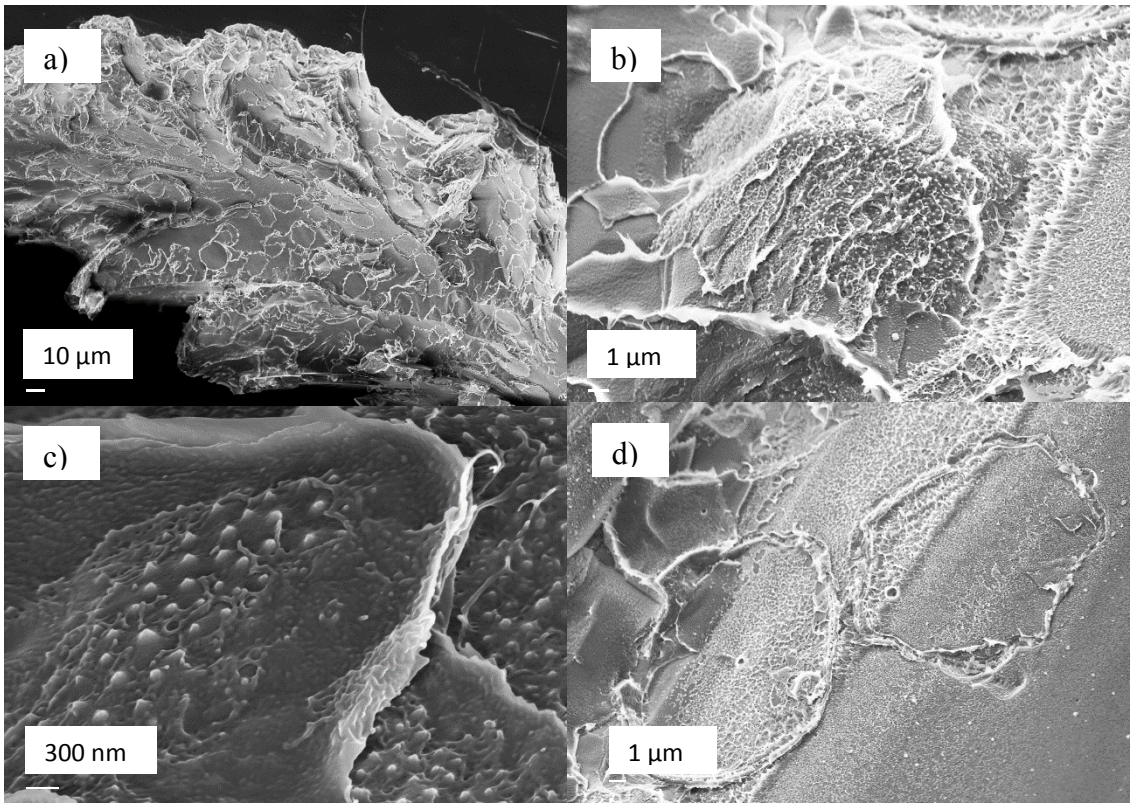

Figure 5.7: HTMECH fracture surfaces of ABK pollen in PVAc.

Figure 5.7b show the large amount of broken cross sections of ABK after fracture, which is observed much less with ABR pollen. The HTMECH fracture surfaces also further reveal the increased coverage of polymer and strongly attached residual polymer on ABK surfaces after fracture. Pollen with smaller surface structures were adhered more effectively to polymer

matrices than pollen with larger structures, thus we may infer that wetting of ABK pollen is improved versus ABR pollen. Sporopollenin is believed to be a hydrophilic particle, due to the presence of polar functional groups, such as hydroxyls and carboxyls. PVAc is also hydrophilic due to its polar functionalities [27, 28]. It has been observed that microscopically rough or spiked surfaces can improve wettability of hydrophilic surfaces [29-33]. Thus, wetting of polymer surrounding pollen grains is likely to be affected by pollen surface roughness and surface features. Some studies have shown that patterned surfaces with higher spacing to diameter ratios and lower aspect ratios tend to be more fully wetted [34, 35]. Considering Table 5.1, ABK pollen has an aspect ratio of ~.6-1.7 and a spacing to diameter ratio of ~1.08-3. ABR has an aspect ratio of ~.88-1.1 and a space to diameter ratio of 1.2-2. Due to the range of these values it is challenging to draw a conclusion about how aspect ratio and space to diameter ratio may affect wetting. However, at a certain point below the spine tips the diameter of the spines becomes larger very rapidly. The spines of ABR are actually higher aspect ratio if the very wide bases are not considered (>2.5). Thus, the larger spines on ABR may actually have the effect of a high aspect ratio surface feature which may inhibit wetting of the polymer matrix more so than surface features on ABK.

Figure 5.8 shows freeze fractured surfaces of ABD pollen incorporated in PVAc. As shown in Table 5.1, ABD is very similar to ABR, except for a slightly smaller diameter, slightly larger pores, and more open apertures. Figure 5.8b and Figure 5.8c, show that although interfacial adhesion is optimized, where intact grains are visible, the surface of ABD pollen is often exposed and free of polymer coating, similar to ABR pollen (Figure 3.6). Broken pollen cross sections are also apparent, though not as frequent as ABK pollen. Figure 5.9 shows the HTMECH fracture surfaces of PVAc with ABD pollen, which lead to similar observations as the

freeze fractured surfaces. These images are also very similar to the freeze fractured surfaces of ABR pollen composites. This may indicate that the dominate shape characteristics that affect wetting and adhesion at the pollen polymer interface, are the size and spacing of spines. Characteristics related to pores, apertures, and grain diameter are less significant.

In summary, the interfacial morphology of composites with ABR and ABD are very similar, and this is believed to be due to the similarities of the chemistry of the sporopollenin and the spine shape and sizes. The high aspect ratio of the spine tips may diminish the degree of wetting and adhesion at the interface, resulting in exposed surfaces of the pollen grain observed after freeze fracturing or HTMECH testing. On the other hand, ABK possesses low aspect ratio bumps on its surface, which may lead to enhanced wetting and adhesion indicated by the absence of significant ABK surface exposure in the freeze- and HTMECH-fractured samples.

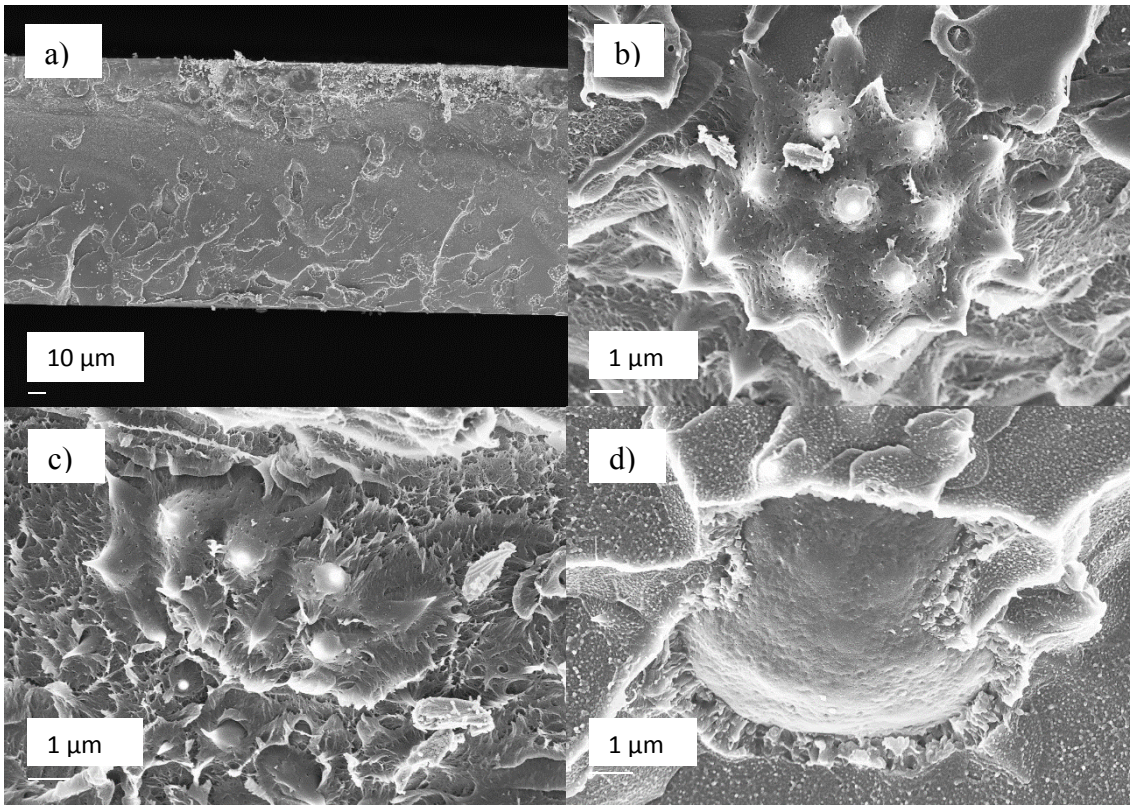

Figure 5.8: Freeze fractured cross sections of ABD pollen in PVAc.

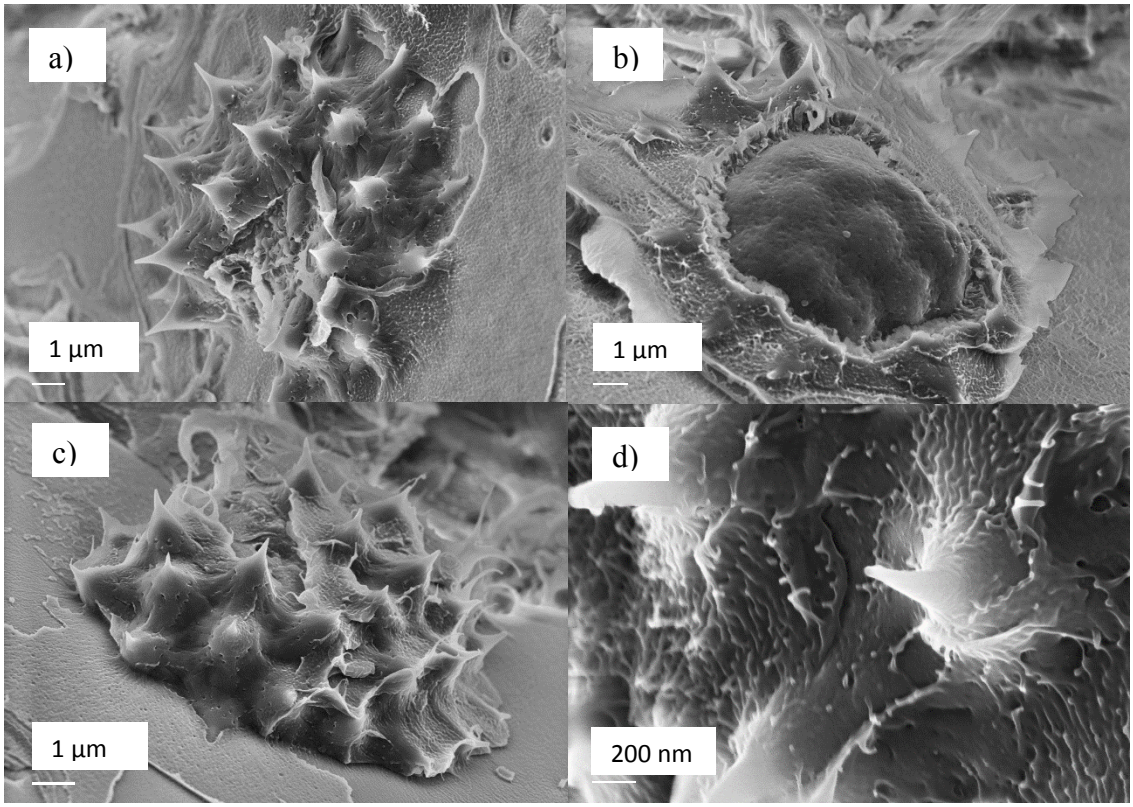

Figure 5.9: HTMECH fracture surfaces of ABD pollen in PVAc.

The polymer matrix heavily coats ABK pollen grains, making them hard to visibly locate in SEM imaging and intimately fills the groves between the surface bumps (indicated by webbing patterns in Figure 5.6f. Also, there is a much higher amount of broken ABK cross sections on fracture surfaces, than ABR and ABD composites which may be attributed to enhanced adhesion with ABK grains or its thinner exine.

Figure 5.10 shows the mechanical properties of composites with varied pollen species. In general, the trends are similar to those observed for AB pollen types investigated in Chapter 3. AB pollen types stiffen

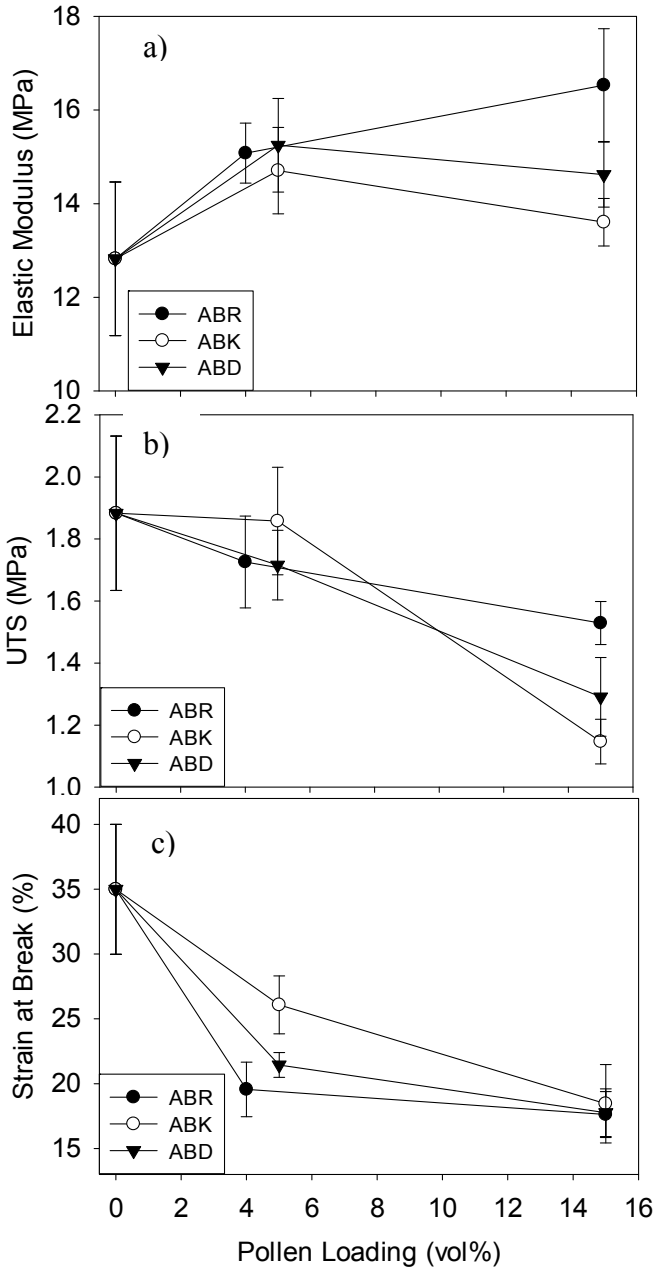

Figure 5.10: Elastic modulus (a), UTS (b), and strain at break (c) of composites with ABR, ABK, and ABD. The error bars are 95% confidence intervals.

the polymer matrix due to elimination of interfacial voids (versus as received untreated pollen grains), but still decrease both tensile strength and strain at break with increased pollen loading. All the pollen grains used displayed an apparent plateauing behavior at higher loadings also observed in Chapter 3 with ABR pollen, which was ascribed to increased proximity of pollen grains (particle-particle interactions) and particle agglomeration [3]. The drop in apparent

reinforcement is most apparent with ABK pollen. This may be due to the thinner exine shell of ABK versus ABR and ABD pollen, or to the effect of ABK's distinct reticulate surface microstructure, composed of many tiny grooves, on its effective modulus. Additionally, as seen in Table 5.1, ABK pollen is the largest of the three pollen grains. Thus, at similar pollen loadings, ABK pollen grains lie in closer proximity to one another. As can be seen in Figure 5.6a and Figure 5.7a, ABK pollen grains are in closer proximity to one another in composites than ABR and ABD composites, at the highest pollen loadings. Thus, particle-particle interactions may play a larger role in the decreased ineffectiveness of stiffening with ABK pollen. There is no definitive evidence in the mechanical properties of enhanced adhesion in ABK composites, despite its improved interfacial morphology versus ABR and ABD. Tensile strength decreases continually in all cases. ABK's 5% loading seems to have higher tensile strength than the other samples, however overlapping error bars indicate these differences may not be significant. At the highest loading ABK and ABD composites appear to have lower tensile strengths than ABR composites. Again, strain at break decreases continually. ABK pollens seem to degrade strain at break less than ABR and ABD at 5% loadings, however, at the highest loadings, all films display similar strain at break values. Thus, despite visual evidence of possibly improved adhesion of PVAc to ABK versus ABR and ABD, mechanical properties do not convincingly corroborate these observations. Hence we conclude that the difference between reticulate and echinate morphology does not play a significant role in observed mechanical reinforcement, assuming that the chemistry between the three AB-treated pollen species is similar.

5.5 Conclusions

In this work, the effect of the size of surface microstructures on wetting, interphase adhesion, and mechanical properties is explored. First, interfacial morphology and mechanical

properties of PVAc composites highly loaded with silane functionalized ragweed pollen and silane functionalized silica particles are compared in order to examine the effects of a 'rough' particle versus a completely smooth sphere. The rougher echinate pollen imparted higher tensile strength and strain at break on PVAc matrices than the smooth silica particles. Separation at the silica-PVAc interface, which was not observed for pollen grains, was clearly apparent after mechanical tests of silica-filled PVAc. Pollen shape (nanopores and hollowness) and roughness may enhance wetting and adhesion at the interface when compared to a smooth spherical particle. The species of pollen incorporated in PVAc matrices was varied in order determine the effect of the size of surface nano- and micro- structures on wetting, adhesion, and composite properties. Pollen with small echinate spines and grooves (ABK) were better adhered to PVAc in SEM images, compared to pollen with larger echinate structures. However, mechanical properties did not indicate that this apparent enhanced adherence for ABK resulted in more effective stress transfer at the interface.

5.6 References

1. Limited, R.T., *High Performance Fillers 2005: Cologne, Germany, 8-9 March 2005*. 2005: Rapra.
2. Wypych, G., *Handbook of Fillers, 3e*. 2010: ChemTec Publishing.
3. Fu, S.-Y., et al., *Effects of particle size, particle/matrix interface adhesion and particle loading on mechanical properties of particulate–polymer composites.* Composites Part B: Engineering, 2008. **39**(6): p. 933-961.
4. Ash, B.J., et al., *Mechanical properties of Al2O3/polymethylmethacrylate nanocomposites.* Polymer Composites, 2002. **23**(6): p. 1014-1025.
5. Lučić, S., V. Kovačević, and D. Hace, *Mechanical properties of adhesive thin films.* International Journal of Adhesion and Adhesives, 1998. **18**(2): p. 115-123.
6. Spitalsky, Z., et al., *Carbon nanotube–polymer composites: Chemistry, processing, mechanical and electrical properties.* Progress in Polymer Science, 2010. **35**(3): p. 357-401.
7. Vollenberg, P.H.T. and D. Heikens, *The mechanical properties of chalk-filled polypropylene: a preliminary investigation.* Journal of Materials Science, 1990. **25**(7): p. 3089-3095.

8. Wang, W., et al., *Effective reinforcement in carbon nanotube–polymer composites.* Philosophical Transactions of the Royal Society A: Mathematical, Physical and Engineering Sciences, 2008. **366**(1870): p. 1613-1626.
9. Hall, S.R., H. Bolger, and S. Mann, *Morphosynthesis of complex inorganic forms using pollen grain templates.* Chemical Communications, 2003(22): p. 2784-2785.
10. Hall, S.R., et al., *Fabrication of Porous Titania (Brookite) Microparticles with Complex Morphology by Sol−Gel Replication of Pollen Grains.* Chemistry of Materials, 2006. **18**(3): p. 598-600.
11. Jenik, M., et al., *Pollen-imprinted polyurethanes for QCM allergen sensors.* Analytical and Bioanalytical Chemistry, 2009. **394**(2): p. 523-528.
12. Liu, T. and Z. Zhang, *Mechanical properties of desiccated ragweed pollen grains determined by micromanipulation and theoretical modelling.* Biotechnology and Bioengineering, 2004. **85**(7): p. 770-775.
13. Thio, B.J.R., J.-H. Lee, and J.C. Meredith, *Characterization of Ragweed Pollen Adhesion to Polyamides and Polystyrene Using Atomic Force Microscopy.* Environmental Science & Technology, 2009. **43**(12): p. 4308-4313.
14. Feng, C. and L. Dong-Xu, *Morphology-controlled synthesis of SiO 2 hollow microspheres using pollen grain as a biotemplate.* Biomedical Materials, 2009. **4**(2): p. 025009.
15. Wang, Y., et al., *Carbon Microspheres with Supported Silver Nanoparticles Prepared from Pollen Grains.* Langmuir, 2005. **21**(23): p. 10846-10849.
16. Wang, Y., et al., *Replication of biological organizations through a supercritical fluid route.* Chemical Communications, 2005(23): p. 2948-2950.
17. Lee, J.H., et al., *Pollen: A Novel, Biorenewable Filler for Polymer Composites.* Macromolecular Materials and Engineering, 2011. **296**(11): p. 1055-1062.
18. Fadiran, O.O. and J.C. Meredith, *Surface treated pollen performance as a renewable reinforcing filler for poly(vinyl acetate).* Journal of Materials Chemistry A, 2014. **2**(40): p. 17031-17040.
19. Piffanelli, P., J.H.E. Ross, and D.J. Murphy, *Biogenesis and function of the lipidic structures of pollen grains.* Sexual Plant Reproduction, 1998. **11**(2): p. 65-80.
20. Wiermann, R. and S. Gubatz, *POLLEN WALL AND SPOROPOLLENIN.* International Review of Cytology-a Survey of Cell Biology, 1992. **140**: p. 35-72.
21. Blackmore, S., et al., *Pollen wall development in flowering plants.* New Phytologist, 2007. **174**(3): p. 483-498.
22. Dominguez, E., et al., *Pollen sporopollenin: degradation and structural elucidation.* Sexual Plant Reproduction, 1999. **12**(3): p. 171-178.
23. Hemsley, A.R. and I. Poole, *The Evolution of Plant Physiology*. 2004: Elsevier Science.
24. Southworth, D., *Solubility of Pollen Exines.* American Journal of Botany, 1974. **61**(1): p. 36-44.
25. Sormana, J.-L., S. Chattopadhyay, and J.C. Meredith, *High-throughput mechanical characterization of free-standing polymer films.* Review of Scientific Instruments, 2005. **76**(6): p. 062214-9.
26. Paul, J., et al., *A review of models for single particle compression and their application to silica microspheres.* Advanced Powder Technology, 2014. **25**(1): p. 136-153.
27. Drelich, J., Laskowski, and K.L. Mittal, *Apparent and Microscopic Contact Angles*. 2000: Taylor & Francis. 149-170.

28. Ucar, I., et al., *Combined XPS and contact angle studies of ethylene vinyl acetate and polyvinyl acetate blends.* Applied Surface Science, 2011. **257**(22): p. 9587-9594.
29. Bico, J., U. Thiele, and D. Quéré, *Wetting of textured surfaces.* Colloids and Surfaces A: Physicochemical and Engineering Aspects, 2002. **206**(1–3): p. 41-46.
30. Geoghegan, M. and G. Krausch, *Wetting at polymer surfaces and interfaces.* Progress in Polymer Science, 2003. **28**(2): p. 261-302.
31. Kavousanakis, M.E., C.E. Colosqui, and A.G. Papathanasiou, *Engineering the geometry of stripe-patterned surfaces toward efficient wettability switching.* Colloids and Surfaces A: Physicochemical and Engineering Aspects, 2013. **436**(0): p. 309-317.
32. Quéré, D., *Wetting and Roughness.* Annual Review of Materials Research, 2008. **38**(1): p. 71-99.
33. Quéré, D., *Rough ideas on wetting.* Physica A: Statistical Mechanics and its Applications, 2002. **313**(1–2): p. 32-46.
34. Kulkami, S.A., S.B. Ogale, and K.P. Vijayamohanan, *Tuning the hydrophobic properties of silica particles by surface silanization using mixed self-assembled monolayers.* Journal of Colloid and Interface Science, 2008. **318**(2): p. 372-379.
35. Shah, G.J., M. Sitti, and Ieee, *Modeling and design of biomimetic adhesives inspired by gecko foot-hairs*. IEEE ROBIO 2004: Proceedings of the IEEE International Conference on Robotics and Biomimetics. 2004. 873-878.

CHAPTER 6

CONCLUSIONS AND RECOMMENDATIONS

6.1 Summary and Conclusions

This work provides a foundation for exploiting pollen grains as sustainable filler for creating high strength, light weight polymer composites. The results demonstrate the successful completion of the specific objectives outlined in Chapter 1. The key findings for each objective are summarized as follows:

6.1.1 Characterizing Important Interfacial Properties of Pollen

The first part of this objective was optimization of an acid-base hydrolysis treatment of as received, defatted pollen. We successfully optimized well established acid-base hydrolysis extraction procedures in order to obtain largely intact pollen grains, with surfaces free of debris. This was demonstrated with three different pollen species (short ragweed, Kentucky blue june, and dog fennel). It was found that using low stirring rates combined with highly diluted titrations was key for keeping pollen grains intact and free of debris. This optimization had important effects on all our results. In Chapter 2, intact and clean pollen grains were found to be important for achieving a useful packing of ILC columns, because surface impurities impacted retention behavior of chemical probes and fragments lead to further variation in column packing. Also, the cleaner, purer surface resulted in smoother chromatograms and enhanced retention due to the further isolated sporopollenin shell, compared to as-received pollen. In Chapters 3 to 5 it was observed that acid-base treated pollen grains were more easily functionalized than non treated grains due to the higher purity of sporopollenin and possibly by the presence of reactive functional groups such as hydroxyls. Also, debris likely had a detrimental effect on wetting and

adhesion at the interface for pollen-polymer composites. We suggested that uniformity of pollen grains is a unique characteristic when compared to more polydisperse conventional fillers, so we aimed to obtain pollen grains that were mostly intact and their shapes retained. In fact, as mentioned in Appendix A.1, the acid-base hydrolysis treatment actually caused pollen grains to be more round and plump than in their original as received state, which may be due to improved hydration of the exine shells.

Next, we aimed to investigate the effects of the acid-base hydrolysis treatment on pollen interfacial properties. We successfully showed that the acid-base hydrolysis improved pollen surface interactions with both solids and liquids. In Chapter 2, ILC studies showed acid-base pollen exposed and/or generated polar functional groups on the pollen surface. This resulted in specific interactions with chemical probes and increasing retention with increasing probe basicity. In Chapter 3 and 4 we found acid-base pollens displayed improved interfacial morphology versus as-received pollen grains, again due to polar functional groups leading to increased surface interactions. This was demonstrated with various pollen species as well as shown in Chapter 5.

Finally, we aimed to develop and use inverse liquid chromatography (ILC) to characterize pollen chemical and physical interactions of pollen with potential matrix chemistries. We successfully demonstrated the first use of ILC in characterizing a biological particle (to our knowledge). As-received untreated pollen displayed unchanging retention of chemical probes, while retention increased on acid-base pollen as chemical probes became increasingly polar, due to interactions with hydroxyl groups on AB pollen. This suggested that surface interactions are limited to weak van der Waals forces for D pollen, while AB pollen is capable of stronger polar interactions, possibly including hydrogen bonding. The ILC results supported the results in Chapters 3, 4, and 5 strongly, which indicated that acid-base pollen was more polar than as received pollen due to improved presentation of surface polar groups.

6.1.2 Engineering a More Effective Pollen-Polymer Composite

First, we aimed to explore the effects of the acid-base hydrolysis treatment and organosilane functionalization of pollen in polyvinyl acetate (PVAc) matrices. We demonstrated the first successful use of pollen as a sustainable, light-weight, and reinforcing filler in PVAc. Acid-base pollens eliminated interfacial voids observed with as received pollen, effectively stiffening PVAc with increased pollen loading. This is due to exposed polar functional groups and increased surface interactions. Composites prepared with acid-base pollen also showed no significant change in weight of at the composite loadings explored herein (up to 15 vol. %). Further functionalizing the pollen with an organosilane optimizes the interfacial morphology and results in simultaneous stiffening and strengthening of PVAc-pollen composites. A pollen modulus was able to be estimated from elastic modulus data of composites, and is reported to be ~62-70 MPa. Acid-base and functionalized pollen both displayed increased widths of the glass transition region, indicating the restriction of polymer chains near these pollen surfaces that suggests strong surface attractive interactions.

Next, we explored the effects of the acid-base hydrolysis treatment of pollen in waterborne epoxy matrices. Again, we demonstrated the first successful use of pollen as a sustainable, light-weight, and reinforcing filler in an epoxy. As received pollen displayed a thick, soft interphase surrounding pollen grains, due to the leeching of intracellular material which strongly bonds with amine crosslinker. As a result of the amine depletion, the epoxide in this region did not fully cure, leading to decreased mechanical properties with increased pollen loading. Acid-base pollen eliminated the visible interphase and was strongly coated by epoxy. This optimized interphase resulted in simultaneous stiffening and strengthening of AB pollen-filled epoxy materials. Unlike PVAc, both as received and acid-base pollen elevated glass transition temperature (acid-base to a higher degree), indicating epoxy is more compatible with pollen than PVAc and previous

polymers studied. A pollen modulus was able to be estimated from elastic modulus data of epoxy composites, and is reported to be ~67 MPa from HTMECH data and ~8005-8170 MPa from conventional tensile testing.

Finally, we aimed to determine the effects of size of pollen microstructures on wetting, adhesion, and composite properties. First, functionalized pollen was found to impart higher tensile strength and strain at break on PVAc matrices than smooth functionalized silica particles, when both particles were treated with the same surface functionalization (vinyltrimethoxysilane). Separation occurred at the silica-PVAc interface after mechanical tests, an effect that was not observed in pollen-PVAc composites, indicating that pollen shape (nanopores and hollowness) and roughness may enhance wetting and adhesion at the interface when compared to smooth spherical particles. By varying the species of pollen incorporated in PVAc matrices it was observed that pollen with smaller surface structures were wetted more effectively by polymer matrices than pollen with larger structures. However, mechanical properties were similar for the various pollen species considered, indicating that the enhanced wetting did not translate to enhaced adhesion at the interface during mechanical strain.

6.2 Recommendations and Future Work

Based on the findings of this work, a number of key scientific questions have been raised. The following section seeks to provide possible strategies for approaching these issues in future studies.

Only one study has determined mechanical properties of dessicated pollens [1]. Atomic force microscopy (AFM) may also be utilized to further determine mechanical properties of pollen grains, utilizing normal AFM cantilevers or cantilevers with glass beads attached [2-5]. AFM cantilevers may pierce the sporopollenin shell top layer, while a glass bead cantilever may result in more structural compression of the sporopollenin shell. ILC can be used further to

continue to develop our understanding of the pollen surface. ILC can also be used for the determination of adsorption and desorption isotherms with probes at finite concentrations [6-9]. This is useful for determining uptake of chemical probes. In a pulse method, injections of known quantities of solute result in a pulse chromatographic peak. Two pulse methods used for isotherm determination are peak maximum (PM) and elution by characteristic point (ECP). In frontal analysis, solute concentration in the mobile phase is changed to a new constant value, resulting in a boundary breakthrough curve. Two frontal methods are frontal analysis (FA) and frontal analysis by characteristic point (FACP). PM and FA methods are accurate, but can be time consuming, while ECP and FACP derive complete isotherms from only one experiment. In order to properly calculate uptake and determine isotherms, it is important to understand and know significant parameters such as the mass of solid in the column, concentrations of injections, and maximum solute concentration of in the mobile-phase, depending on the method chosen. ILC has even been used to estimate fundamental values such as surface energies of different surfaces, which could be of great interest with such a complex particle as pollen [10, 11]. ILC was only conducted with short ragweed pollen. Investigating as received and treated pollen grains of various species in order to probe differences in surface properties between species would be interesting since it is known that the chemical composition of sporopollenin can vary between species [12]. ILC can be used to probe how these variations may affect surface interactions. Additionally, ILC may be used further to probe the retention of high molecular weight probes which may be more useful for predicting potentially compatible matrix chemistries.

Many more polymers could be investigated as potential matrices for pollen-polymer composite. Because functionalization appears to be an effective strategy, it would also be interesting to investigate other polymers that are reactive with hydroxyl groups, e.g., urethanes

and epoxies. Also, we could return to our initial work with PS and PCL in order to determine if acid-base hydrolysis of pollen would yield similar results as reported in this thesis, where acid-base pollens displayed enhanced wetting and adhesion and also resulted in reinforcement due to the elimination of interfacial voids. Further, pollen grains could be functionalized with appropriate functional groups for compatibility with less polar thermoplastics, such as PS and PCL, in order to further tune interfacial and mechanical properties. In relation to PCL previously studied, acid-base pollen may actually be a good filler for grafting PCL chains on the pollen surfaces via -OH groups to initiate ring opening polymerization of PCL [13-15], thereby fabricating a biodegradable polymer with natural pollen filler. Continuing along these lines, focusing on "green" composites is of interest. Pollen filler could be incorporated in recyclable polymers, such as polyolefins, reducing the use of non-biodegradable polymer. Entirely "green composites" can be fabricated by incorporating pollen filler with additional biodegradable polymer matrices such as polyesters, polysaccharides, natural rubbers, and some polyamides, to name a few. Polylactic acid is a widely used natural polymer of interest [16-18]. Biodegradable polymers often suffer from poor mechanical properties [19-21]. Pollen is a tough natural filler that may be incorporated in these polymers to enhance mechanical strength if adhesion is optimal. Also, as shown in this work, the pollen shell is stable up to ~450 C. Materials filled with natural fillers often suffer from low thermal decomposition over 200 °C, resulting in polymer processing temperatures that are kept below approximately 200 °C. Thus, pollen filler may allow for higher polymer processing temperatures versus other natural organic fillers. Finally, pollen might be able to be recovered when recycling both natural and non-biodegradable polymers.

Fabricating pollen-polymer composites with industrially relevant processing techniques such as extrusion, injection molding, compression molding, may constitute future work as well.

More challenges may arise with incorporation and effective dispersion of pollen in polymers subjected to such processing due to the high viscosities and temperatures encountered in melt processing. Again, pollen may have an advantage over other natural organic fillers due to the shell's thermal resistance (stable to ~450 C) allowing for higher processing temperatures. Materials filled with natural fillers often suffer from poor adhesion between the fillers (hydrophilic) and the polymer matrix (generally hydrophobic). The hydrophilic and hygroscopic characteristics of natural fillers influence both filler dispersion and interfacial adhesion. The presence of humidity can lead to the formation of water vapor during processing, which in turn can cause interfacial void formation and poor mechanical properties. Thus, research is often focused on utilizing chemical modifications and adhesion promoters to improve the interfacial adhesion and dispersion of natural organic fillers in polymer matrices. Is acid-base treatment of pollen alone still effective in improving wetting, adhesion, and reinforcement of matrices when polymers are processed with industrially relevant processing techniques? These are important questions that should be answered in relation to pollen as a filler, especially with industrially-relevant processing techniques. In relation to the effect of the size of microstructures of interfacial and composite properties, it would be interesting to continue this work by investigating a more complete range of pollen loadings and choosing more model pollen grains for incorporation in polymers. One species of interest is olive pollen (*Olea europaea*) due to its reticulum (network-like pattern) surface, which could allow improved mechanical interlocking of polymer chains with the pollen surface. Poplar pollen (*Populus nigra*) is another pollen species of interest due to its different degree of surface roughness versus the species studied in this work.

In this work we optimized previously-established sporopollenin extraction proedures. It would be interesting to develop new methods for isolation of pollen exine that may be more

simple. The established procedures often have several steps (such as the acid and base steps or more) and often employ harsh solvents or even dangerous chemicals such as HF. Even for the procedure optimized in this work additional titration and centrifugation steps were added to improve the established procedures for larger batches of pollen. One alternative that may be interesting for further investigation is ionic liquids for sporopollenin extraction. Ionic liquids are solid salts that melt below 100 °C. They are often powerful green solvents solid at room temperature and less harmful that traditional solvent. They have been shown to dissolve cellulose [22, 23], which is in pollen grains intine layer. Thus it is likely that the solvents also extract intracellular material. It may be possible to use ionic liquids to extract exines, dissolving intracellular material and some cellulosic content. Since ionic liquids are currently expensive, this alternative would be a tradeoff between higher cost and potentially simpler procedure that has less steps and is safer.

Finally, the unique characteristics of pollen grains has inspired some interesting ideas. This work showed the potential of using pollen to maintain or possibly lightweight polymers. Treated pollen grains are hollow particles and coating the pollen surface in order to entrap air in pollen grains would further enhance their weight reduction capability. Such a coating procedure may involve placing pollen in polymer solution for a short amount of time in order to deposit polymer only on the inside and the outside of the pollen grain. Perhaps, even with extended exposure to polymer, effective washing of exposed pollen will wash away polymer in the center of the pollen leaving only polymer on the inner and outer surface. SEM images of recovered acid-base pollens seem to suggest this may be possible. The insides of the pollen grains were coated with a thick layer of epoxy, however it was still apparent where pollen pores existed although the outer surface was also covered with epoxy. The visibility of pores may reveal that

the pollen grains are not coated completely when and air is not entrapped in the pollen core. However, with further work, perhaps epoxy or a more optimal polymer may be used to achieve this goal. Finally, pyrolysis of pollen is an idea that was explored herein and that has been examined by others [24, 25]. Pyrolysis of pollen yields carbon microspheres with unique morphologies derived from a sustainable source which may also have increased surface area. These carbon microspheres could have several applications. First, we could continue to utilize carbon microspheres in composites work. Carbon fillers are often used in polymers such as polystyrene. Carbons also have applications in areas such as water treatment, adsorption and separations [26-29]; thus, pollen could be an additional sustainable source of carbon for such areas.

6.3 References

1. Liu, T. and Z. Zhang, *Mechanical properties of desiccated ragweed pollen grains determined by micromanipulation and theoretical modelling.* Biotechnology and Bioengineering, 2004. **85**(7): p. 770-775.
2. Cappella, B., et al., *Mechanical properties of silicone methacrylate microparticles determined by AFM Colloidal Probe Technique.* Polymer, 2014. **55**(5): p. 1209-1216.
3. Vakarelski, I.U., et al., *Deformation and Adhesion of Elastomer Microparticles Evaluated by AFM.* Langmuir, 2001. **17**(16): p. 4739-4745.
4. Tan, S., R.L. Sherman, and W.T. Ford, *Nanoscale Compression of Polymer Microspheres by Atomic Force Microscopy.* Langmuir, 2004. **20**(17): p. 7015-7020.
5. Park, S.-J., M.B. Goodman, and B.L. Pruitt. *Measurement of mechanical properties of Caenorhabditis elegans with a piezoresistive microcantilever system*. in *Microtechnology in Medicine and Biology, 2005. 3rd IEEE/EMBS Special Topic Conference on*. 2005.
6. Yla-Maihaniemi, P.P. and D.R. Williams, *A comparison of frontal and nonfrontal methods for determining solid-liquid adsorption isotherms using inverse liquid chromatography.* Langmuir, 2007. **23**(7): p. 4095-4101.
7. Donnet, J.B., et al., *Characterisation of a precipitated silica surface by inverse liquid chromatography Part I.* Kautschuk Gummi Kunststoffe, 2004. **57**(4): p. 151-159.
8. Maafa, D., H. Balard, and J.B. Donnet, *The study of adsorption of iodine on carbon black by inverse liquid chromatography.* Rubber Chemistry and Technology, 2007. **80**(5): p. 895-906.
9. Antworth, C.P., R.R. Yates, and W.T. Cooper, *Applications of inverse chromatography in organic geochemistry—I. Characterization of polar solute-soil organic matter*

interactions by high performance liquid chromatography. Organic Geochemistry, 1989. **14**(2): p. 157-164.
10. Donnet, J.B., et al., *Surface energy of silica xerogels and fumed silica by inverse gas chromatography and inverse liquid chromatography.* Rubber Chemistry and Technology, 2002. **75**(5): p. 811-824.
11. Bednar, I., et al., *Surface energies of hydrophobic interaction chromatography media by inverse liquid chromatography.* Journal of Chromatography A, 2012. **1220**(0): p. 115-121.
12. Guilford, W.J., et al., *High Resolution Solid State 13C NMR Spectroscopy of Sporopollenins from Different Plant Taxa.* Plant Physiology, 1988. **86**(1): p. 134-136.
13. Huang, Q., J. Huang, and P.R. Chang, *Polycaprolactone grafting of cellulose nanocrystals in ionic liquid [BMIM]Cl.* Wuhan University Journal of Natural Sciences, 2014. **19**(2): p. 117-122.
14. Lönnberg, H., et al., *Synthesis of Polycaprolactone-Grafted Microfibrillated Cellulose for Use in Novel Bionanocomposites–Influence of the Graft Length on the Mechanical Properties.* ACS Applied Materials & Interfaces, 2011. **3**(5): p. 1426-1433.
15. Lönnberg, H., et al., *Grafting of Cellulose Fibers with Poly(ε-caprolactone) and Poly(l-lactic acid) via Ring-Opening Polymerization.* Biomacromolecules, 2006. **7**(7): p. 2178-2185.
16. Oksman, K., M. Skrifvars, and J.F. Selin, *Natural fibres as reinforcement in polylactic acid (PLA) composites.* Composites Science and Technology, 2003. **63**(9): p. 1317-1324.
17. Graupner, N., A.S. Herrmann, and J. Müssig, *Natural and man-made cellulose fibre-reinforced poly(lactic acid) (PLA) composites: An overview about mechanical characteristics and application areas.* Composites Part A: Applied Science and Manufacturing, 2009. **40**(6–7): p. 810-821.
18. Huda, M.S., et al., *"Green" composites from recycled cellulose and poly(lactic acid): Physico-mechanical and morphological properties evaluation.* Journal of Materials Science, 2005. **40**(16): p. 4221-4229.
19. Baruah, S.D., *Biodegradable Polymer: The promises and the problems.* Sci Cult, 2011. **77**: p. 466-470.
20. Gunatillake, P.A. and R. Adhikari, *Biodegradable synthetic polymers for tissue engineering.* Eur Cell Mater, 2003. **5**: p. 1-16; discussion 16.
21. Vroman, I. and L. Tighzert, *Biodegradable Polymers.* Materials, 2009. **2**(2): p. 307-344.
22. Swatloski, R.P., et al., *Dissolution of Cellose with Ionic Liquids.* Journal of the American Chemical Society, 2002. **124**(18): p. 4974-4975.
23. Wang, H., G. Gurau, and R.D. Rogers, *Ionic liquid processing of cellulose.* Chemical Society Reviews, 2012. **41**(4): p. 1519-1537.
24. Wang, Y., et al., *Carbon Microspheres with Supported Silver Nanoparticles Prepared from Pollen Grains.* Langmuir, 2005. **21**(23): p. 10846-10849.
25. Xia, Y., et al., *Biotemplated fabrication of hierarchically porous NiO/C composite from lotus pollen grains for lithium-ion batteries.* Journal of Materials Chemistry, 2012. **22**(18): p. 9209-9215.
26. Bansal, R.C. and M. Goyal, *Activated carbon adsorption*. 2005: CRC press.
27. Sircar, S., T. Golden, and M. Rao, *Activated carbon for gas separation and storage.* Carbon, 1996. **34**(1): p. 1-12.

28. Siriwardane, R.V., et al., *Adsorption of CO2 on molecular sieves and activated carbon.* Energy & Fuels, 2001. **15**(2): p. 279-284.
29. Sontheimer, H., et al., *Activated carbon for water treatment.* 1988.

APPENDIX A

A.1 Optimization of Acid-Base Hydrolysis Procedure

As mentioned in previous chapters, an acid-base treatment (hereafter labeled as AB) was used to clean and isolate the exine shell for characterization of pollen surface properties before and after the treatment, incorporation in polymer films, and preparation for further functionalization. Extraction of sporopollenin shells is well established in literature [1, 2], however the procedures had to be optimized for treatment of larger batches of pollen (10 grams or more). With treatment of larger batches of pollens, issues with broken pollen grain, pollen grains covered with debris, and irregularly shaped pollen became more prevalent. Here, we present a more in depth description of the optimization of the procedure and the results obtained.

Typically, 10 grams of pollen were well dispersed and mixed in 80 mL of DI water in a 500 mL flask. 6 grams of KOH were dissolved in 20 mL of water and added to the pollen-water mixture to make a 6w/v% KOH solution. This was gently stirred for 24 hours at room temperature. The mixture was neutralized with HCl and subsequently washed with hot water and ethanol in between centrifuging at 2800 rpm (vial caps were punctured in order to avoid vial breakage). The pollen was then dried in a convection oven at 60 °C overnight. Figure A.1 and Figure A.2 show ragweed and dog fennel pollen, respectively, after the base hydrolysis step. Both figures show that base step affects the shape of pollen grains (shrinking or collapsing) and causes debris to be deposited on the surfaces. Our base hydrolysis appears to extract pollen internal material leaving empty shells, but does not fully dissolve the internal material. Thus large amounts of undissolved internal material are present on pollen surfaces after the base step. A key variable for obtaining mostly intact pollen grains was using a gentle stir. Initially high stir rates above 200 rpm (sometimes reaching ~1100 rpm) with a 40 cm stir bar were utilized for this

procedure. This resulted in fragmentation of pollen grains and a large amount of broken shells, as shown in Figure A.1. Stir rates were decreased to 155 rpm or lower to optimize the procedure. Figure A.2 shows dog fennel pollen after base hydrolysis and with the lower stir rates, resulting in nearly all pollen grains remaining intact.

Base hydrolyzed grains were then re-suspended in water, sonicated to detach as much debris as possible, and centrifuged. The grains were added to a 500 mL flask while still suspended in a small amount of water. 200 mL of 85% H_3PO_4 was added to this flask, and was refluxed at 50 °C for 7 days again with gentle stirring. The mixture was then centrifuged in several vials at 1.5 rpm with punctured vial caps. Due the phosphoric acid's larger density, the pollen grain settled out at the top of the solution. A large 25 mL glass syringe with a long metal syringe needle was utilized to collect and discard the phosphoric acid at the bottom of the vial. The volume of the remaining pollen-phosporic acid mixture was estimated by comparison to known volumes of water, in order to determine how much sodium hydroxide was required to neutralize the mixture. The mixture was diluted 4x the estimated volume with DI water and sodium hydroxide was dissolved in an equal amount of water. The diluted pollen mixture was combined to the sodium hydroxide mixture to create a neutral solution. These optimized neutralization steps proved to be key for attaining clean and intact pollen grains. Finally, the pollens were washed with hot water, acetone, and ethanol in between centrifuging at 2800 rpm. The acid hydrolyzed pollen was dried in a convection oven at 60 °C. The acid-base hydrolysis process caused the pollen grains to lose ~80% of their original weight.

Figure A.3 and Figure A.4 show short ragweed pollen after the acid hydrolysis step. Figure A.3 shows that with a high stir rate and non-optimal neutralization ragweed pollen becomes highly fragmented, broken, and is covered with surface debris. Figure A.4 shows that

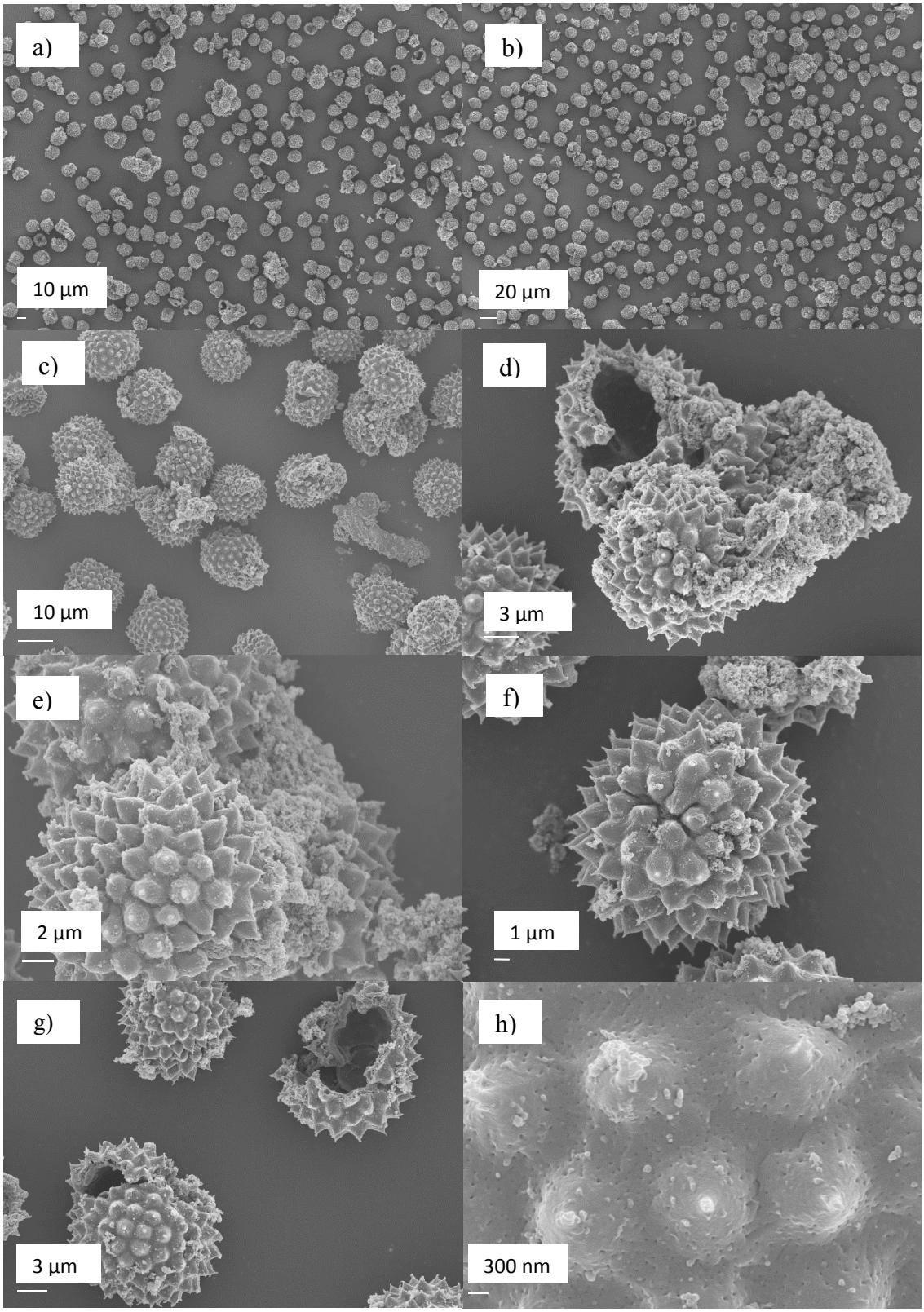

Figure A.1: Short ragweed pollen grains after base hydrolysis step. High stir rate.

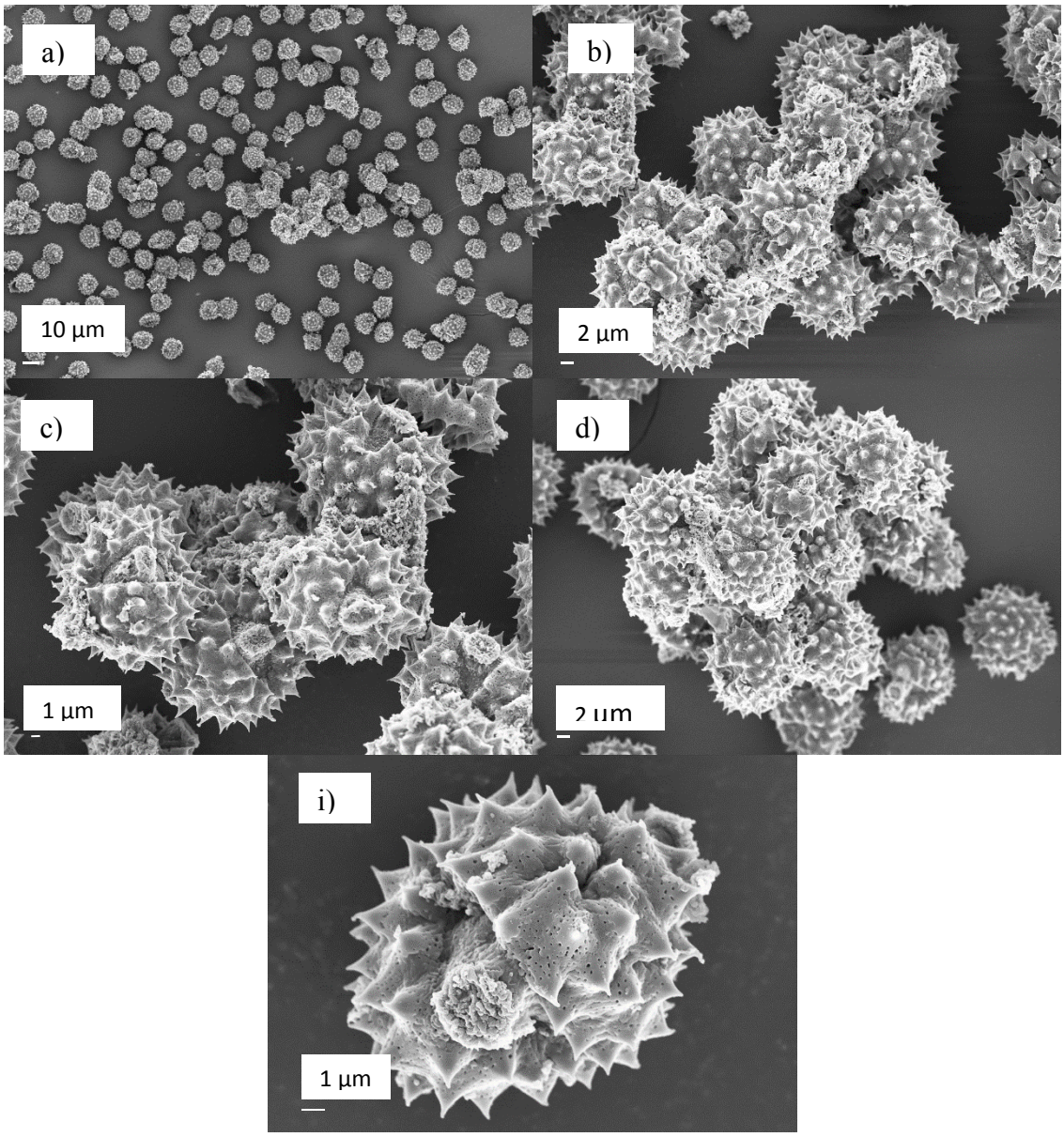

Figure A.2: Dog Fennel pollen grains after base hydrolysis step. Low stir rate.

low stir rates combined with optimal neutralization procedures results almost entirely intact pollen grains with surfaces free of debris. The few examples of broken shells so that the inner layer of the exine is clear of debris as well. The acid hydrolysis step also appears to impart pollen grains with a more spherical and plump shape. This further apparent with species besides ragweed pollen as shown in Figure A.5 to Figure A.8. Figure A.5 shows that nearly all Kentucky blue june pollens are collapsed in their as received state. However, after acid-base hydrolysis the

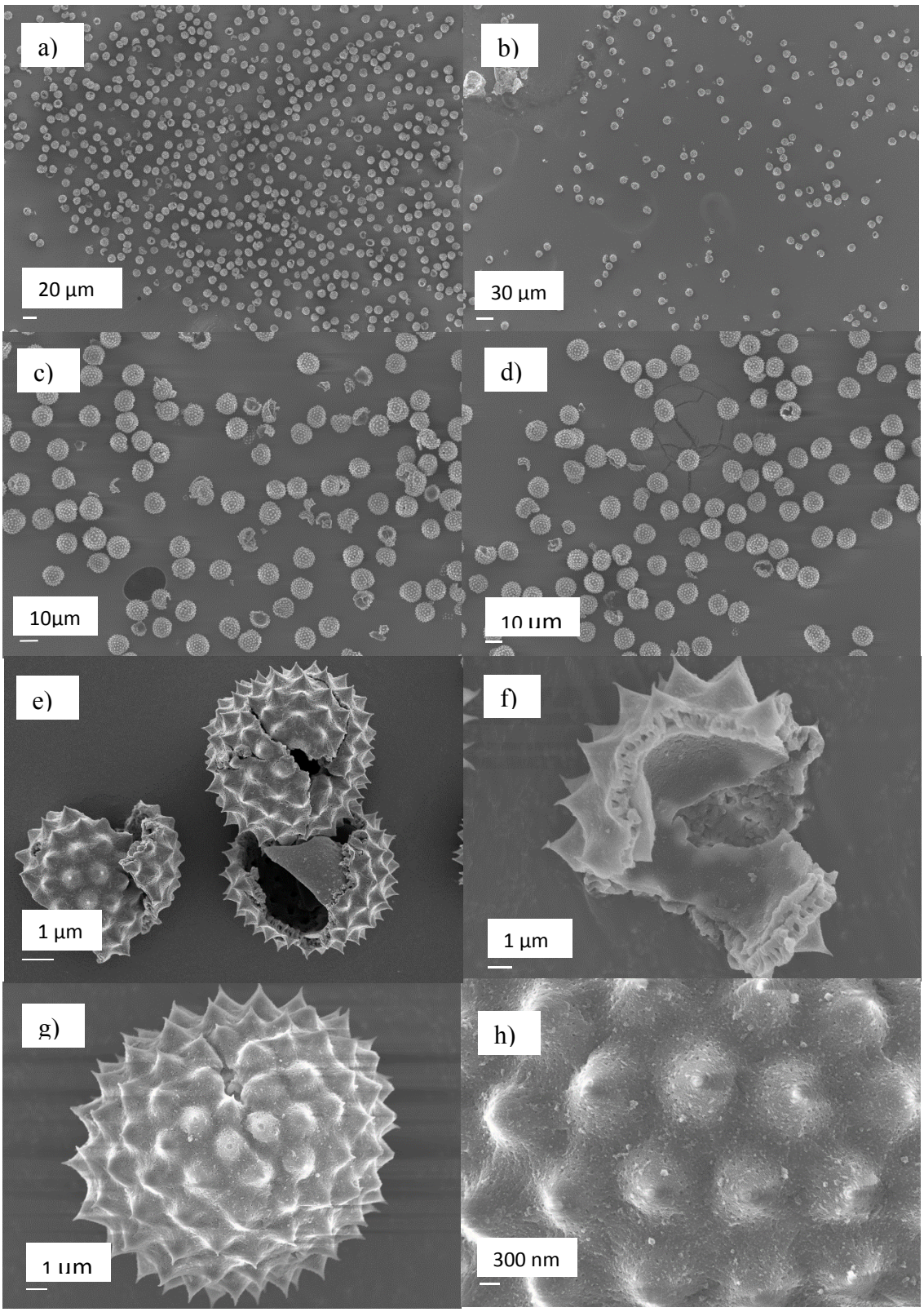

Figure A.3: Ragweed pollen after acid hydrolysis step. High stir rate and non-optimal neutralization.

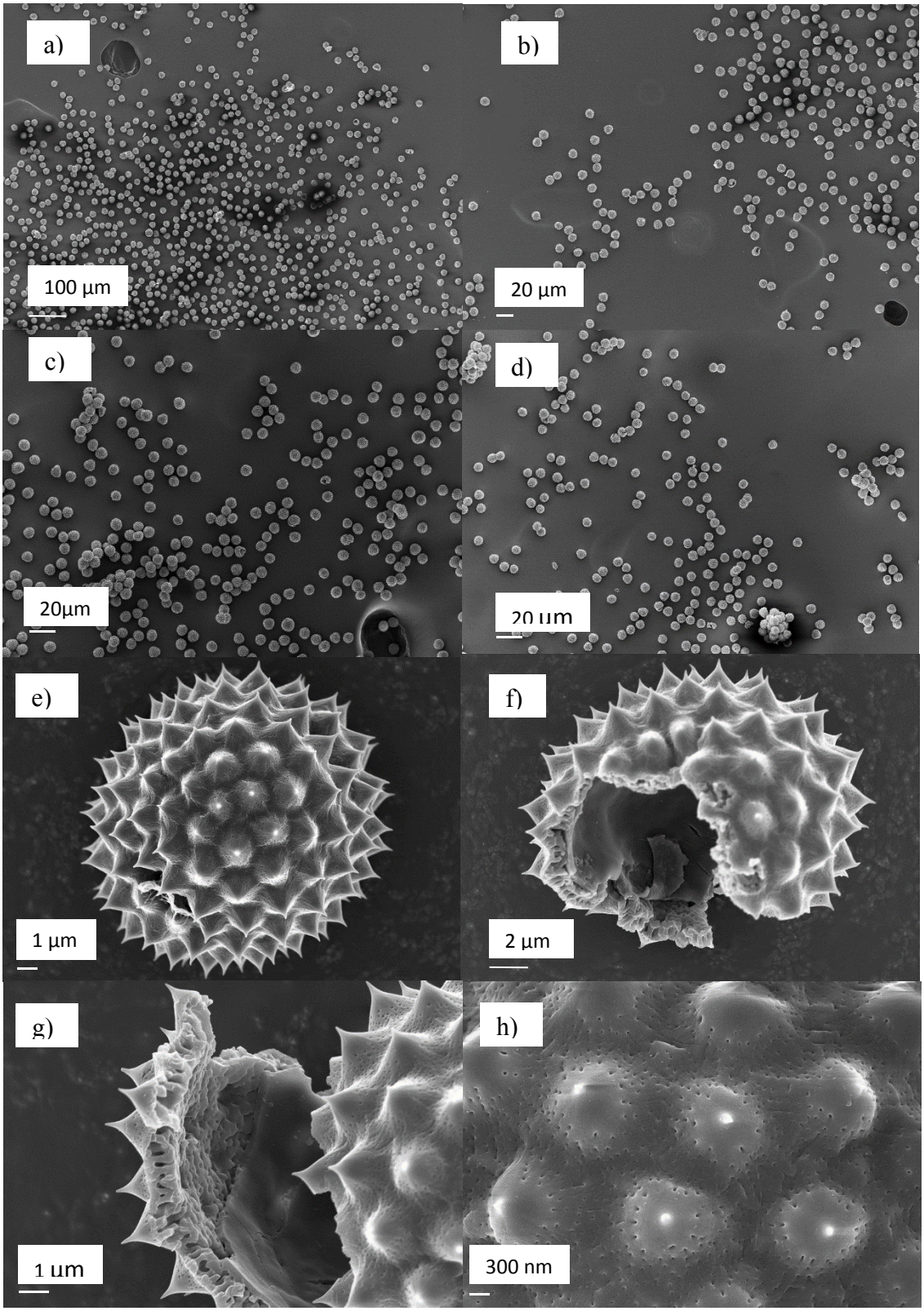

Figure A.4: Ragweed pollen after acid hydrolysis step. Low stir rate and optimized neutralization.

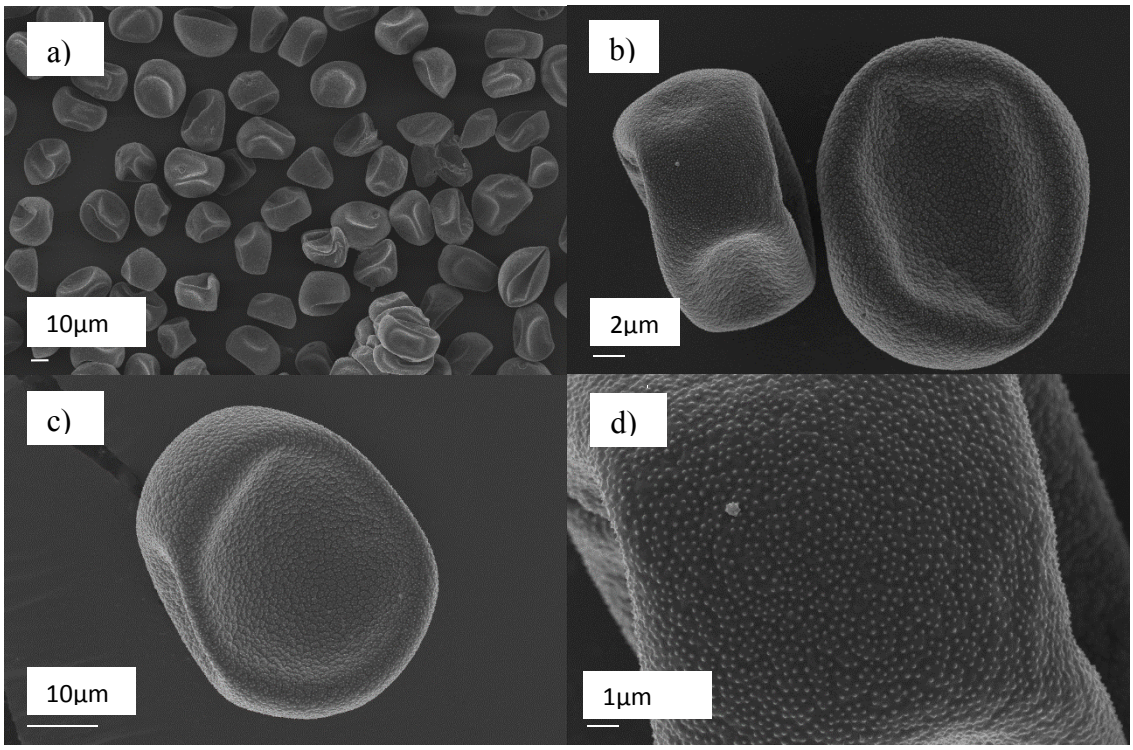

Figure A.5: Defatted Kentucky blue june pollen.

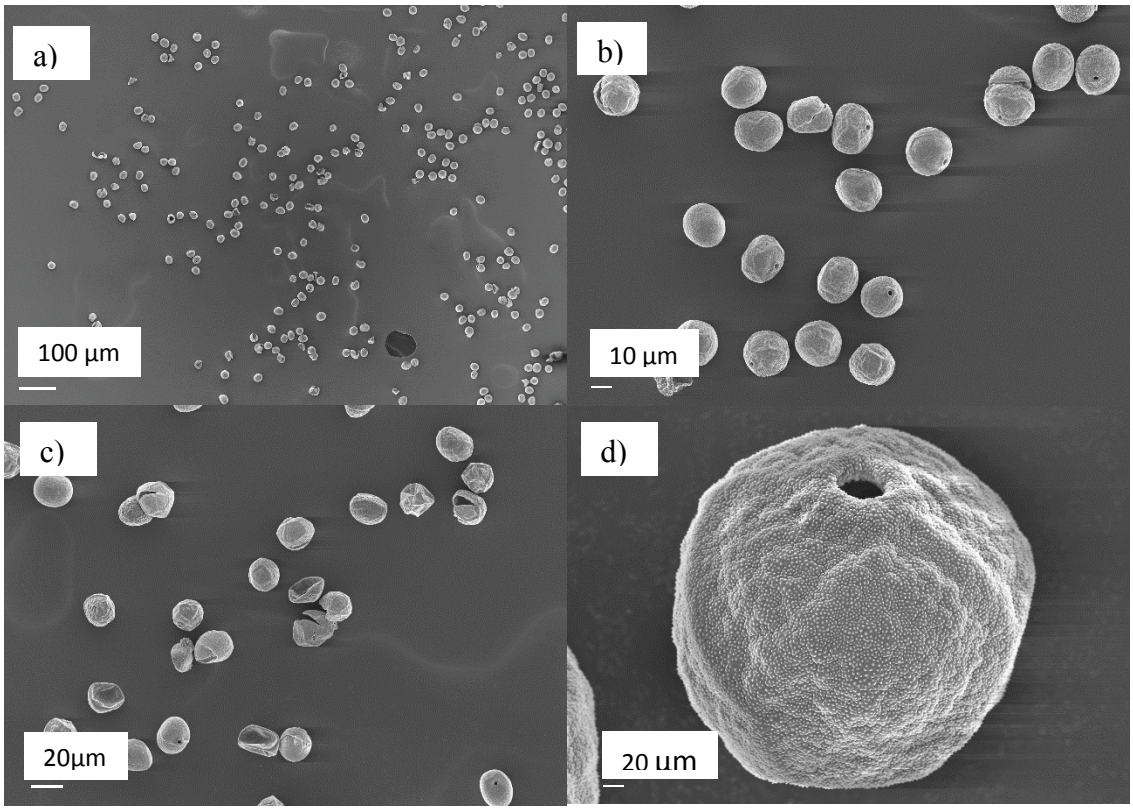

Figure A.6: Acid-base hydrolyzed Kentucky blue june pollen.

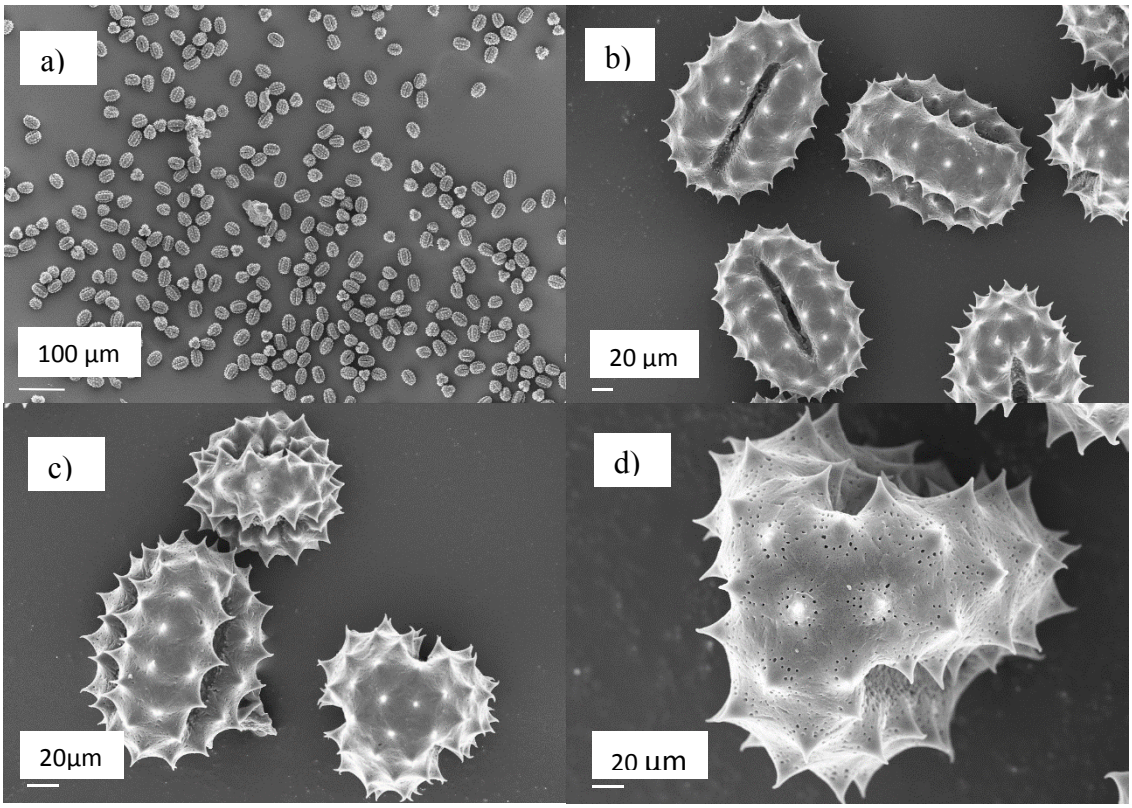

Figure A.7: Defatted dog fennel pollen grains.

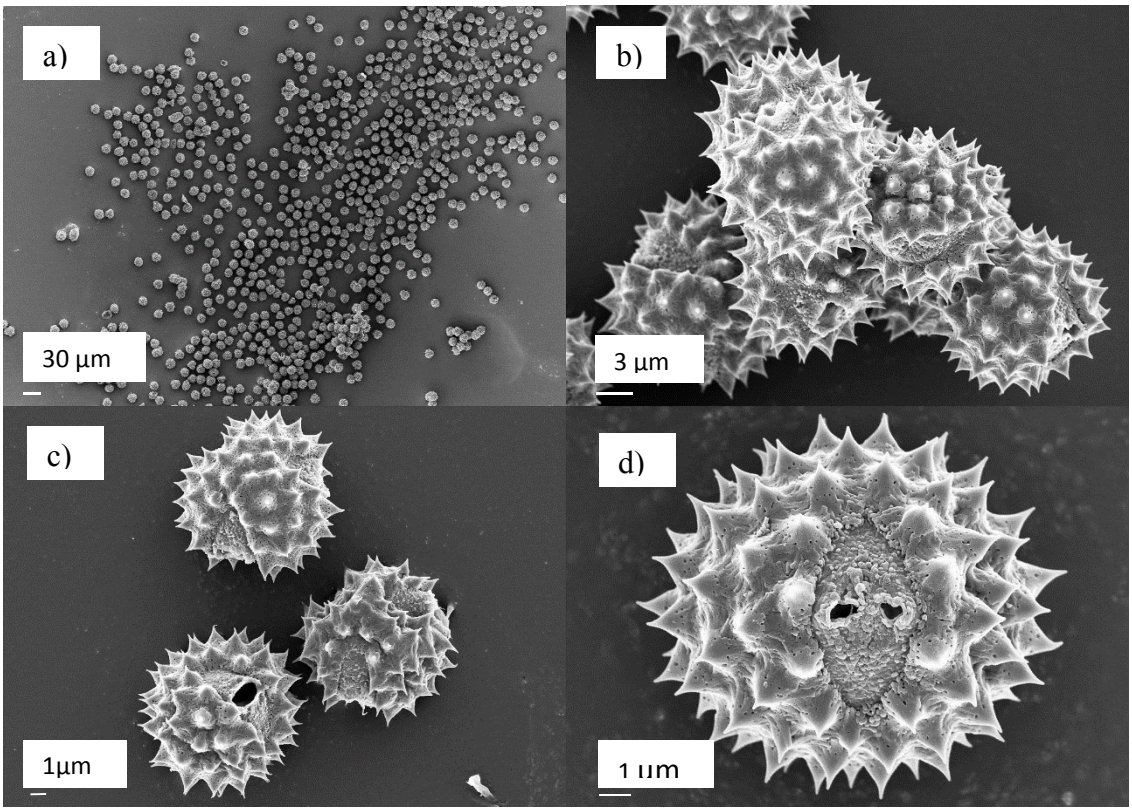

Figure A.8: Acid-base hydrolyzed dog fennel grains.

grains are mostly intact, have clear surfaces, and are no longer collapsed, displaying much more spherical and rounded shapes. Figure A.7 and Figure A.8 show similar results for dog fennel pollen. This may occur because natural grain are dehydrated. However, after acid-base hydrolyzed grains may have an increased water uptake due to the addition of polar functional groups (hydroxyls and carboxyls) allowing the shell to be more hydrated and resulting in swollen rounded pollen grains.

A.2 References

1. Southworth, D., *Solubility of Pollen Exines.* American Journal of Botany, 1974. **61**(1): p. 36-44.
2. Wiermann, R. and S. Gubatz, *POLLEN WALL AND SPOROPOLLENIN.* International Review of Cytology-a Survey of Cell Biology, 1992. **140**: p. 35-72.